

***Exploring the Piezoresistive Characteristics of Solution Styrene
Butadiene Rubber composites under static and Dynamic Conditions
- A Novel Route to Visualize Filler Network Behavior in Rubbers***

Von der Fakultät Maschinenwesen
der
Technische Universität Dresden
zur
Erlangung des akademischen Grades
Doktoringenieur (Dr.-Ing.)
angenommene Dissertation

M.Tech. Subramani Bhagavatheswaran, Eshwaran
Geb. am 08 Mai 1989 in Bhilai Nagar, Indien

Tag der Einreichung: 14.08.2018

Tag der Verteidigung: 04.02.2019

Erste- Gutachter: Prof. Dr. rer. nat. habil. Gert Heinrich

Zweite- Gutachter: Prof. Dr. Jyrki Vuorinen

Vorsitzender: Prof. Dr. –Ing. Habil. Maik Gude

Written in memory of my loving parents
Dr. B. Subramani & Dr. C.R. Rajashree

Dedicated to

My beloved wife, dearest friend, and
pillar of support
Nisha

&

My dear brother
Krishnan

Acknowledgements

It gives me immense pleasure to sincerely thank everyone who has helped me in different ways to complete this dissertation successfully. This success would have never been possible without the support from my coworkers, friends and family members. I would like to convey my deepest gratitude to all these kind-hearted people.

First and foremost, my sincere thanks to Prof. Gert Heinrich for giving the opportunity to carry out my doctoral thesis under his guidance at IPF Dresden. I sincerely thank him for his valuable guidance, endless encouragement and also for motivating me to learn the German language. He is a genuine example of dedication and this made me realize how one should develop an understanding in their subject. Finally, as a person, I respect his humbleness and friendly personality.

I have no words to express my thankfulness to Dr. Amit Das who has been guiding me throughout. Apart from inducing scientific orientation in me, he has set himself as an example of commitment and passion for research. Being my most critical audience, he has shaped my research invaluable. Apart from being my mentor, he has also been a family to me and has been supportive all throughout my difficult times.

I would like to earnestly thank Prof. Sven Wießner for his constant guidance, support, and advice. I am grateful for his enthusiastic and unrelenting support during the course of time. I have really enjoyed our countless inspiring discussions which also helped me to shape my intellect. He is the main reason for me having learned the German language. I show my greatest respect and most sincere gratitude from the core of my heart for his humbleness and friendliness.

I would express my warmest thanks to Dr. Klaus W. Stöckelhuber for the helpful discussions, suggestions, and encouragement. I admire him for his lively and humble behavior. My sincere thanks to Mr. Rene Jurk for his kind support and I admire him for his jovial personality. Special thanks to my officemate Mr. Thomas for his kindness and especially for organizing all the nice department excursions. A special

thanks to Dr. Wolfgang Jenschke for the technical support. I am very much thankful to Mrs. Anne Hofmann and Mrs. Gudrun Schwarz for all the kind help. I am thankful to members and co-workers of other departments who have helped me in many respects during the whole Ph.D. work.

I am very much thankful to my friends Sankar Raman, Tamil Selvan, Minoj, Parthiban, Anik, Sakrit, Shib Shankar and Tahir. Special thanks to my family friends Mr. Boopathy, Mrs. Selvi Boopathy, Dr. Krishnakumar, Dr. Renuka Krishnakumar, and Krisitha. I am grateful to all of these kindhearted people for all the help and support, especially, for the wonderful times chatting, traveling to many places, having nice dinners and enjoying movies together.

Finally and most important of all, is to thank my near and dears. Most special thanks for my wife Nisha for her never-ending support, encouragement, patience, love and for being there throughout the stressful times. Heartfelt thanks to my parents, Dr. B. Subramani and Dr. C.R. Rajashree for their motivation from the very beginning and having faith in me. I hope they would be happy and proud of my accomplishment. Respectful and humble thanks to my grandparents for all the blessings. I would like to convey a special piece of thanks to my brother, Krishnan, for his boundless love and support. I am very much thankful to my in-laws Mr. Sankaran and Mrs. Ananthi Sankaran for their wishes and constant encouragement. Finally, thanks to my uncle and aunt, Mr. Mohan and Mrs. Jayashree Mohan for all the relentless support and motivation.

Abstract

For the development of intelligent vehicle tires, especially for future self-driving cars, suitable strain sensors are mandatory. The design of such a strain sensor must fulfill several criteria and most important of them all, it must be easily mounted or implanted into the tire and the elastic nature of the sensors must synchronize with the deformation of the tire. This work is therefore focused on understanding the piezoresistive characteristics of a composite developed from tire rubber. Thus, a commercially available grade of solution styrene butadiene rubber (SSBR) was primarily chosen as the matrix rubber along with butadiene rubber (BR) and natural rubber (NR).

The initial focus was given to develop simple strain sensors by exploiting the concept of piezoresistivity with conductive rubber composites based on SSBR filled with carbon black and carbon nanotubes. As the internal structure of the filler particles was found to rearrange or alter during deformation, it was important to study the piezoresistive performance with respect to critical material parameters such as crosslink density, hardness, and stiffness of the composite in details. The developed sensors were able to be stretched to several hundred percents of their original length and strain sensitivity as much as ~ 1000 (gauge factor) was achieved.

Quasi-static cyclic tests indicated the ability of the developed materials to respond and recover within the given time frame. This motivated to assess the suitability of these materials for dynamic sensing. As a consequence, the dynamic piezoresistive characteristics were studied for the conducting SSBR composites. The temporal changes in electrical resistance of the SSBR composites were monitored real-time during dynamic mechanical studies. The influence of critical parameters such as filler content, test frequency, test temperature, and matrix crosslink density was taken into consideration.

The filler network was found to rearrange in the rubber matrix during dynamic loading, witnessed from the changes in electrical resistance over time. The findings

offered a preliminary understanding of the filler network behavior inside the SSBR matrix. Situations that eased the filler mobility such as high temperature, low frequency, and low crosslink density resulted in the minimal effect on the filler network changes. For a given strain cycle, the samples responded with two distinct responses pertaining to the loading and unloading, reflecting as two signals. Filler network reconfiguration during unloading was found to be the reason for the second piezoresistive response. The behavior of the second peaks was analyzed in detail at different conditions.

The stress relaxation, an inevitable process pertaining to viscoelastic materials, resembled the overall piezoresistance change of the material. The two properties were therefore correlated, and a relationship was deduced, offering the possibility to monitor the mechanical performance using electrical resistance data. Apart from evaluating the phase shifts between stress and strain ($\delta_{\sigma-\epsilon}$) during the dynamic tests, phase shifts were also evaluated between resistance and strain ($\delta_{R-\epsilon}$) as well as between stress and resistance ($\delta_{\sigma-R}$). The piezoresistive phase shift values ($\delta_{\sigma-R}$) were found to be larger than the mechanical phase shifts values ($\delta_{\sigma-R} > \delta_{\sigma-\epsilon}$). It perceived information regarding the time taken by the filler network to respond for the applied strain.

To realize the concept of dynamic piezoresistivity in commercial use, (i) SSBR filled with conventional carbon blacks N220, N330, and N660 and (ii) NR and BR (two more rubbers that are widely used in tire industry) filled with Printex carbon black were tested for their piezoresistive behavior under dynamic conditions. The experimental results were promising and guaranteed the applicability of the concept for all rubber - filler combinations that display piezoresistive characteristics.

This basic scientific study would be the stepping stone to understand dynamic piezoresistivity in rubbers, which would help in developing rubber-based sensors that are capable of performing under dynamic conditions for the future. Moreover, the study offered a much deeper insight not only on the dynamic piezoresistivity but also on the behavior and changes in the filler network during dynamic deformation.

Kürzfassung

Für die Entwicklung von intelligenten Fahrzeugreifen, insbesondere für zukünftige selbstfahrende Autos, sind geeignete Dehnungssensoren notwendig. Die Konstruktion eines solchen Sensors muss mehrere Kriterien erfüllen: am wichtigsten ist, dass er einfach in den Reifen eingebaut oder implantiert werden kann und dass die Verformung des Sensors mit der Verformung des Reifens synchronisiert ist. Daher konzentriert diese Arbeit sich auf das Verständnis der piezoresistive Eigenschaften eines bekannten Reifenkautschuks, gefüllt mit leitfähigen Füllstoffpartikeln. Eine kommerziell erhältliche Sorte von Lösungs-Styrol-Butadien-Kautschuk (SSBR), Butadien-Kautschuk (BR) und Naturkautschuk (NR), welche in der modernen Reifenindustrie weit verbreitet sind, wurden deshalb als Matrix-Kautschuk gewählt.

Der Fokus lag zunächst auf der Entwicklung einfacher Dehnungssensoren unter Ausnutzung des Konzepts der Piezoresistivität mit leitfähigen Gummimischungen auf Basis von SSBR, welche mit leitfähigem Ruß und Kohlenstoff-Nanoröhrchen gefüllt sind. Da sich die innere Struktur der Füllstoffpartikel während der Verformung verändert, war es wichtig, das piezoresistive Verhalten in Bezug auf kritische Materialparameter wie Vernetzungsdichte, Härte und Steifigkeit des Komposits im Detail zu untersuchen. Die Sensoren konnten auf mehrere hundert Prozent ihrer ursprünglichen Länge gestreckt werden, wobei eine Empfindlichkeit bis zu ~1000 (Gauge Faktor) erreicht wurden.

Quasistatische zyklische Tests zeigten die Fähigkeit der entwickelten Materialien, innerhalb des vorgegebenen Zeitrahmens zu reagieren und sich zu erholen. Dies motivierte dazu, die Eignung dieser Materialien für die dynamische Sensorik zu beurteilen. In der Folge wurden die dynamischen piezoresistiven Eigenschaften für die elektrisch leitfähigen SSBR-Verbundwerkstoffe untersucht. Die zeitlichen Veränderungen des elektrischen Widerstandes dieser SSBR-Verbundwerkstoffe wurden während dynamisch-mechanischer Studien in Echtzeit überwacht. Der Einfluss kritischer Parameter wie Füllstoffgehalt, Matrixvernetzungsdichte, Messfrequenz, und Messtemperatur wurde dabei berücksichtigt.

Es wurde festgestellt, dass sich das Füllstoffnetzwerk während der dynamischen Belastung in der Elastomermatrix neu anordnet, wie die Veränderungen des elektrischen Widerstands im zeitlichen Verlauf zeigen. Diese Ergebnisse bieten ein vorläufiges Verständnis des Verhaltens des Füllstoffnetzwerks der SSBR-Matrix. Situationen, die die Füllstoffmobilität begünstigen, wie hohe Temperatur, niedrige Frequenz und niedrige Vernetzungsdichte, führten zu minimalen Auswirkungen auf das Füllstoffnetzwerk. Für einen gegebenen Dehnungszyklus reagierten die Proben mit zwei getrennten Signalen, welche dem Be- und Entlasten des Materials entsprechen und sich als zwei Peaks in der Widerstandsmessung widerspiegeln. Der Grund für das zweite piezoresistive Signal ist die Rekonfiguration des Füllstoffnetzwerks während der Entlastung. Das Verhalten dieser zweiten Peaks wurde unter verschiedenen Bedingungen detailliert analysiert.

Die Spannungsrelaxation, ein unvermeidlicher Prozess bei viskoelastischen Materialien, ähnelte der gesamten Piezowiderstandsänderung des Materials. Diese beiden Eigenschaften wurden daher korreliert und ein Zusammenhang abgeleitet, der die Möglichkeit bietet, die mechanische Leistung anhand von elektrischen Widerstandsdaten zu überwachen. Neben der Auswertung der Phasenverschiebungen zwischen Spannung und Dehnung ($\delta_{\sigma-\epsilon}$) bei dynamischen Tests wurden auch die Phasenverschiebungen zwischen Widerstand und Dehnung ($\delta_{R-\epsilon}$) sowie zwischen Spannung und Widerstand ($\delta_{\sigma-R}$) bewertet. Die piezoresistiven Phasenverschiebungswerte ($\delta_{\sigma-R}$) erwiesen sich als größer als die mechanischen Phasenverschiebungswerte ($\delta_{\sigma-R} > \delta_{\sigma-\epsilon}$). Dies bietet Informationen über die Zeit, die das Füllernetzwerk benötigt, um auf eine angelegte Belastung zu reagieren.

Um das Konzept der dynamischen Piezoresistivität im kommerziellen Einsatz zu realisieren, wurden (i) SSBR gefüllt mit konventionellen Rußen N220, N330 und N660 und (ii) NR und BR (zwei weitere Kautschuke, die in der Reifenindustrie weit verbreitet sind) gefüllt mit leitfähigem Ruß auf ihr piezoresistives Verhalten unter dynamischen Bedingungen getestet. Die experimentellen Ergebnisse sind vielversprechend und garantieren die Anwendbarkeit des Konzepts für alle Gummi-Füllstoff-Kombinationen mit piezoresistiven Eigenschaften.

Diese grundlegende wissenschaftliche Studie ist ein wichtiger Schritt, um die dynamische Piezoresistivität in Kautschuken zu verstehen, was bei der Entwicklung von zukünftigen, dynamisch arbeitenden Sensoren auf Kautschukbasis helfen kann. Darüber hinaus liefert diese Studie einen viel tieferen Einblick nicht nur in die dynamische Piezoresistivität, sondern auch in das Verhalten und die Veränderungen im Füllstoffnetzwerk während der dynamischen Verformung.

Abbreviations

NR	Natural rubber
SBR	Styrene butadiene rubber
SSBR	Solution polymerized styrene butadiene rubber
BR	Butadiene rubber
Phr	Parts per hundred rubber
ISAF	Intermediate super abrasion furnace
HAF	High abrasion furnace
FEF	Fast extruding furnace
HMF	High modulus furnace
SCB	Super conducting carbon black
CB	Carbon black
CNT	Carbon nanotubes
MWCNT	Multi walled carbon nanotubes
L/D	Aspect ratio = Length / diameter
T _g	Glass transition temperature
DMA	Dynamic mechanical analyser
Vol %	Volume percent
1D	One dimension
2D	Two dimension
3D	Three dimension
Rel. resistance	Relative resistance

Symbols

R_0	Initial electrical resistance (unstrained sample)
R	Instantaneous electrical resistance (after stretching)
ΔR	Change in electrical resistance ($R - R_0$)
$\Delta R / R_0$	Relative change in electrical resistance
δ	Phase shift
$\delta_{\sigma-\varepsilon}$	Phase shift between stress and strain
σ'	Electrical conductivity
P	Volume fraction of filler
P_c	Volume fraction of filler at percolation threshold
σ	Stress
τ	Relaxation time
E'	Storage modulus
E''	Loss modulus
R^2	Coefficient of determination

Contents

Abstract.....	iii
Kurzfassung	v
Abbreviations.....	ix
Symbols	x
Contents	xi

Chapter 1 - Introductions

1.1 General introductions.....	1
1.2 Challenges.....	2
1.3 Motivation.....	4
1.4 Goal.....	5
1.5 Structure of the thesis.....	6

Chapter 2 - Literature survey

2.1 Conducting rubbers.....	9
2.2 Percolation network of fillers.....	11
2.2.1 Influence of Filler aspect ratio on the percolation threshold	13
2.2.2 Influence of Filler dispersion and Morphology	15
2.3 Piezoresistivity	16
2.3.1 Simple uni-axial piezoresistivity	18
2.3.2 Piezoresistivity under dynamic conditions	20
2.4 Dynamic Mechanical Properties	21
2.5 Stress relaxation	23

Chapter 3 - Materials, compounding and characterization

3.1 Materials	25
3.1.1 Rubbers.....	25
3.1.2 Fillers.....	26

3.1.3 Other chemicals	28
3.2 Compounding.....	28
3.2.1 Preparation of rubber and filler masterbatch	28
3.2.2 Compounding in Two roll mill	29
3.2.3 Heated press.....	29
3.2.4 Compounding formulations	30
3.3 Characterization	33
3.3.1 Vulcameter.....	33
3.3.2 Determination of crosslink density	33
3.3.3 Electrical conductivity	34
3.3.4 Simple uni-axial piezoresistance measurements.....	34
3.3.5 Hysteresis / Cyclic piezoresistance measurements	35
3.3.6 Electrical resistance coupled dynamic mechanical analysis.....	36
3.3.7 Stress relaxation fitting	38
Chapter 4 - Exploring the quasi-static piezoresistive behaviour of SSBR composites	
4.1 Introduction.....	41
4.2 Electrical conductivity of the composites	41
4.2.1 Influence of crosslink density on electrical conductivity	42
4.2.2 Influence of process oil on electrical conductivity	43
4.3 Uniaxial piezoresistivity	44
4.3.1 Influence of filler content	44
4.3.2 Strain sensitivity	46
4.4 Cyclic piezoresistivity.....	52
Chapter 5 - Exploring the piezoresistive properties of SSBR composites under dynamic conditions	
5.1 Introduction:.....	55
5.2 Introduction to dynamic tests.....	55
5.2.1 Difference in relaxation under static and dynamic conditions	57

5.2.2 Mean stress and mean electrical resistance	59
5.3 Time sweep measurements	60
5.3.1 Influence of the four major parameters (filler content, temperature, frequency and crosslink density) on mean resistance.....	60
5.3.2 Major parameters and electrical resistance amplitude	62
5.3.3 Analyzing the nature of the dynamic piezoresistive response	64
5.4 Dynamic temperature sweep measurements	67
5.4.1 Influence of major parameters on mean and dynamic resistance	67
5.4.2 Major parameters and second peaks	70
5.5 Dynamic strain sweep measurements	71
5.6 Hysteresis profiles under temperature sweep experiments	73
 Chapter 6 - Predicting the mechanical performance and filler network behaviour using dynamic piezoresistivity	
6.1 Introduction.....	75
6.2 Correlating stress and resistance relaxations	75
6.2.1 Different filler loading.....	76
6.2.2 Major parameters and stress relaxation behavior	78
6.2.3 Correlating the relaxation parameters.....	80
6.3 Evaluating the phase shifts (δ) between stress, strain, and resistance.....	81
6.3.1 Phase shift values during time sweep experiments.....	83
6.3.2 Phase shifts during temperature sweep experiments	86
6.4 Relation between second peaks and viscoelastic properties of the polymer.....	89
6.4.1 Time sweep measurements	89
6.4.2 Temperature sweep measurements	91
 Chapter 7 - Investigating the potentials of dynamic piezoresistivity for commercial applications	
7.1 Introduction.....	93
7.2 Piezoresistive behavior of SSBR with conventional carbon blacks.....	93

7.2.1 Time sweep.....	93
7.2.2 Temperature sweep.....	97
7.2.3 Strain sweep.....	98
7.2.4 Summary.....	98
7.3 Piezoresistive behavior of NR, BR, and SSBR with conducting carbon blacks	99
7.3.1 Time sweep measurements	99
7.3.2 Summary.....	101
7.4 Scope for further research	101
7.4.1 Possible extensions of the current work	101
7.4.2 Dynamic piezoresistive studies under compression force	102
7.4.3 Dynamic piezoresistive studies with graphene nanoplatelets and Ionic liquids	102
7.4.4 Studying carbon black and silica hybrid filler systems	103
7.4.5 Studying the interparticle distance using tunneling theory.....	103
Conclusions.....	105
References.....	109
List of figures.....	121
List of tables.....	125
Eidesstattliche Erklärung	126
List of publications	127
Bio data	130

Chapter 1

Introduction

1.1 General introductions

We live in an era where a variety of materials are being used which would not have been thought of in the earlier ages. They range from glass, ceramics, polymers, and their combinations known as ‘composites’. Out of the many materials known, one important discovery is rubbers. Columbus discovered natural rubber during one of his expeditions. A lot of further developments in the field of rubbers happened during the World War II. As of today, many synthetic rubbers have been invented to meet the current needs and demands. Nowadays synthetic rubbers supersede natural rubber in terms of economic viability.

Rubbers are in general well known for their outstanding electrical insulation. However, many attempts have been made to make rubbers electrically conductive. Metals and various carbon allotropes are incorporated into the rubber to improve their thermal and electrical conductivity [1-3]. With the advent of novel carbonaceous materials such as carbon nanotubes, graphenes, etc., the number of research works on conductive rubber composites has increased tremendously [4].

Developing conductive elastomeric materials with desirable mechanical as well as electric properties is always a challenge. As the outcome, plenty of reports can be found [5-8]. Several strategies are followed to develop such materials, which take into account, for example, design concepts (insertion of fine metal wires) [9], synthesis of conducting polymers [10] and incorporation of carbon-based conducting solid particles [11, 12] and metals [13] into polymers. In general, the conducting properties of a composite is governed by the intrinsic conductivity of the incorporated filler particles, as well as, their dispersion *i.e.*, a well-percolated network [14, 15]. It is believed that a very well-established strong filler-filler network of conducting particles in the polymer matrix would improve the electrical conductivity of the resulting composite.

One of the main ideas behind the development of such electrically conducting rubbers is to use them as sensors. There are a plenty of reports on conducting elastomer based

sensors for strain [16], solvent [17], and vapor [18] sensing. These materials are known to cater a variety of applications ranging from simple solvent and vapor leakage detection (also called as polymeric nose and tongue) [19], to mechanical structure failure [20] and even complex health monitoring (also called as polymeric skin) [21]. However, such materials have not yet been realized for real-time use. There are a few challenges one must overcome before assuring the commercial applicability of such flexible rubber-based sensors.

1.2 Challenges

Flexible rubber-based conductors are still a challenging subject with vast research capabilities [4, 22, 23]. Many works report the changes in the electrical conductivity of such flexible conductive rubbers depending on the strain, temperature, surrounding atmospheric conditions, etc. [24-27]. [Figure 1.1](#) depicts the loss in electrical conductivity of different rubber based conducting materials when exposed to strain, temperature, and solvents. Hence, there are hardly any reports on common commercially produced rubber products with high electrical conducting properties.

Most of the conductive elastomeric materials have a strong drawback with their strain dependent electrical conductivities *i.e.* the materials exhibit a piezoresistive characteristic, where the electrical conductivity is sharply affected by strain [28]. The piezoresistive behavior in rubber is very sensitive to the filler network dynamics during cyclic or repeated loading. After several cycles, the piezoresistive response could be altered due to rearrangement of the filler network inside the soft rubber. [Figure 1.2](#) shows the inability of CNT and CB filled NR composites to yield stable piezoresistive response under a controlled cyclic hysteresis experiment. The resistance values were found to either increase or decrease after a few strain cycles. Therefore, for practical applications, a detailed understanding of the material behavior with respect to different parameters like crosslinking degree, nature of the filler, aspect ratio of the filler, material stiffness and extensibility is required.

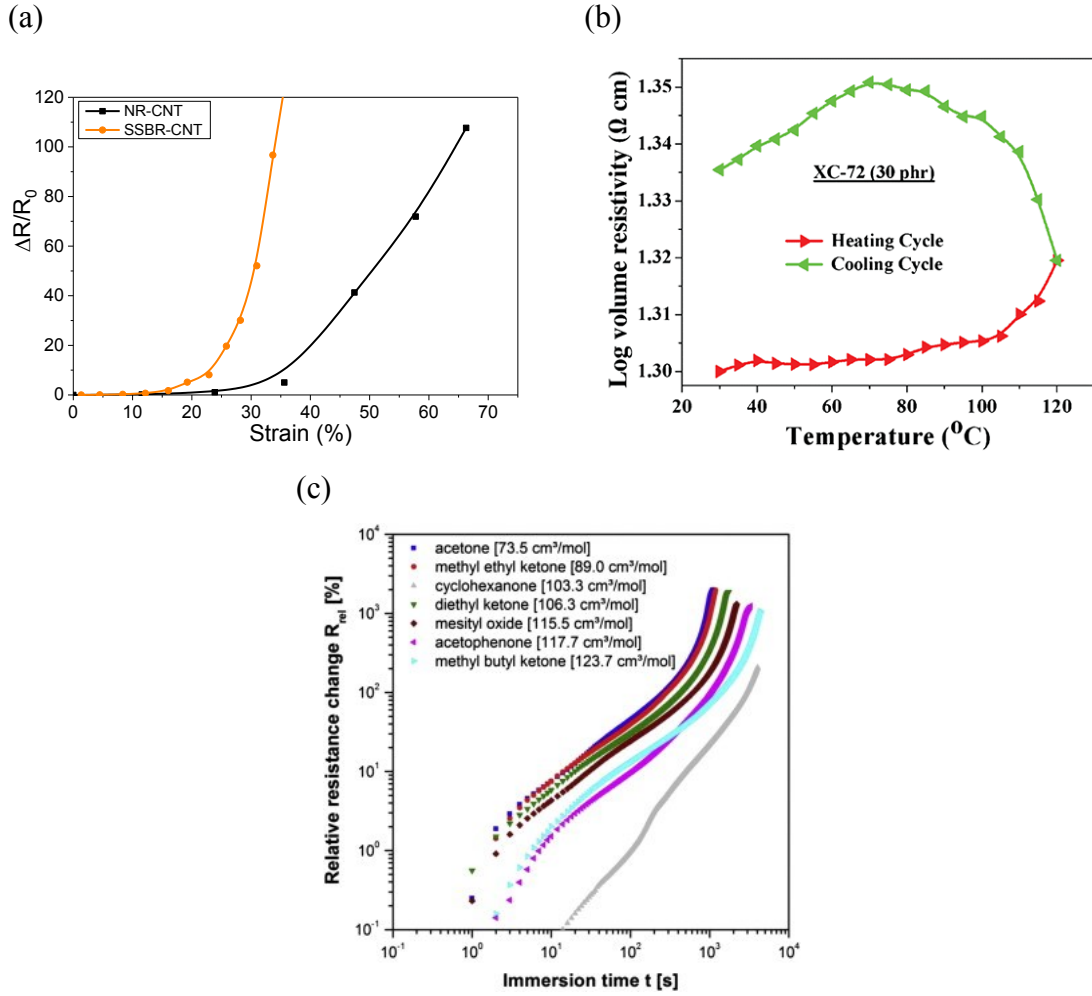


Figure 1.1: (a) Change in electrical resistance of CNT filled NR and SBR samples upon mechanical stretching [29]. (b) Change in electrical resistance of carbon black filled silicone rubber samples at different temperatures[30](Reproduced with permissions from John Wiley and Sons). (c) Change in electrical resistance of CNT filled polycarbonate samples upon exposure to various solvents [31] (Reproduced with permissions from Elsevier).

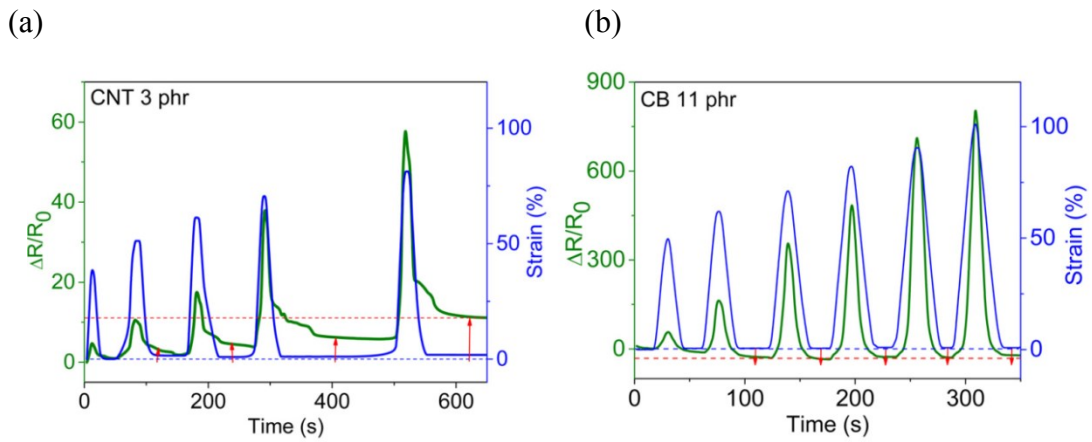


Figure 1.2: Electrically conducting NR samples filled with (a) CNT and (b) CB samples to yield non-reliable electrical hysteresis behavior under cyclic loading [32]

In repeated loading situations, *e.g.* flexible robotic arms joints, artificial skin, etc., the polymer material could be subjected to a defined loading pattern or also indefinite loads at undefined intervals. For such cases, a much more predictable material performance and piezoresistivity behavior are necessary. Moreover, in course of cyclic piezoresistive experiments, an atypical second resistance response (Figure 1.3) is observed since 1986 [33] until today [34]. Very few publications could be found that report and discuss this anomaly [33-38]. A clear explanation concerning the behavior of such second piezoresistive response is however still lacking.

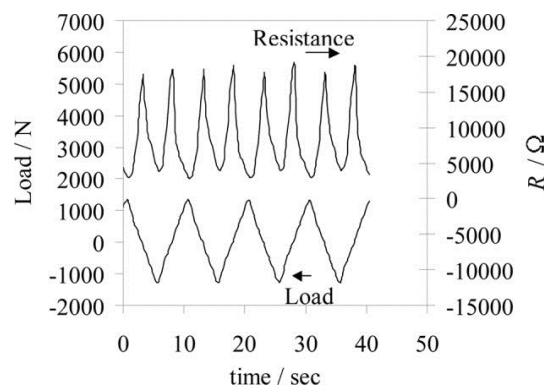


Figure 1.3: Appearance of second piezoresistive response in course of cyclic loading experiment [37] (Reproduced with permissions from John Wiley and Sons).

1.3 Motivation

Tire manufacturers are convinced that we are running to a point where deep innovation in rubber compound as well in complete tire design is needed for the next generation. There are some publications concerning this issue like the analysis of strain on a tire tread during movement of the vehicle [9, 39]. There are also few reports about the strain sensing of tires using different methods like flexible metal wires [9], commercial strain gauges [40], capacitance based micro-patterning of metal by photolithography [41] etc. These types of sensors represent challenges in tire application due to their differences in stiffness. Therefore, instead of physically mounting a foreign material into the tire, it would be ideal if, the tire itself comes with damage sensing abilities or develop strain sensors with rubbers used in tires so that analogous properties could be achieved.

Especially for the latter case, one has to develop a system where the stiffness and dynamic modulus of the rubber-based strain sensors are similar to the tire rubber component to achieve a stable and robust performance. Commercial passenger car tire treads comprise mostly of styrene butadiene rubber (SBR) and butadiene rubbers (BR). However, in-depth research on SBR based strain sensors is scarce. In practical situations, tires are subjected to high frequencies for long durations, where they undergo intense dynamic deformation and scientific works on strain sensing, catering for such dynamic applications are none. Literary works could be found either on quasi-static cyclic tests with rubbers or dynamic piezoresistive properties of rigid thermoset materials. No works could be found that focuses on understanding the dynamic piezoresistive performance of rubber composites. Much deeper insights are therefore necessary to understand the dynamic piezoresistivity of conductive rubber composites in order to realize their use as sensors.

1.4 Goal

Inspired by the aforementioned challenges, the dynamic piezoresistivity behavior of conductive composites prepared from a commercial grade of SSBR is studied. This would help to understand the material's behavior under dynamic conditions and in-turn help in developing dynamic strain sensors. To initially assess the piezoresistive capabilities of SBR composites, simple uni-axial piezoresistive tests are performed. Later, the dynamic piezoresistive performance of the same material is studied in a dynamic mechanical analyzer (DMA). In general, DMA's are used to mimic the load conditions experienced by a tire rubber. So, this basic scientific study on dynamic piezoresistivity would be the stepping stone for developing rubber-based sensors in the future, that would be capable of performing under dynamic conditions.

As rubber is an insulating medium, the changes in electrical conductivity are purely driven by the filler network. So, the observed piezoresistive effect arises mainly due to the changes in the filler network inside the rubber matrix. Therefore, this method would additionally offer a new possibility to visualize filler networking and filler cluster changes during dynamic mechanical deformations.

1.5 Structure of the thesis

In Chapter 1, a general introduction is given with the persistent challenges that exist in the field of piezoresistive materials. The motivation and the prime goals of the work are highlighted.

Chapter 2 provides a detailed literature analysis about the evolution and development of conducting rubbers. The percolation theory is discussed with its relevance on conducting rubber composites. The concept of piezoresistivity pertaining to rubber composites is explained along with the challenges and hurdles in understanding the dynamic piezoresistance in details.

Chapter 3 describes in detail about the materials used in this study, the compound formulations, the sample preparation techniques and also the various characterization techniques that were employed.

In Chapter 4, basic piezoresistive characteristics of composite prepared with SSBR (an important rubber used in tire production) are studied in detail, as the first step in understanding their piezoresistive behavior. For this purpose, SSBR was filled with a special commercially available carbon black having exceptional electrical conductivity and with multiwall carbon nanotubes. Parameters such as filler content, crosslink density and material stiffness that mainly influence the piezoresistive effect are investigated. In an attempt to realize them as potential strain sensors, the sensitivity of the materials is calculated in the most sensitive regime and simple mathematical equations are fitted to compare their performances. Finally, the behavior of these materials is assessed under a cyclic load.

In Chapter 5, an attempt has been made to understand the relationship between dynamic mechanical properties and electrical behavior of conductive SSBR composites. In a dynamic mechanical analyzer, the sinusoidal strain was applied and the stress, as well as the temporal changes in electrical resistance, was monitored simultaneously. Critical parameters such as filler content, dynamic frequency, temperature and matrix crosslink density were varied. The findings were also helpful in visualizing the behavior of filler network and their influence over the material's

dynamic performance. These experiments are found to be helpful to understand the behavior of rubber products that are constantly experiencing dynamic forces such as tires, conveyor belts, dynamic seals, shafts, dampers, etc.

In Chapter 6, efforts are given to correlate the mechanical stress relaxation with the electrical resistance, thereby; a governing relationship between the same could be established. This allows the prediction of the mechanical performance from the electrical resistance data or vice versa. The prime motive of such a study is its realization real-time, wherein the mechanical stress relaxation in a rubber product could be estimated during its service. A characteristic piezoresistive phase shift between mechanical stress and electrical resistance ($\delta_{\sigma-R}$) is deduced from the dynamic piezoresistance studies. The second peaks that are observed during unloading are studied in details and their kinetics is evaluated with respect to time and temperature by analyzing the intensities of the first and second peaks.

In Chapter 7, the dynamic piezoresistivity is tested for SSBR filled with conventional fillers N220, N330, and N660, in order to check the relevance of the developed concept for commercial rubber products. Additionally, two other rubbers that are generally used in the tire industry, namely NR and BR are filled with conductive carbon black and assessed for their dynamic piezoresistive capabilities. At last, a few interesting studies that can be extended from the current work are highlighted with examples.

Chapter 2

Literature Survey

2.1 Conducting rubbers

Since many years attempts are being continuously made to produce electrically conductive rubbers. The first patent was filed by Trueman in 1882 [42]. Successive works have been reported from many countries, e.g. Bormann [43] from Germany, Granier from France [44], the Continental AG group in Germany [45], Dunlop from England [15] and many cable industries [46-48]. **Table 2.1** summarizes a few of the very first attempts to produce conductive rubber. The primary motive as per **Table 2.1** was to develop rubbers capable of dissipating static electricity. Graphite, oil black, and acetylene black were used in large quantities to achieve the desired electrical conductivity [15]. The electrical conductivity inside the rubber matrix is assumed to occur through the filler, *i.e.* the carbon black, which forms a network throughout the rubber matrix [49]. It is interesting to note from the table that the first patent for developing conducting tires was filed in the year 1940 [50]. Therefore, since then attempts are being made to commercially produce electrically conductive tires.

Table 2.1: Few initial works on the development of conductive rubber

Patent year	Company / person	Targeted application	Filler type	
1882	E. Trueman		Graphite	[42]
1909	Bourne	Electrodeposition	Gas carbon, etc.	
1925	Nederlandsche Technische Handel Maatschappij	Carrying currents	Graphite, Carbon, metals in powder form	[51]
1933	Hollandsche Draad- en Kabelfabriek N.V.	Anti-corona shields for cables	Graphite	[52]
1937	Boggs and Simplex Wire & Cable Co.			[53]
1937	Continental Gummiwerke A. G.	Conducting carding	Graphite	[54]
1937	Goodrich Rubber Co.	Composite extensible sheet for deicing. etc.	Graphite	[55]
1940	U. S. Rubber Co.	Conductive tires	Acetylene (cement)	[50]
1941	Thomas and Hutchinson Instrument Co.	Electrodeposition	Carbon and colloidal metals	[56]

Following the boom in carbon black manufacturing and development, different grades of carbon black were introduced into the market and Abdel-Bary *et.al.* [57] reported the influence of various types of carbon blacks, namely intermediate super abrasive

furnace (ISAF), high abrasion furnace (HAF), fast extrusion furnace (FEF) and general-purpose furnace (GPF), on the electrical conductivity of SBR rubber. In his study, carbon blacks were used in different quantities and the optimal amount of carbon black required to achieve electrical conductivity was determined from experimental trial and errors. Li *et.al.* [58] studied the influence of different grades of conventional carbon blacks (N330, N472, N550, N770, and SCB) on various properties of EPDM composites. The electrical conductivity measurements highlighted the influence of surface area on the final conductivity of the derived composites. Higher surface area blacks are in general found to offer better conductivity to the composites. However, the surface area is one important criterion for choosing the conducting filler but is not the sole parameter for electrical conductivity of the composite.

Later on, special grades of carbon black with high electrical conductivity were developed and many works report outstanding electrical performance of composites developed from such specialty carbon blacks [59]. With the advent of novel fillers like carbon nanotube [60], graphene [61], etc., and exploiting the advancements in rubber technology, developments in the field of electrically conducting rubber composites are enormous [62-67]. It was even attempted to produce conducting rubber composites utilizing various metals, metal oxides, and ceramics as fillers [21, 67-72]. Efforts have been made to produce sophisticated rubber based products with high electrical conductivity over the recent years for various applications such as artificial muscles [73-76], smart clothing and electronic textiles [77-81], artificial skins [70, 82-84], paper electronics [81, 85-87], prosthetic limbs [88, 89], biomedical devices [72, 90, 91], electronic eyes [92], soft and humanoid robots [93-96], and flexible and stretchable electronics [22, 97-100] such as transistors [101, 102] and optoelectronic devices [103-106]. Considering the requisites of certain applications, rubber based conducting materials are the only option that would meet the stringent of demands. For example, in manufacturing low cost soft robotic components like robust stretchable electrodes, flexible interconnections, etc., the electrical conductivity should be retained even at high strains. Conducting rubber composites are the only class of materials that could fulfill these demands [107].

2.2 Percolation network of fillers

Rubbers could be made electrically conductive only if the amount of conducting fillers inside the rubber matrix exceeds a certain critical concentration. The critical concentration required to make the (insulating) rubber electrically conductive were used to be determined by random experimental methods, until the percolation theory was developed. Once the amount of filler exceeds this critical concentration, a remarkable increase in electrical conductivity (several orders of increase in electrical conductivity) is observed. As per the theory, at this critical point, at least one electrically conductive filler pathway is assumed to have formed inside the rubber matrix. The phenomenon of electrical conductivity in an electrically conductive polymer composite could be explained and modeled using the percolation concepts.

The first percolation theory was proposed by Hammersly and Broadbent in 1957 [108]. Later in 1979, Stauffer developed the percolation theory using an array of squares, wherein, the term ‘Percolation threshold’ was introduced to define the minimum concentration required to successfully achieve clustering inside the lattice [109]. Later on, many conductivity models have been developed to evaluate the percolation concentration of conductive fillers for a polymer composite. The models are generally classified into four main classes based on their approach: (i) statistical, (ii) geometrical, (iii) structural, and (iv) thermodynamic methods [14]. Statistical models are most frequently found in the literature. It depicts the conductivity of the composite based on the probability of physical particle contacts in the given system. The most well-known model being reported for percolation theory is developed by Kirkpatrick [110] and Zallen [111]. Based on the volume fraction of the conducting filler, computer-based simulations could yield the concentration of fillers necessary to percolate in the rubber matrix. The power law equation proposed by Kirkpatrick and Zallen is:

$$\sigma' = (P - P_c)^t \quad \text{Eq 2.1}$$

Where σ' is the electrical conductivity (S/m), P is the volume fraction of conducting fillers, P_c is the percolation concentration (also known as the critical concentration of fillers to achieve electrical conductivity) and t is the critical exponent that defines the

(geometrical) state of the percolated network. Eq 2.1 is a very basic model used to predict the percolation threshold of conductive composites. The background of percolation phenomenon could be visualized with the following simple example in Figure 2.1:

(i) At low concentration of conducting fillers (Region A in Figure 2.1), the conductive particles are scattered randomly inside the rubber matrix, mostly isolated and could also be enveloped by the insulating rubber matrix. This would result in less improvement in electrical conductivity, or the electrical conductivity of the composite would be similar to the rubber matrix.

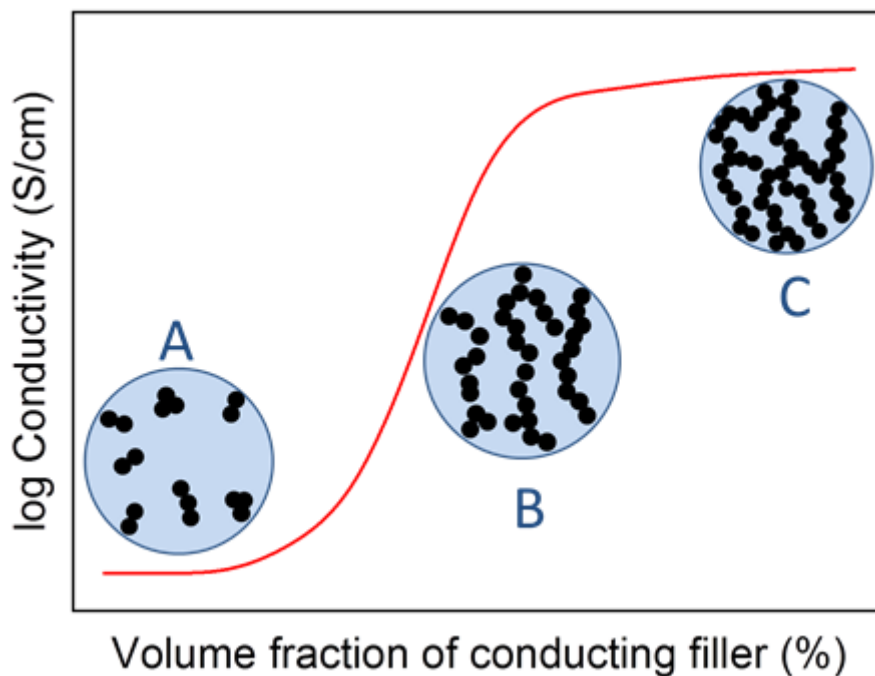


Figure 2.1: Schematic representation of the dependence of electrical conductivity on filler volume fraction.

(ii) As more conducting particles are added into the rubber (Region B in Figure 2.1), the conducting particles start to form a network spanning through the rubber matrix, gradually transforming the insulating composite to a conductive composite. The filler concentration in this region is known as percolation concentration or critical concentration, where a drastic increment in electrical conductivity occurs.

(iii) When more conducting filler particles (higher than the percolation value) are incorporated into the rubber matrix (Region C in Figure 2.1), the percolated network becomes dense. Whereas, the conductivity of the rubber composite increases at a slower rate.

Many experimental studies reported a wide range of t value (critical exponent in Eq 2.1) from 1 to 12 [112, 113]. Agglomeration of conducting fillers inside the rubber could result in a lower t value [26]. In the case of graphene (two-dimensional filler), the t value could be below 1.3, implying a 2D percolated structure [114]. CNT (one-dimensional high aspect ratio filler) displayed higher t values of over 2.0, indicating a 3D conductive percolated network [115, 116]. Kirkpatrick reported $t \sim 1.6$ in his work [110] and many works on CNT polymer composites report an average value of $t \sim 1.8$. The value of t is mostly independent of the nature of fillers [117] and depends only on the dimensionality of the system [118]. Theory calculation shows that $t \sim 1.0 - 1.3$ denote a 2D filler network and $t \sim 2.0$ correspond to the formation of 3D filler network [4].

Several factors affect the percolation concentration and restrict the maximum achievable conductivity. The percolation threshold depends on various criteria, such as shape and size of the conductive filler (*i.e.* aspect ratio), and mainly on the state of dispersion and distribution [26, 27, 119]. In general, the conducting properties of the composites are governed by the intrinsic conducting nature of the filler particles, as well as, the state of the percolated network [15, 26].

2.2.1 Influence of Filler aspect ratio on the percolation threshold

For spherical particles, the aspect ratio is 1 ($L/D = 1$) and therefore, a much higher filler concentration is necessary to form a percolated network in the rubber [120]. In the case of fillers like carbon fibers, or carbon nanotubes, which are tubular or rod-like shaped, they have a much higher aspect ratio ($L/D > 100$). In these cases, a percolated conducting network is formed in the rubber at much lower concentrations [113]. Also, according to the percolation theory, the percolation threshold decreases with an increase in the aspect ratio of the conductive fillers. In situations where the

electrical conductivity should be achieved without affecting the properties of the polymer matrix, high-aspect-ratio fillers such as CNT, carbon nanofiber, silver nanowire, and graphene are preferred [4].

Bauhofer *et.al.* [113] summarized the percolation thresholds and the maximum conductivities achieved for various CNT filled polymers. The lowest percolation concentration was 0.0021 wt.% for an Epoxy / MWCNT composite and the MWCNT had an aspect ratio of 200. They reported MWCNT filled VMQ composite with a percolation concentration of 2.4 wt.%, where the CNT had an aspect ratio of 500. Moreover, the high-aspect-ratio conducting fillers always resulted in a higher conductivity. Natarajan *et.al.* [32] reported NR composites with percolation thresholds of ~ 10.5 phr and ~ 2.7 phr for highly conducting carbon black and MWCNT respectively in Figure 2.2a. The higher aspect ratio of CNT is therefore found to offer higher electrical conductivity at much lower volume fractions.

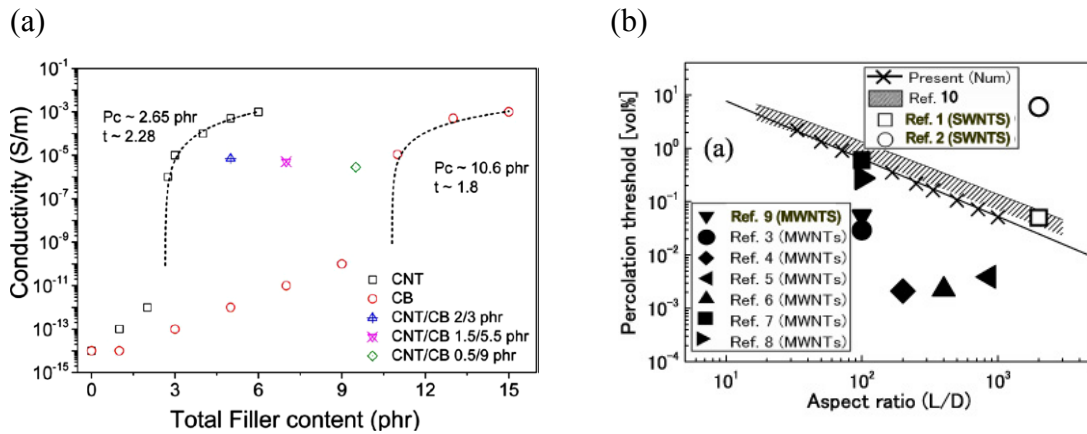


Figure 2.2: (a) Influence of filler aspect ratio on electrical conductivity [32] [reproduced with permissions from ACS] and (b) Influence of CNT aspect ratio on the percolation threshold [117] [reproduced with permissions from IOP Science]

Subramaniam *et.al.* [11] observed a percolation threshold of ~ 2 phr for MWCNT in their CR/Ionic liquid composites. Hu *et.al.* [117] used an empirical model to predict the percolation threshold of the fillers in Figure 2.2b. $P_c = (L/D)^{-1.1 \pm 0.03}$, in which L and D represent the length and diameter of the incorporated filler particles. Lower P_c values are observed for composites containing graphene or functionalized graphene sheets (1-dimensional fillers), as well as for CNTs (2-dimensional filler). In the case of spherical fillers such as carbon blacks or metal particles, the P_c is higher.

2.2.2 Influence of Filler dispersion and Morphology

Filler dispersion plays a major role in determining the final conductivity of the rubber composites. A poor dispersion would result in higher agglomeration and therefore yield in less network formation and reduced conductivity. An ideal dispersion on the other hand (in which all the filler particles are covered by a rubber layer) would also result in poor or no conductivity [49]. Finer carbon blacks are known to increase the probability of network formation in the rubber matrix and result in higher electrical conductivity [49].

Moreover, high-aspect-ratio conductive fillers easily aggregate and filler aggregation restricts the maximum achievable electrical conductivity. This has always been a problem while producing such conducting rubber composites. Mierczynska *et.al.* [121] observed composites of SWCNT with a high degree of agglomeration being less conductive than the well dispersed MWCNT samples. Effective dispersion is, therefore, necessary to achieve high conductivity in high-aspect-ratio conducting fillers while fabricating conductive rubber composites. To overcome this issue various strategies were often employed to achieve good dispersion of conducting nanofillers. For example, modification of the filler surface, utilizing different processing techniques, adapting different methods in filler incorporation, and preconditioning the fillers before incorporation into the rubbers [122-126].

In order to achieve a finer dispersion and reduce the percolation threshold, composite processing is being approached with several techniques. Zhan *et.al.* [127] have reported that NR composites prepared by compounding in the latex stage displayed higher electrical conductivity (~5 orders) in comparison to conventional mixing methods (Figure 2.3a). The latex processing is expected to offer much finer dispersion of the graphene in the rubber matrix after vulcanization. Bokobza *et.al.* [128] utilized carbon black and CNT simultaneously in a SSBR matrix and observed that double loading of fillers improved the dispersion of CNT. Higher electrical conductivity and lower percolation threshold values evidenced a better dispersion of the CNT. Das *et.al.* [129] utilized a pre-dispersion of CNT in ethanol and ultra-sonicated the mixture. Due to its high aspect ratio, the CNT is in a highly entangled state and is said to be one of the major issues affecting the dispersion. By this pre-dispersion process,

the CNT is expected to de-entangle. The pre-dispersed CNT mixture is then mixed with the rubber to achieve an even dispersion and distribution of the conducting filler. From Figure 2.3b, it could be noted that in comparison to the conventional mixing process, the pre-dispersed CNT offered much higher electrical conductivity and lower percolation threshold. Sau *et.al.* [130] demonstrated the benefits of blending two rubber systems in order to achieve higher electrical conductivity. In comparison to carbon black filled EPDM and NBR composites, the 50/50 blend of these two rubbers proved to be effective by displaying a higher electrical conductivity.

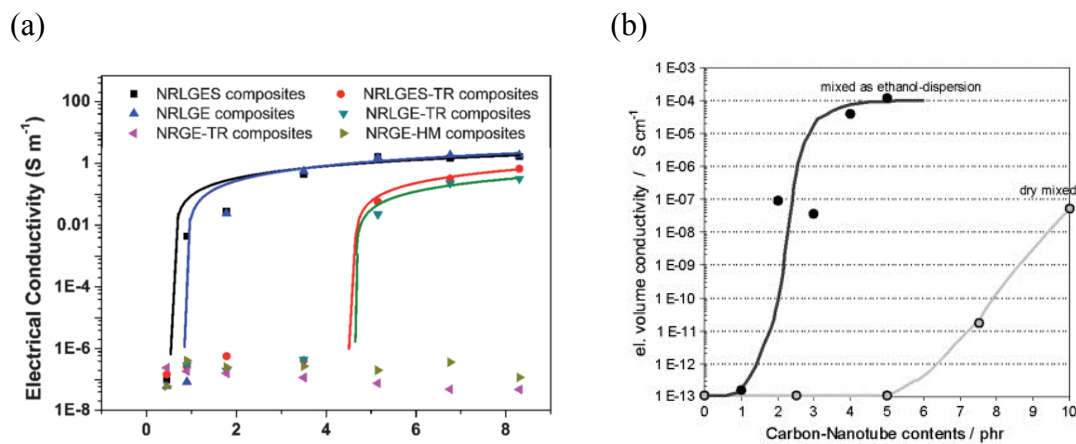


Figure 2.3: Effect of filler dispersion (a) Improvement in electrical conductivity due to latex mixing [127] (Reproduced with permissions from Royal Society of Chemistry). (b) Improvement in electrical conductivity due to pre-dispersion of CNT in ethanol [129] (Reproduced with permissions from Elsevier).

2.3 Piezoresistivity

“Piezoresistivity is defined as the change in resistance of semiconductors or metals from an applied mechanical stress”[131]. The discovery of piezoresistance dates back to the late nineteenth century (1856) when Lord Kelvin observed changes in resistance in copper and iron wires. He found different ‘changes in resistance’ for the two materials, while elongation remained the same [132]. The term “piezoresistance” was coined by Cookson in 1935 when he defined the term as the change in conductivity with stress [133]. The term “piezo” is rooted from the term “πιέζειν” from the Greek, meaning ‘to press’.

In rubber composites, however, the phenomenon relies on the change in the interparticle distances between conducting fillers and due to the disruption of the percolated filler network during mechanical deformation. When an external strain is applied, it directly affects the physical contact and/or the tunneling gap between the conducting fillers, causing a change in the electrical conductivity of the composite [26]. The tunneling model [112, 134] that defines the electrical resistance of a composite based on interparticle distance is given in Eq 2.2 and Eq 2.3

$$R = \frac{L}{N} \cdot \frac{8hs}{3a^2\gamma e^2} \cdot e^{\gamma s} \quad \text{Eq 2.2}$$

$$\gamma = \frac{4\pi}{h} \sqrt{2m\phi} \quad \text{Eq 2.3}$$

Where R is the electrical resistance of the nanocomposite, L is the number of particles forming a single conductive pathway, N is the number of conductive pathways, h is the Plank constant, s is the interparticle distance between conductive fillers, a^2 is the effective cross-section where tunneling occurs, e and m are the charge and mass of electron, and ϕ is the height of the potential barrier between adjacent particles. Eq 2.2 in simple terms is often expressed as $R \propto s$.

$$\frac{R}{R_o} = \frac{N_o}{N} \cdot \frac{s}{s_o} \cdot e^{\gamma(s-s_o)} \quad \text{Eq. 2.4}$$

When the material is stretched, the filler particles are separated and could lead to an increase in the interparticle distance or even breakdown of the conductive paths at much larger strains. Assuming the initial resistance of the material as R_o before stretching, the mechanical strain would increase the resistance to a higher value R . This change results from the increase in distance interparticle distance from s_o to s and the loss in numbers of conductive paths from N_o to N [13, 135]. The relative resistance is depicted in Eq 2.4.

2.3.1 Simple uni-axial piezoresistivity

The concept of piezoresistance in rubbers was first observed by Bulgin [15] who used various rubbers and carbon blacks and observed a loss in electrical conductivity during mechanical stretching. Later on, several works too reported the loss in electrical conductivity when conducting rubber samples were subjected to uniaxial tension or compressive forces [25, 27, 136-140]. Many works then followed to address this issue, where the unique behavior was analyzed and studied in detail. The effect was then named piezoresistivity and was tested with different combinations of rubbers, fillers, etc. These works serve as the base to understand the concept of piezoresistivity in rubbers, which then led to the development of a variety of applications. One such development is sensing (e.g. strain, damage monitoring, solvent, vapors, etc.).

Several works could be found that exploits the piezoresistive nature of various rubbers and fillers, thereby utilizing them for strain sensing applications [140-145]. Piezoresistance based strain sensing reports, in general, are often based on tensile or compression tests, where the mechanical deformation and electrical resistance are correlated [146-148]. Natarajan *et.al.* [29, 32] reported NR based composites with carbon black and CNT that displayed piezoresistive capabilities. The concept of piezoresistivity was utilized to develop strain sensors that could be used for different applications requiring different strain sensitivities. Their materials show linear as well as nonlinear dependencies for the applied strain. Tadakaluru *et.al.* [149] reported CNT and graphite film-based NR sensors with high sensitivity and high range strain sensing (up to 620%) with high durability. These high-strain sensors were targeted to be used as multifunctional sensors for force, speed, pressure, acceleration, frequency, structural vibrations, earthquakes or in health monitoring. Bifulco *et.al.* [150] fabricated simple conducting rubber sensors to record muscle contraction. Their new sensor does not require any preparation of patient's skin and can be comfortably worn as an elastic cuff.

Lin *et.al.* [151] meticulously designed a blend system of NR/SBR wherein, during fabrication in the latex stage, modified graphene is selectively targeted to bond with the NR particles as shown in [Figure 2.4](#). Upon vulcanization, the graphene particles

are found mostly in the NR phase. By this approach, the percolation concentration was reduced by 1/10 in comparison to conventional mixing technique and the sensitivity and stretchability of the finally fabricated sensors increased significantly. Yamada *et.al.* [152] developed silicone rubber-based CNT strain sensors for detecting human body movements. Unlike conventional rubber mixing, in this case, the CNT films were carefully aligned on a substrate and then coated with silicone rubber. The sensitivity and durability of these sensors are very good. However, this is a very tedious process for sensor fabrication. Kim *et.al.* [153] reported a very cost-effective technique to manufacture rubber-based strain sensors with exceptional biocompatibility, durability (10,000 cycles), and sensitivity. The cost-effectiveness of the process resulted in manufacturing sensors for \$1~\$5/gram. The application is targeted for the biomedical sector as wearable electronics.

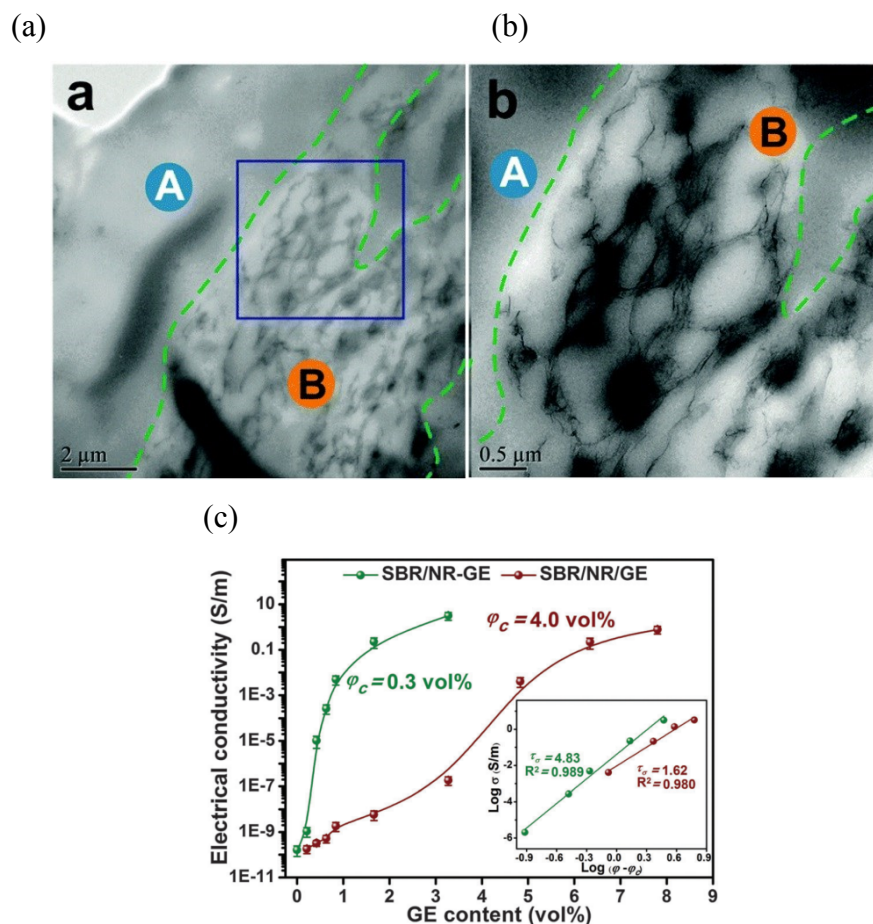


Figure 2.4 : (a) Concentration of CNT within the NR phase and (b) magnified image as highlighted by a blue box. (c) Reduction in the percolation concentration of graphene. [All images are reproduced from [151] with permissions from Royal Society of Chemistry].

It has been observed that a well-established strong filler-filler network would improve the electrical behavior of the composites. A loose and weak percolated network of conducting particles inside flexible elastomers can be permanently destroyed during dynamic operations, resulting in an irreversible change in the electrical conductivity. Therefore, for high durability, a permanent or stable conducting network is expected for use in cyclic or continuous loading situations. Kost *et.al.* [33] reported the cyclic piezoresistive behavior of silicone rubber filled with a highly conductive carbon black (AkzoNobel, Ketjenblack) for up to 80 % strain. The rubber composites displayed a certain irrecoverable resistance (resistance set) at high strains. Moreover, for each strain cycle, two resistance responses were noticed, which depends mainly on the strain amplitude. Ciselli *et.al.* [38] performed cyclic experiments on EPDM/CNT composites. For the applied constant cyclic strain, two responses were observed in the resistance signal. The first resistance change peaks correspond to the increase in strain and the second resistance change peaks correspond to the unloading or while de-straining the sample. This atypical second peak became stronger and prominent with time after more test cycles.

2.3.2 Piezoresistivity under dynamic conditions

Dynamic piezoresistivity experiments are similar to cyclic piezoresistance tests, whereas the test frequencies here are much higher and the loading conditions are complex. The changes in resistance are monitored and studied over a continuous sinusoidal dynamic pulse. Very few works have attempted to study the dynamic piezoresistive effect in polymers.

Voet *et.al.* [154] performed dynamic strain sweep experiments on SBR and SBR/BR blends. The resistance patterns were sinusoidal in accordance with the applied stress, wherein during loading (stretching), a proportionate increase in electrical resistance was observed and upon unloading the resistance decreased. However, at higher deformation amplitudes, second resistance responses were noticed during the unloading cycles. The effect was reasoned to be due to the high interactions between the carbon black fillers, and the breakdown and reformation process lead to the formation of aligned transient filler network. The double conductivity amplitude and

the phase angle between the applied strain and observed resistance were calculated using an oscilloscope. Anand *et.al.* [155] performed dynamic studies on Epoxy/CNT composites, where the dynamic load was given to the epoxy stripes by fixing them on the piezo-ceramic substrate. By increasing the excitation voltage of the substrate, a maximum frequency of up to 500 Hz was achieved. The relative resistance change was found to be high with higher dynamic strains and higher test frequencies. Vega *et.al.* [27] attempted to study the phase shifts between stress, strain, and resistance on epoxy-based polymer composites. In their study, the measurement frequency and temperature were varied between 0.05 Hz to 1 Hz and 20 °C to 200 °C respectively. The phase shifts between strain and resistance were evaluated and studied for its relation to the viscoelastic behavior of the matrix. The above works are encouraging, but the main drawback is the loading scenario, as Vega *et.al.* [27] reported relatively higher strain but at frequencies $< 1\text{ Hz}$ and Anand *et.al.* [155] reported results for higher frequencies up to 500 Hz, but the strain was very low (max. 30% μ -strain). Owing to the stiffness of the epoxy matrix, the applied strain in both cases is very less (μ -strain range) and the main principle for the change in resistance in such cases relay on the tunneling mechanism.

Therefore, the explanations from the hard epoxy resins cannot be used to describe the piezoresistivity in rubbers under dynamic conditions. Also, the experimental conditions should mimic the continuous high strain and high-frequency loading situations experienced by dynamic rubber products. Such experiments must, therefore, be carried out in sophisticated dynamic mechanical analyzers. Moreover, during such cyclic experiments, atypical secondary responses are observed in rubbers and only a few papers report on the atypical second electrical resistance response [35-38]. Clear explanations and the behavior of such secondary piezoresistive response are lacking and deeper insights are necessary to understand the dynamic piezoresistivity of conductive rubber composite systems.

2.4 Dynamic Mechanical Properties

Rubbers are viscoelastic in nature and therefore when they are subjected to mechanical deformation, there are always two different responses from the rubbers

pertaining to their viscous and elastic nature, respectively. The two responses can be clearly distinguished and analyzed using dynamic mechanical spectroscopy. From such measurement, a complex modulus (E^*) is obtained, which is a combination of the storage modulus (E' , real part) and the loss modulus (E'' , imaginary part)[156]. Figure 2.5a schematically depicts the two different moduli and the loss factor ($\tan \delta$) which is derived from the shift in phase angle (δ) or the time lag between the applied dynamic stress and the obtained dynamic strain. Eq 2.5 defines the complex dynamic modulus E^* and Eq 2.6 defines the damping factor $\tan \delta$ in relation to the loss and storage moduli.

$$E^*(t) = |E^*| e^{i\delta} = |E^*| \cos \delta + i |E^*| \sin \delta = E' + iE'' \quad \text{Eq.2.5}$$

$$\text{Loss factor} = E'' / E' = |E^*| \sin \delta / |E^*| \cos \delta = \tan \delta \quad \text{Eq.2.6}$$

Figure 2.5b illustrates the dependence of elastic and viscous moduli over temperature for a SSBR compound. It could be noted from the figure that the $\tan \delta$ also varies with temperature and the value $\tan \delta_{\max}$ denotes the glass transition temperature (T_g) of the material [156]. Dynamic mechanical studies are therefore not only useful in characterizing the viscoelastic properties of a material but also, they yield information regarding the glass transition temperature.

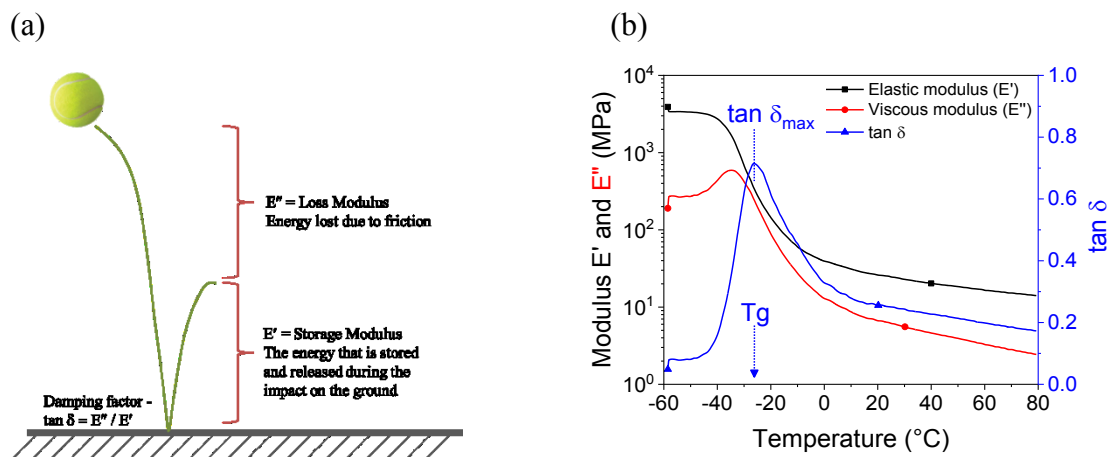


Figure 2.5: (a) Schematic representation of storage modulus (E') and loss modulus (E'') and (b) an example temperature sweep curve of unfilled SSBR

2.5 Stress relaxation

Another very common effect seen in rubbers due to their inherent viscoelastic nature is the stress relaxation [157]. When rubbers are subjected to a constant long time deformation as shown in Figure 2.6a, for *e.g.* in sealing applications, where they are pressed between two structures; the sealing force is very high initially, but over time, the material relaxes and the sealing force decreases leading the rubber component to fail. This is mainly due to the viscoelastic nature of the material.

Many physical models are available that defines the stress relaxation behavior of rubbers using spring and dashpot elements. The spring represents the elastic nature, while the dashpot represents the viscous nature of the material. One of the popular models that can perfectly define the stress relaxation in rubbers is the Maxwell-Wiechert model shown in the inset of Figure 2.6b, comprising combinations of several springs and dashpot elements [158]. Eq 2.7 represents the stress relaxation and Figure 2.6b depicts the significance of the terms in the equation in an example relaxation curve.

$$\sigma = \sigma_R + \sum_{n=0}^k \sigma_n e^{-t/\tau_n} \quad \text{Eq. 2.7}$$

Where σ_R is the residual stress at the infinite time, σ_n are the stress relaxation coefficients (relaxation strength) and τ_n are the relaxation times.

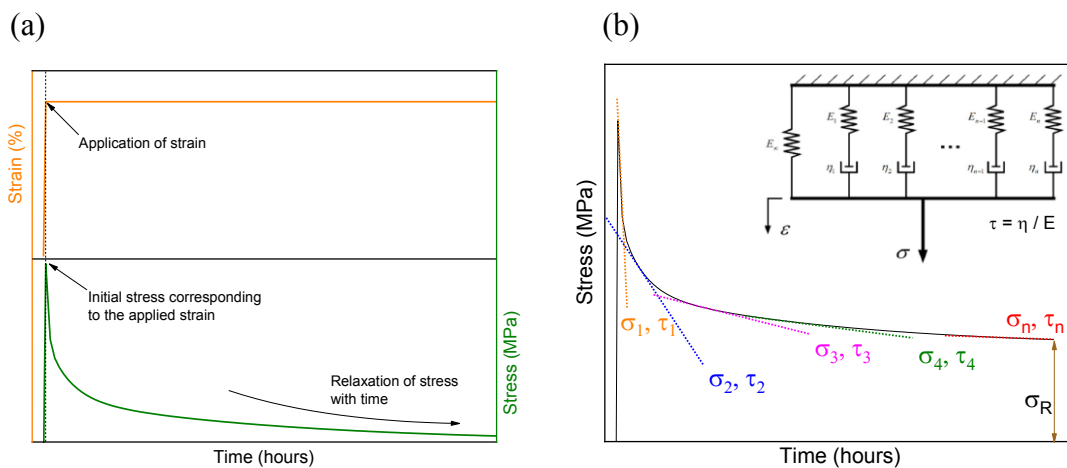


Figure 2.6: (a) An example stress relaxation curve and (b) Stress relaxation curve indicated with the relaxation parameters namely relaxation coefficient and relaxation time. (Inset: Representation of the Maxwell Model with combinations of springs and dashpots)

Chapter 3

Materials, compounding and characterization

3.1 Materials

3.1.1 Rubbers

3.1.1.1 Solution styrene butadiene rubber (SSBR)

The main rubber used to study and understand the piezoresistive properties was solution vinyl styrene butadiene rubber (SSBR). It's commercially available as Buna VSL 2525-0 M from Lanxess AG, Germany. Basic properties of the rubber are summarized in Table 3.1 and the chemical structure is given in Figure 3.1.

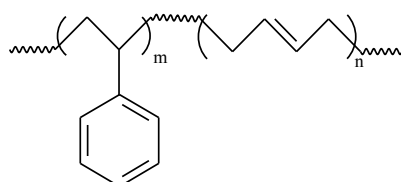


Figure 3.1: Chemical structure of SSBR

Table 3.1 Basic properties of the utilized SSBR

Parameters	Unit	Quantity
Mooney Viscosity	ML(1+4) @ 100°C	54
Styrene content	wt. %	25
Vinyl content	wt. %	25
Tg	°C	- 49
Specific gravity	g/cc	0.98
Total ash content	wt. %	≤ 0.2

3.1.1.2 Natural rubber (NR)

For testing the piezoresistivity on other commercial rubbers, electrically conductive natural rubber composites were prepared from Standard Malaysian Rubber (SMR 10). The specifications of the utilized SMR 10 are summarized in Table 3.2 and the chemical structure is given in Figure 3.2.

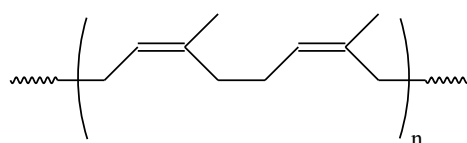


Figure 3.2 Chemical structure of NR

Table 3.2 Basic properties of the utilized NR

Parameters	Unit	Quantity
Max. dirt content	wt. %	0.08
Max. ash content	wt. %	0.75
Max. Nitrogen content	wt. %	0.06
Max. Volatile matter	wt. %	0.08
Wallace rapid plasticity (P°)	min	30
Min. plasticity retention index	%	50

3.1.1.3 Butadiene rubber (BR)

Electrically conductive butadiene rubber composites were prepared with a commercially available neodymium grade: Buna CB 24 from Arlanxeo, Germany, and its basic specifications are summarized in Table 3.3 and the chemical structure is given in Figure 3.3.

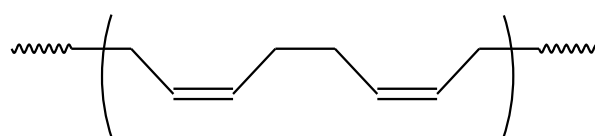


Figure 3.3 Chemical structure of BR

Table 3.3 Basic properties of the utilized BR

Parameters	Unit	Quantity
Mooney Viscosity	ML(1+4) @ 100°C	44
Organic acid	wt. %	≤ 1
Cis 1,4 content	wt. %	≥ 96
Max. Volatile matter	wt. %	≤ 0.5
Specific gravity	g/cc	0.91
Total ash content	wt. %	≤ 0.5

3.1.2 Fillers

3.1.2.1 Carbon black

One of the main conducting fillers utilized to understand the piezoresistive effects in SSBR is a highly conductive carbon black (abbreviated as CB). A commercially

available grade, Printex XE-2B and was obtained from Orion Engineered Carbons. Table 3.4 summarizes the basic specifications and Figure 3.4 shows the fine particle size of Printex black in the SSBR matrix. This specific grade of carbon black comprises very high structure and offers a very high surface area. Other conventional carbon blacks (abbreviated as CCB) were also used in the study, namely N220 (ISAF), N330 (HAF) and N660 (GPF). These commercially available grades of carbon blacks were procured from Orion Engineered Carbons, Köln, Germany.

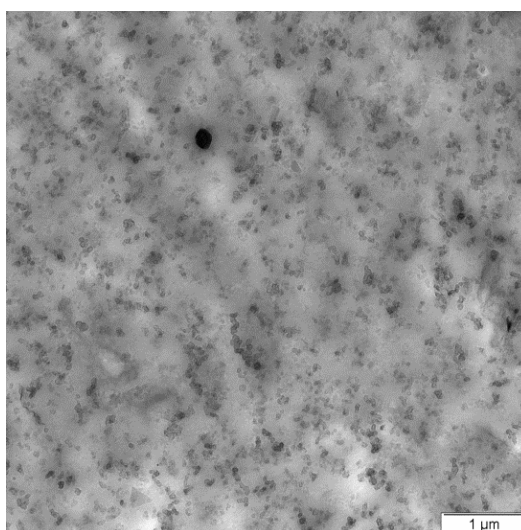


Figure 3.4: TEM Picture of Printex (12 Phr) inside the SSBR matrix

Table 3.4 Basic properties of the utilized Printex XE-2B grade

Physical Properties	Unit	Metric	Comments
Oil Absorption	ml/100g	420	ASTM D 2414
Loss on Ignition (Heating Loss)	%	≤ 2.0	ASTM D 1509
Statistical thickness surface area	m ² /g	1000	ASTM D 6556
Iodine Absorption Number	mg/g	1125	ASTM D 1510
Fines	%	< 12	ASTM D 1508
Individual Pellet Hardness	g	< 20	ASTM D 5230 (Ø 1.4 - 1.7 mm)
Sieve Residue	ppm	< 500 ppm	ASTM D 1514

3.1.2.2 Carbon nanotubes

Another conductive filler used in this study are multiwalled carbon nanotubes (MWCNT). They were obtained from Nanocyl S.A., Belgium and are commercially available as Nanocyl NC7000. The basic properties of the utilized grade of CNT as per the manufacturer's datasheet are summarized in Table 3.5.

Table 3.5: Basic properties of the utilized Nanocyl NC7000 grade

Physical Properties	Unit	Metric	Comments
Average diameter	nm	9.5	TEM
Average length	μm	1.5	TEM
Carbon purity	%	90	TGA
Metal oxide	%	< 1	ICP-MS
Surface area	m^2/g	250 ~ 300	BET analysis
Volume resistivity	$\Omega\cdot\text{cm}$	10^{-4}	Raw powder

3.1.3 Other chemicals

The basic rubber compounding ingredients such as Zinc oxide, stearic acid, and sulfur were obtained from Acros Organics and the vulcanizing accelerator n-cyclohexyl-2-benzothiazole sulfenamide (CBS) was obtained from Lanxess AG., Germany.

3.2 Compounding

3.2.1 Preparation of rubber and filler masterbatch

Large quantities of SSBR masterbatch were prepared in a Haake Rheomix 3000 PolyLab OS (Thermo Scientific GmbH, Karlsruhe), shown in Figure 3.5a, which has a chamber volume of 360 cm^3 . A fill factor of 0.7 was set and the total mixing was performed within 10 minutes at a mixing temperature of $80\text{ }^\circ\text{C}$ and with a rotor speed of 60 rpm. For smaller quantities of the masterbatch, a Haake Rheomix 600 PolyLab OS (Thermo Scientific GmbH, Karlsruhe), shown in Figure 3.5b was utilized, which has a chamber volume of 85 cm^3 . A fill factor of 0.7 was set and the total mixing was performed within 10 minutes at a mixing temperature of $80\text{ }^\circ\text{C}$ and with a rotor speed of 60 rpm.

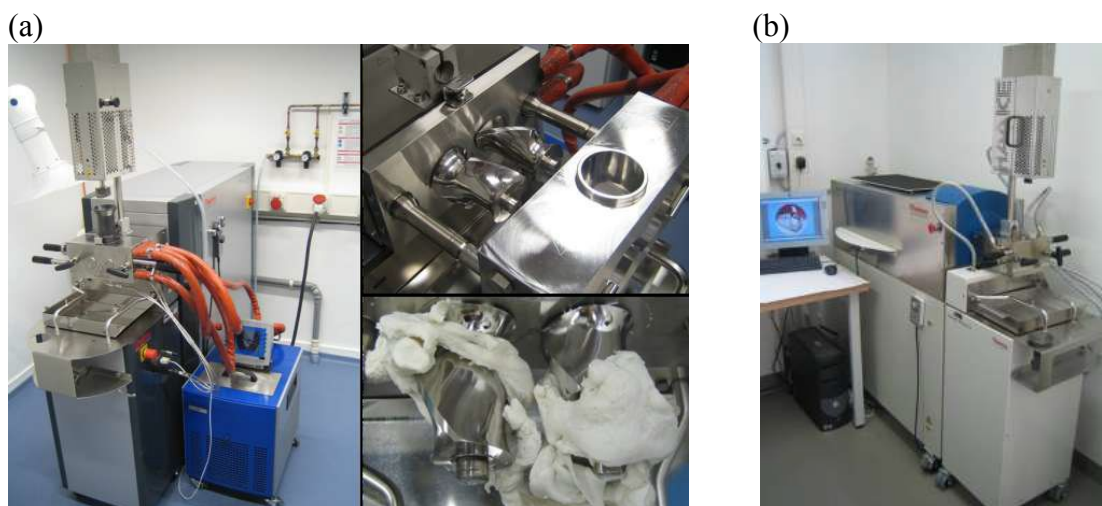


Figure 3.5: (a) Haake Rheomix 3000 with large mixing chamber (360 cm³) with pictures of the rotors and the masticated rubber. (b) Haake Rheomix 600 with the small mixing chamber (85cm³)

3.2.2 Compounding in Two roll mill

Rubber filler masterbatch was mixed with other ingredients such as zinc oxide, stearic acid, Sulfur and CBS in a laboratory-sized two-roll mill (Polymix 100L, Servitec GmbH, Wustermark, Germany), shown in Figure 3.6. The milling temperature and friction ratio were set at a constant 50 °C and 1:1.2 respectively.



Figure 3.6: Two-roll mill

3.2.3 Heated press

The compression press from Fontijne Holland (TP 1000) was used to vulcanize the sheets at 160 °C with 150 kN force according to their optimum cure time (T_{90})

obtained from a rubber process analyzer. In Figure 3.7 a view of the utilized compression press is shown. The hydraulic cylinder can generate a maximum press force of 1 MN between the platens and the maximum possible press temperature is 300 °C.



Figure 3.7: Heated press utilized to prepare the samples

3.2.4 Compounding formulations

In Table 3.6 and Table 3.7, formulations of carbon nanotubes (CNT) and conducting carbon black (CB) with different amounts of sulfur and accelerator are given. Changing the amounts of sulfur and accelerator would help in achieving different crosslink densities in the rubber matrix. The ratio of sulfur to accelerator was always kept constant at 4:3, to ensure a proportional increase of sulfidic bonds in the vulcanizate. Moreover, for preparing masterbatches with CNT, pre-dispersed and ultrasonicated mixtures of CNT in ethanol were utilized to ensure disentanglement and better dispersion of the CNT [129].

Table 3.8 summarizes the composites produced with different levels of hardness using aromatic oils. Increasing the dosage of aromatic oil helps in achieving composites with lower hardness. Conducting composites with different rubbers (NR, BR, and SSBR) were produced with Printex carbon black and Table 3.9 summarizes their compounding recipes. Finally, SSBR composites were produced with commercially available conventional carbon blacks, namely N220, N330, and N660, which is given in Table 3.10.

Table 3.6: Basic rubber compounding formulation (ingredients) with CNT

Compound Nr.	1	2	3	4	5	6	7	8	9	10	11	12	13	14	15	16	17	18
SSBR	100																	
ZnO	5																	
Stearic acid	2																	
CNT	1	2	3			3.5			4			5						
Sulfur	2	2	1	2	3	4	1	2	3	4	1	2	3	4	1	2	3	4
CBS	1.5	1.5	0.75	1.5	2.25	3	0.75	1.5	2.25	3	0.75	1.5	2.25	3	0.75	1.5	2.25	3

Table 3.7: Basic rubber compounding formulation (ingredients) with conductive carbon black (CB)

Compound Nr.	1	2	3	4	5	6	7	8	9	10	11	12	13	14	15	16	17	18	19	20
SSBR	100																			
ZnO	5																			
Stearic acid	2																			
Carbon black	5	7.5	10			11			11.5			12			13					15
Sulfur	2	2	1	2	3	4	1	2	3	4	2	1	2	3	4	1	2	3	4	2
CBS	1.5	1.5	0.75	1.5	2.25	3	0.75	1.5	2.25	3	1.5	0.75	1.5	2.25	3	0.75	1.5	2.25	3	1.5

Table 3.8: Compound formulations of conductive carbon black and carbon nanotube with SSBR and aromatic process oil

Mix no.*	1	2	3	4	5	6
SSBR	100					
Zinc Oxide	5					
Stearic acid	2					
Carbon black (CB)	10.5			-		
Carbon nanotubes (CNT)	-			3.5		
Aromatic oil	1	2.5	5	1	2.5	5
Sulfur	2					
CBS	1.5					

*All the weights were taken in *phr*, where *phr* stands for parts per hundred parts rubber.

Table 3.9: Compound formulations of conductive carbon black with different rubbers

Mix no.*	1	2	3
BR	100		
NR		100	
SSBR			100
Zinc Oxide	5		
Stearic acid	2		
Carbon black (CB)	12		
Sulfur	2		
CBS	1.5		

*All the weights were taken in *phr*, where *phr* stands for parts per hundred parts rubber.

Table 3.10 : Compound formulations of conventional carbon blacks with SSBR

Mix no.*	1	2	3
SSBR	100		
Zinc Oxide	5		
Stearic acid	2		
ISAF - N220	60		
HAF - N330		60	
GPF - N660			60
Sulfur	2		
CBS	1.5		

*All the weights were taken in *phr*, where *phr* stands for parts per hundred parts rubber.

3.3 Characterization

3.3.1 Vulcameter

The optimum cure time of the compounds is obtained from a rubber process analyzer, RPA elite from TA instruments and shown in Figure 3.8. The measurement conditions were 160 °C with 6.98 % strain at a frequency of 1.67 Hz for 1 hour. The optimum cure time t_{90} is calculated from the time to take to reach 90% of the maximum torque.



Figure 3.8: A view of the utilized rubber process analyzer

3.3.2 Determination of crosslink density

The crosslink density was measured by equilibrium solvent swelling method [159, 160]. Three different geometries: circle (\varnothing 9 mm), square (10 x 10 mm²) and triangle ($\frac{1}{2}$ x 10 x 20 mm²) specimens were punched from a 2 mm thick rubber sheet, weighed and let to swell in toluene for 72 hours at room temperature (\sim 25 °C) in sealed glass vials. The samples were kept in dark to prevent effects of degradation. After 72 hours, the samples were taken out of the solvent, wiped to remove the excess solvent on the surface and weighed in a high precision balance. Finally, the swollen samples were dried at 60 °C until constant weight was achieved. The initial weight, swollen weight and final dried weight of samples were used to calculate the crosslink density of gum and filled composites. The Flory-Rehner equation Eq. 3.1 was used to estimate the density of crosslinks in the swollen rubber network [161].

$$\ln(1 - v_r) + v_r + \chi v_r^2 = -\frac{\rho_r}{M_c} V_s \left(1 - \frac{2v_r^{2/3}}{f}\right) v_r^{1/3} \quad \text{Eq.3.1}$$

where ρ_r is the density of the rubber compound, V_s is the molar volume of toluene (106.2 mL/mol), M_c is the molecular weight of the chain segments between two crosslinks, χ is the Flory-Huggins interaction parameter (0.413 for SBR-toluene) and f is the functionality of crosslink (for phantom model network the functionality is assumed as tetra-functional crosslinks, hence $f = 4$). The volume fraction of rubber (v_r) in the filled composite was determined by Eq. 3.2 [160]

$$v_r = \frac{(w_d - f_{ins} w_i) / \rho_r}{(w_d - f_{ins} w_i) / \rho_r + w_0 / \rho_s} \quad \text{Eq.3.2}$$

where, w_i , w_s and w_d are the initial weight of samples before swelling, swollen and dried samples respectively. w_0 is the equilibrium weight of solvent absorbed by the samples, calculated as $[w_0 = w_s - w_d]$. f_{ins} is the weight fraction of the insoluble substances in rubber like carbon black, MWCNT and zinc oxide and ρ_s is the density of toluene (0.867 g/cm³). The final crosslink density of the rubber composites was calculated as $\nu_{FR} = 1/M_c$.

3.3.3 Electrical conductivity

The resistivity/conductivity of insulating rubber samples (showing a specific resistivity $> 10^7 \Omega \cdot \text{cm}$) was measured using a Keithley 8009 (a plate measuring device) in combination with a Keithley electrometer 6517A (Keithley Instruments Inc., USA) on discs with a thickness of 0.5 mm and diameter of 60 mm. The volume resistivity for conducting samples ($< 10^7 \Omega \cdot \text{cm}$) was measured on stripes using a 4-point test fixture (distance between the inner and outer electrodes are 10 mm and 16 mm).

3.3.4 Simple uni-axial piezoresistance measurements

Uniaxial piezoresistive tests were performed with DIN S2 dumbbell specimens in an in-house developed setup as shown schematically in Figure 3.9. The setup can measure a resistance up to 100 M Ω and allows for applying a maximum strain of

300%. The resistance and strain data are recorded real-time in 0.5-second intervals and stored in a computer.

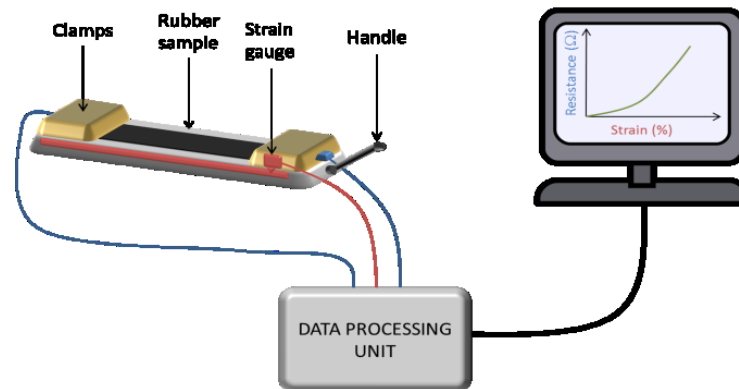


Figure 3.9: Schematic representation of the experimental setup of the piezoresistance measurement device

3.3.5 Hysteresis / Cyclic piezoresistance measurements

Fully automated uni-axial and cyclic piezoresistance tests were performed on DIN S2 dumbbell specimens in an in-house developed setup (see Figure 3.10). The device can measure forces up to 100 N, with a maximum stretch of 300 mm at a maximum rate of 200 mm/min. The coupled multimeter can record resistance precisely from 1 kΩ - 100 MΩ. The stress, strain, and resistance measured real-time in 0.5-second intervals were monitored and saved in a computer.



Figure 3.10: In-house built piezoresistance measurement device with a magnified view of the sample clamps (left)

3.3.6 Electrical resistance coupled dynamic mechanical analysis

To investigate the change in the electrical resistance during dynamic deformation, a Dynamic Mechanical Thermal Spectrometer (DMTS) Gabo Eplexor 2000N (Gabo Qualimeter, Ahlden, Germany) was used. With the aid of an AD converter card, a measurement setup was built, which enables synchronous recording of the measured value of the electrical resistance of a (strip-like) rubber sample and the sinusoidal force and strain acting on it. Therefore, the resistance values could be registered synchronously with the stress and strain data provided by the DMTS. The experimental setup and the schematic representation are shown in Figure 3.11.

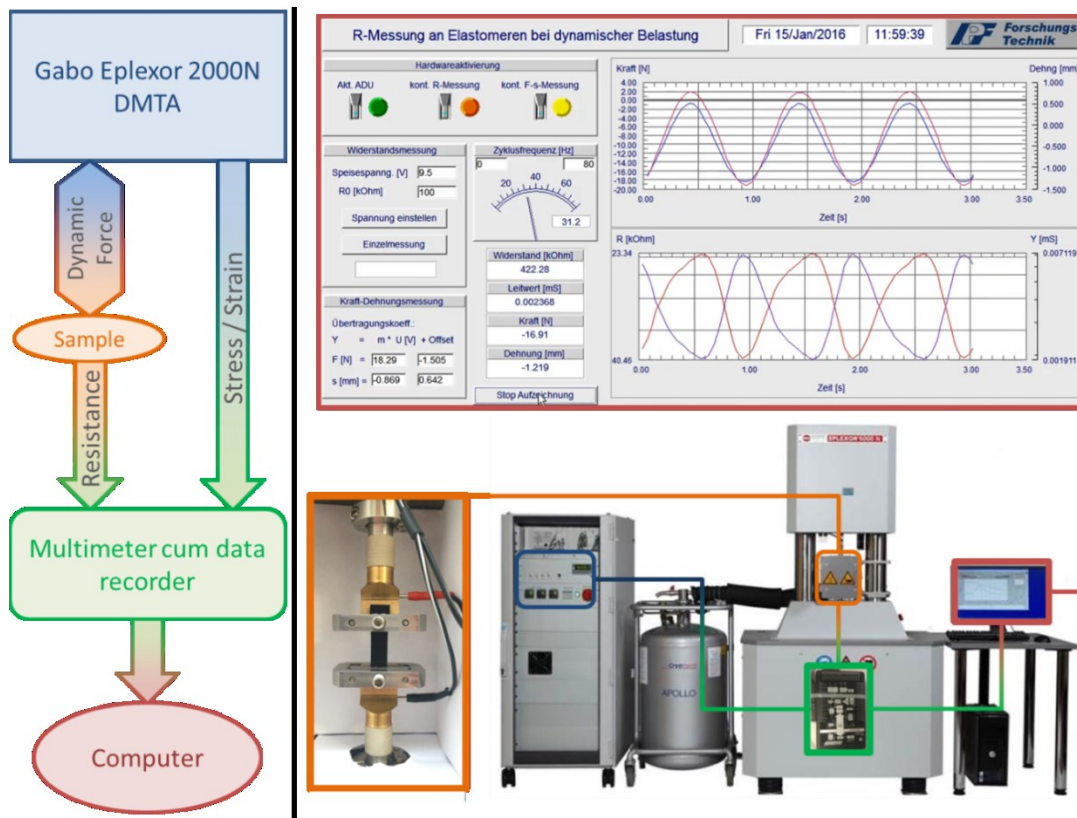


Figure 3.11: Schematic view (left) and experimental setup (right) of the dynamic mechanical analyzer coupled with the in-house built device. [Picture in the orange box on the right depicts the clamping mechanism inside the DMA chamber and image inside the red box on the right depicts a sample data displayed in the computer]

All the tests were performed in tension mode, either by strain or stress controlled modes. The measurements are defined on basis of four parameters: static load,

dynamic load, frequency and test temperature. For strain-controlled mode, static and dynamic strains are defined in the input parameter, and for stress driven mode, the static and dynamic forces are defined in the input parameters. Four major parameters that mainly influence the dynamic property namely (i) filler content, (ii) test frequency, (iii) matrix crosslink density and (iv) test temperature are primarily considered in this study. The experimental parameters of the DMTS coupled resistance measurements are given in Table 3.11 and Table 3.12.

Table 3.11: Various tests conditions utilized for the dynamic piezoresistivity study under strain-driven mode

Experiment	Variable	Static strain (%)	Dynamic strain (%)	Temperature (°C)	Frequency (Hz)	Filler content (phr)
Time sweep (1 hour)	Frequency	60	10	35	0.25, 0.5, 1, 2, 5, 10	12 CB, 3.5 CNT
	Filler content				1	12, 13, 15 CB
	Crosslink density		20			12 CB, 3.5 CNT
	Temperature		30	25, 35, 45		12 CB
Temperature sweep	Filler content	60	30	60 → -10	1	12, 13, 15 CB, 4, 5 CNT
	Crosslink density					12 CB, 4 CNT
	Dynamic strain		10, 20, 30			12 CB
Strain sweep	Filler content	60	0.1 to 30	35	10	12, 13 CB
	Temperature			35, 50		12CB

Table 3.12: Various tests conditions utilized for the dynamic piezoresistivity study under force driven mode

Experiment	Variable	Static force (N)	Dynamic force (N)	Temperature (°C)	Frequency (Hz)	Carbon black content (phr)
Time sweep (1 Hour)	Dynamic strain	6, 9	3, 4.5	35	1	12
	Filler content	6	3			12, 13, 15
	Crosslink density					12
	Temperature			25, 35, 45		12
Temperature sweep	Dynamic strain	6, 9	3, 4.5	60 → -40	1	12

3.3.7 Stress relaxation fitting

The stress relaxation experiments were performed in the Dynamic Mechanical Thermal Spectrometer (DMTS) Gabo Eplexor 2000N (Gabo Qualimeter, Ahlden, Germany). The phenomenological Maxwell - Wiechert model [158], discussed in Chapter 2, [Figure 2.6](#), is utilized to describe the stress relaxation behavior with three relaxation times, given by [Eq. 3.3](#).

$$\sigma(t) = \sigma_f + \sum_{n=1}^3 s_n e^{-t/\tau_{s_n}} \quad \text{Eq.3.3}$$

where $\sigma(t)$ is the stress of the sample at a time ' t ', σ_f is the residual stress, s_n are stress relaxation strengths, τ_s are the relaxation times for the stress. The equation defines three characteristic relaxation times $\tau_{s_1} < \tau_{s_2} < \tau_{s_3}$, a fast relaxation time (τ_{s_1}), followed by a mid-relaxation regime (τ_{s_2}), and a long relaxation time (τ_{s_3}) that represents the long-term properties as shown in [Figure 3.12](#).

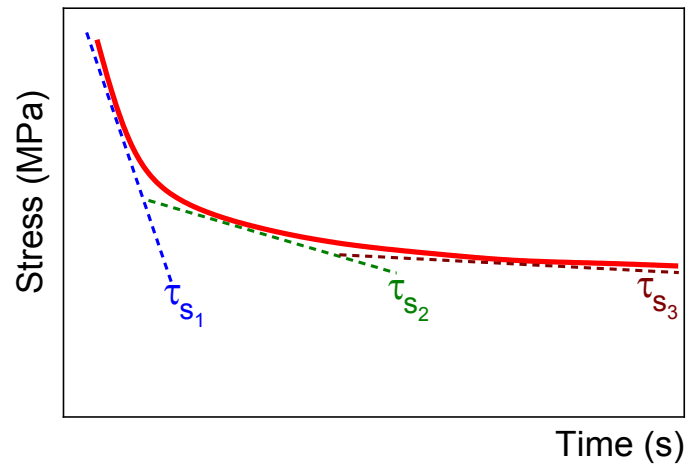


Figure 3.12: An example stress relaxation curve depicting the three characteristic relaxation times τ_{s1} , τ_{s2} and τ_{s3}

Chapter 4

Exploring the quasi-static piezoresistive behavior of SSBR composites

A part of the results from this chapter is published in
Materials today communications, 14, **2018**, 240 – 248

4.1 Introduction

In this chapter, as a first step, basic piezoresistive characteristics of SSBR (an important rubber used in tire production) are studied in detail. Parameters such as crosslink density and material stiffness that influence the piezoresistive effect are primarily investigated. The strain sensitivity of the materials is tailored by controlling the matrix crosslink density and by incorporating aromatic process oils. In an attempt to realize them as potential strain sensors, the sensitivity of the materials is calculated in the most sensitive regime and simple mathematical equations are fitted to compare and predict their performances. Finally, the behavior of these materials under cyclic or repeated loading conditions is studied to understand their repeatability and reproducibility.

4.2 Electrical conductivity of the composites

The electrical conductivities are measured for all the samples including the gum rubber without any filler. The unfilled vulcanizates display the lowest conductance in the order of (10^{-15} S). With the incorporation of fillers, a gradual increase in electrical conductivity is observed. As seen in [Figure 4.1a](#), the electrical percolation starts from 10 phr (4.21 vol. %) for carbon black and 3 phr (1.2 vol. %) for CNT. Therefore, to investigate the effect of crosslink density on the sensing performance, samples with different sulfur contents are only prepared for filler fractions more than 10 phr in the case of CB and 3 phr in the case of CNT.

In [Figure 4.1a](#), it is observed that conductance of 1 μ S could be achieved with just 3.5 phr of CNT, whereas 11 phr of CB is required to achieve this similar value. Though the carbon black used here is a conducting type with a high surface area and high structure, the intrinsic electrically conductive nature and high aspect ratio of CNT ultimately offered a low percolation concentration. [Figure 4.1b](#) presents the logarithm of the conductance as a function of $\log(P - P_c)$. The t values derived from the plots are around 1.1 for CNT and 1.5 for carbon black. The derived values fall in-line with the findings from literature [110].

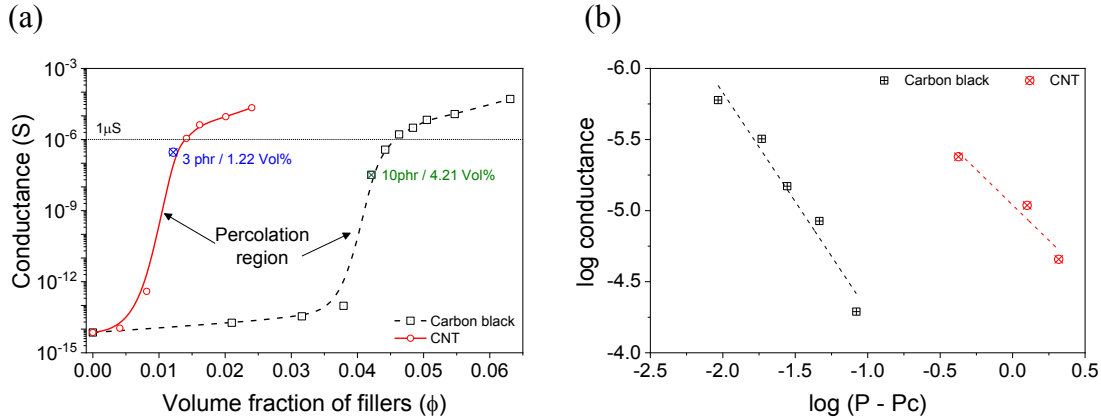


Figure 4.1:(a) Dependence of conductance on the filler content (b) plot of log conductance against $\log(P - P_c)$ with the linear scaling law fit [109, 118]. [P is the filler volume fraction and P_c is the filler volume fraction at percolation threshold]

4.2.1 Influence of crosslink density on electrical conductivity

The ratio of sulfur to organic accelerator was kept constant to ensure a proportional increase of the sulfidic bonds in the vulcanizate. As seen in Figure 4.2a and Figure 4.2b, irrespective of the filler type, conductance values are found to be low for samples with higher cross-link density. Conductance or conductivity of a composite is mainly related to the formation of percolated filler network and any process that hinders the network formation would result in lower electrical conductivity. High sulfur content leads to higher crosslinking degrees and restricts the filler mobility, thus obstructs the network formation of the fillers (filler-filler network formation). This process is taking place during the vulcanization of the rubber compounds [162]. The conductance values are therefore found to decrease significantly with an increase in crosslink density for all the CNT and carbon black composites.

The data were plotted following Eq 2.1 in Figure 4.2c and Figure 4.2d and the critical exponent t values were estimated around $0.42 \sim 0.99$ for various sulfur crosslinked samples [163]. Interestingly, the t values that denote the 2D or 3D network formation are strongly influenced by the crosslink density of the rubber matrix. Irrespective of the crosslinks density, a good percolated filler network is found to be established in all the composites.

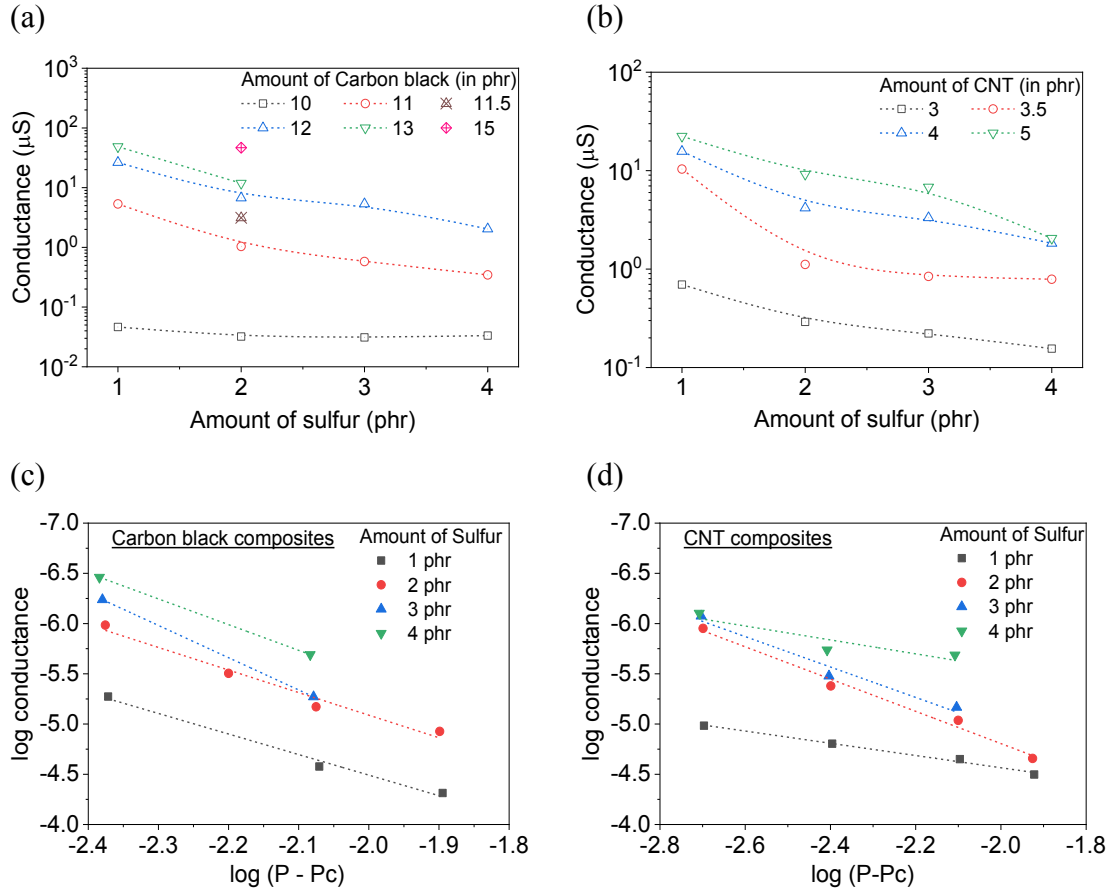


Figure 4.2: Electrical conductance of the rubber composite as a function of sulfur content for (a) carbon blacks and (b) CNT. The plot of $\log \sigma$ against $\log (P - P_c)$ (with the linear fit) for different sulfur contents of (c) carbon black and (d) CNT filled composites.

4.2.2 Influence of process oil on electrical conductivity

Different samples were prepared with a fixed filler concentration near to the electrical percolation with variable amounts of aromatic oil for altering the hardness/stiffness of the composites. Therefore, to study the influence of aromatic oil on the stiffness, the variation in ‘Shore A’ hardness with respect to aromatic oil content is depicted in Figure 4.3a and the electrical conductance is plotted as a function of hardness in Figure 4.3b.

In carbon black and CNT composites, the electrical conductivity increases considerably with the incorporation of process oil. With the addition of 5 phr oil, ~65 % and ~85 % increase in electrical conductivity is observed for carbon black and CNT composites respectively. Incorporation of process oil leads to a plasticizing

effect and thereby results in better distribution of the fillers and paves the formation of more conducting pathways in the rubber matrix. In other words, with the assistance of oil, the electrical percolation threshold could be achieved at relatively lower filler concentrations. Another benefit of plasticization is that rubbers can display higher ultimate elongation values. This would offer rubber-based strain sensors with even higher strain detection range.

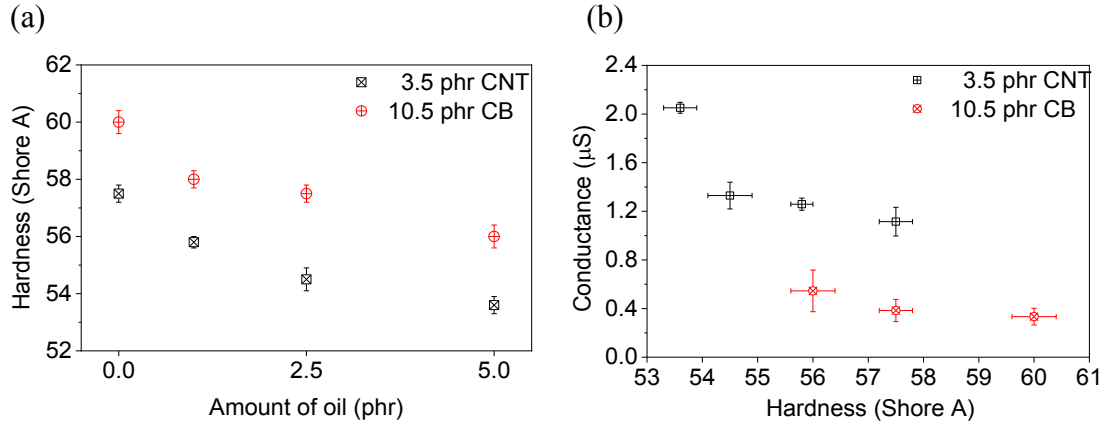


Figure 4.3: (a) Variation in Shore A hardness with respect to plasticizer content and (b) dependence of electrical conductance with respect to the hardness of the composites

4.3 Uniaxial piezoresistivity

4.3.1 Influence of filler content

The electrical resistance-strain relationships for various composites are plotted in Figure 4.4. As seen in Figure 4.1, the difference in electrical resistance of the samples with increasing filler content in the undeformed state is very significant. Therefore, to compare the piezoresistive effect upon stretching, the relative change in electrical resistance was calculated according to Eq 4.1.

$$\text{Relative resistance (\%)} = \frac{R(\varepsilon) - R_0}{R_0} \times 100 \quad \text{Eq. 4.1}$$

where $R(\varepsilon)$ is the electrical resistance of the sample for the applied strain ε and R_0 is the electrical resistance of the unstrained sample. Strain ε is the percentage change in the length of the sample. The electrical resistance displays a non-linear increase with respect to the applied strain, which is well explored and reported in many publications [29, 134, 147]. The carbon black sample with 11 phr CB loading (near to the

percolation concentration of 10.5 phr) shows a strong change in the electrical resistance at relatively lower strains in Figure 4.4a and Figure 4.4b. However, this is not reliable due to its unstable percolated network. In the case of samples with 12 phr and 13 phr of carbon black, a wide range of strains (up to 250 % strain) could be detected with good sensitivity. At even higher filler loading, the strain-dependent behavior of the rubber composites is interesting, *i.e.*, for 15 phr CB filled sample the relative change in resistance is negligible up to 200 % elongation and further from this point, a slow increase in electrical resistance is observed. This kind of material can be used as elastic conductors where the current flow will not be disturbed by the deformation of the sample. Composites with a higher amount of CB may offer higher electrical conductivities, but the strain-dependent electrical changes would be minimal due to the robust electrical conducting pathways of the filler-filler network.

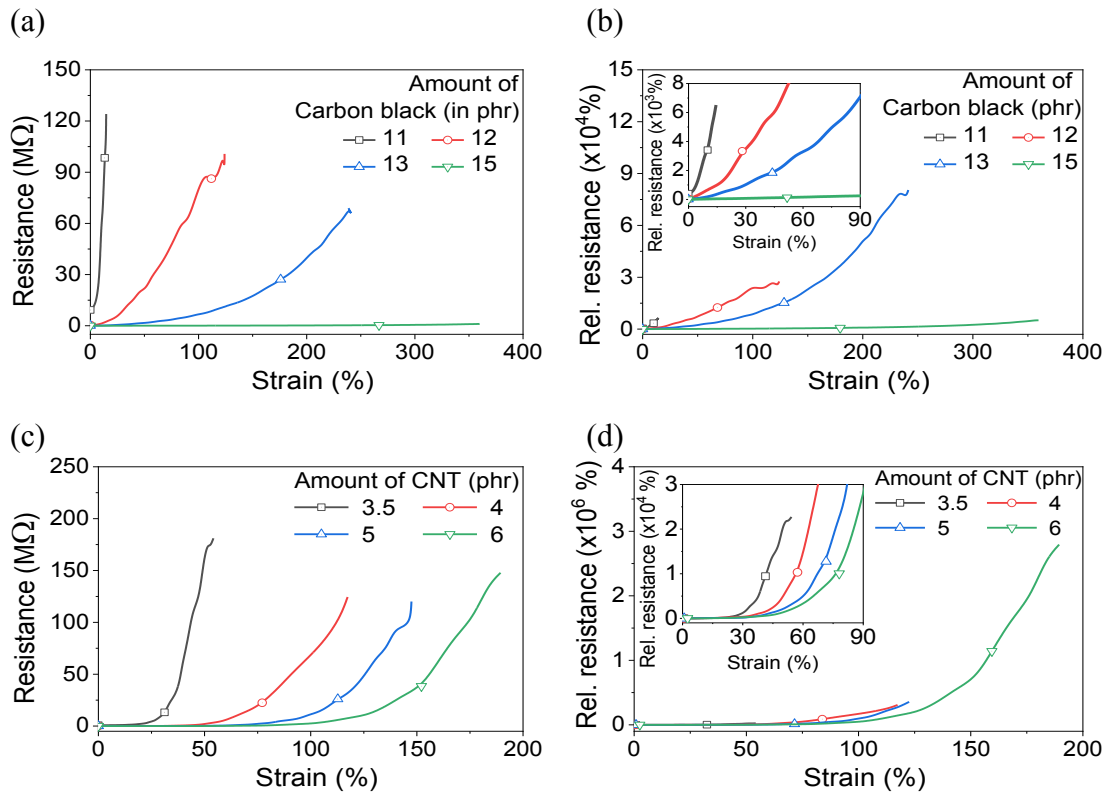


Figure 4.4: Change in (a) resistance and (b) relative resistance with an inset depicting changes in the low strain regime for various carbon black composites. Change in (c) resistance and (d) relative resistance with an inset depicting changes in the low strain regime for various CNT composites.

Similar response profiles are also displayed by the CNT filled samples in [Figure 4.4c](#) and [Figure 4.4d](#). As far as the extent of change in electrical resistance or relative resistance is concerned, MWCNT composites show strong strain dependence at relatively lower elongations than carbon black composites. The high sensitivity of CNT could be ascribed to the low particle size and their aspect ratio. Due to their high aspect ratio and exceptional electrical conductivity, a low concentration would suffice to percolate and form a conductive network. But, when the sample is deformed, the percolated CNT filler network will experience more destruction in comparison to the CB composites. As seen in [Figure 4.4b](#) and [Figure 4.4d](#), the relative change in resistance in the CB composites is in the order of $\sim 10^4$, whereas CNT composites undergo relative resistance change in the order of $\sim 10^6$. Interestingly, even the highly conductive CNT composites lost their electrical conductivity within 200% of strain. The 6 phr of CNT composite, for instance, showed an initial resistance of 5.29 k Ω (un-stretched), which increased to 148 M Ω at 180% strain. Whereas this behavior is not observed for CB composites; highly filled CB composites that display very low initial electrical resistance hardly showed any piezoresistive characteristics. For example, 15 phr CB composite displayed a change from 21 k Ω (un-stretched) to 1.1 M Ω at 360% strain. The piezoresistive behavior or sensitivity of CNT composites towards strain is therefore found to be higher than CB composites.

4.3.2 Strain sensitivity

4.3.2.1 Influence of filler content

Since the responses of the materials are non-linear, it would be more relevant and practical to study the influence of strain on ‘sensitivity’. The sensitivity of a sensor, commonly known as strain gauge factor (GF), is defined as the ratio of the relative change in resistance per unit change of strain, represented by [Eq 4.2](#)

$$\text{Sensitivity} = \frac{\text{Relative resistance}}{\epsilon} = \frac{\frac{R(\epsilon) - R_0}{R_0} \times 100}{\epsilon} \quad \text{Eq. 4.2}$$

where $R(\epsilon)$ is the electrical resistance of the sample for the applied strain ϵ and R_0 is the electrical resistance of the unstrained sample.

Figure 4.5 depicts the sensitivity-strain relationships of carbon black and CNT composites. It can be noted here that MWCNT composites with 5 phr and 6 phr loading show very high gauge factor (>1000) at strains more than 200 %. However, sample with 11 phr CB loading shows a bit lower gauge factor, but its strain responsive behavior is very pronounced at relatively lower strains.

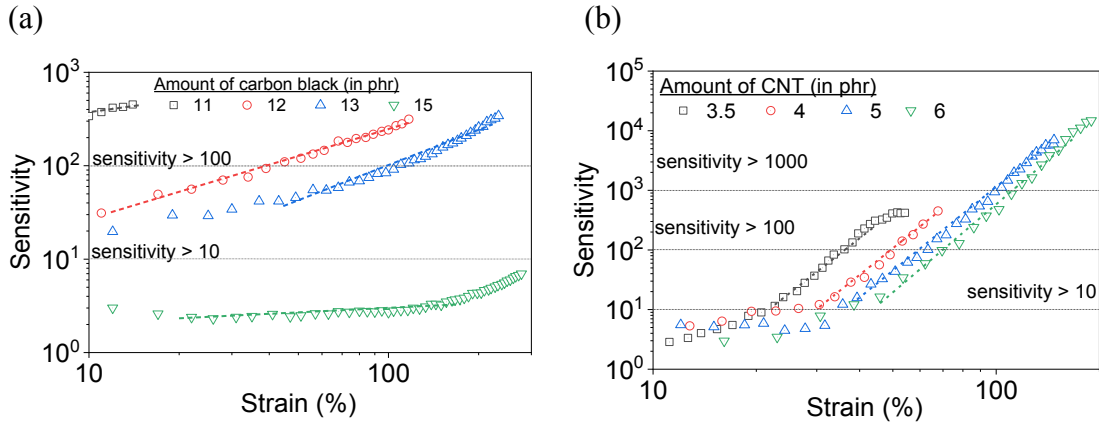


Figure 4.5: Strain sensitivity plots of (a) carbon black composites & (b) CNT composites

Complex theories and fitting functions that describe various segments of the resistance-strain relationship are available in the literature. These functions are usually combinations of exponential functions, power laws, polynomial functions, etc. [29, 164]. In the present case, a simple power law and a simple exponential equation are considered to describe the strain sensing behavior of the rubber composites. Here, fitting is only done for strains > 10 % and when the sensitivity is greater than 1. The simple power law considered is

$$S(\epsilon) = k_1 \epsilon^{m_1} \quad \text{Eq. 4.3}$$

where $S(\epsilon)$ is the sensitivity for the applied strain (ϵ) and m_1 , k_1 are fitting parameters.

The simple exponential function considered is

$$S(\epsilon) = k_2 e^{m_2 \epsilon} \quad \text{Eq. 4.4}$$

where $S(\epsilon)$ is the sensitivity for the applied strain (ϵ) and m_2 , k_2 are fitting parameters.

In Figure 4.5, the value m_1 corresponds to the slopes of the fitted straight lines in the log-log plot of sensitivity against the strain. The fitting parameters k_1 and k_2 represent the sensitivity of the samples towards the imposed strain. It can be noted from Table 4.1 that k_1 and k_2 values are decreasing with increasing filler content. The most interesting observation in the fitting parameter is that the values of k_1 (carbon black) are several orders (up to $\sim 10^6$) higher than k_1 (CNT) values. Most probably, highly anisotropic and entangled structure of the CNT could be associated with such observations. The m -values represent the slopes of the linear fits in Figure 4.5 and refer to the magnitude of the sensitivity change for the applied strain. The exponent m -values are found to decrease with the increase in filler volume fraction for composites filled with either carbon black or CNT. These fitting parameters, therefore, serve as a very good tool to compare and choose the right sensor material for the desired application. Hence by considering the actual operating region, simple equations can rather provide significant information regarding the performance of the sensors.

Table 4.1: Fitting parameters for different samples with 2 phr of sulfur

Samples (in phr)	k_1	m_1	R^2	k_2	m_2	R^2
11 CB	52.5	0.82	0.982	201.83	0.0584	0.967
12 CB	1.87	1.06	0.989	66.14	0.0132	0.988
13 CB	1.46	0.89	0.972	31.97	0.0103	0.998
15 CB	1.30	0.17	0.918	1.76	0.0047	0.980
3.5 CNT	9.41×10^{-6}	4.91	0.998	0.48	0.1497	0.994
4 CNT	1.60×10^{-6}	4.67	0.993	0.54	0.0999	0.988
5 CNT	5.32×10^{-7}	4.61	0.993	3.86	0.0539	0.992
6 CNT	8.97×10^{-8}	4.51	0.996	4.44	0.0449	0.993

4.3.2.2 Influence of crosslink density

Once the right type and amount of filler are identified, the sensitivity could be further fine-tuned by varying the crosslink density or using plasticizers, to tune the hardness of the materials. Figure 4.6a depicts the sensitivity of 12 phr CB sample with different degree of crosslinking. With reference to Figure 4.2a, samples with higher

crosslinking degree display lower electrical conductance and the consequential effect are observed in Figure 4.6a. Samples with higher crosslink density display higher sensitivity to the applied strain. The less crosslinked samples display significant piezoresistive characteristics only in the high strain regime. For example, in 12 phr CB filled sample and crosslinked with 1 phr of sulfur, the sensitivity values hardly change up to 50 % strain. Only at higher elongations (>100 %), the strain-dependent sensitivity changes are prominent. A similar dependence of sensitivity on the crosslink density is observed in Figure 4.6b also for the CNT filled composites.

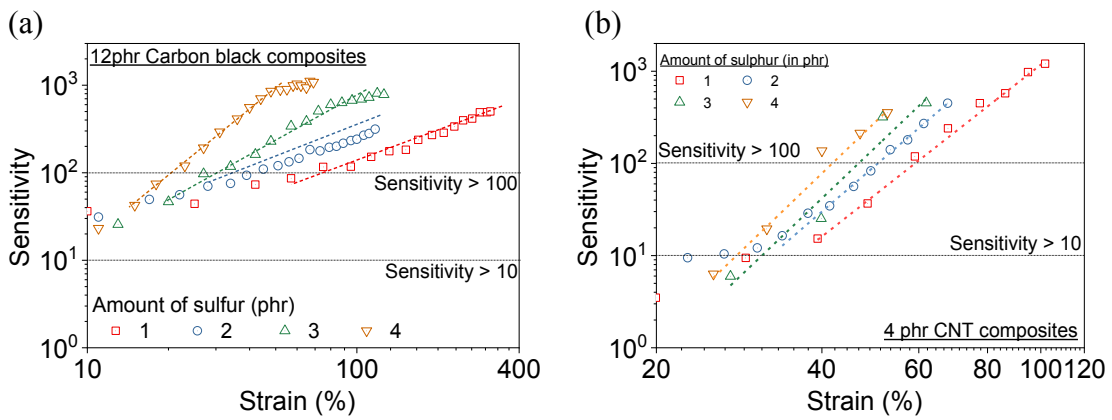


Figure 4.6: Log-log representation of the strain sensitivity with the power law fits for (a) carbon black and (b) CNT composites respectively.

An increase in the number of crosslinks would limit the maximum extensibility of the short polymer chains. Therefore, during stretching, the initial strain would contribute to the alignment of short chains along the stretching direction. The segmental orientations would last until the short chains reach their extensibility limit [165]. Once all the short chains are stretched and cannot take up more loads, the excess strain would then be transferred to align the fillers along the stretching direction. Further increase in strain would disorder/rupture the filler clusters resulting in an increment of the resistance value [25, 165, 166]. Thus, the relatively poor electrical response at lower strain regime could be associated to the fact that the filler clusters seldom respond to low strains.

Finally, the variation in the crosslink density can affect the chain extensibility and in-turn determines the sensitivity of the samples. The advantage of manipulating the crosslink density of the rubber matrix could be explained as follows: In Figure 4.5a,

there is a substantial difference in the sensitivities of samples with 13 phr CB and 15 phr CB. Therefore, achieving an intermediate sensitivity in-between this range is difficult by adjusting filler concentration, but is rather easily possible by optimizing the crosslink density of the rubber matrix. Eq 4.3 and Eq 4.4 are fitted for the curves displayed in Figure 4.6a and Figure 4.6b and the fitting parameters are presented in Table 4.2. As expected, the m_1 and m_2 values for carbon black as well as CNT are falling with the decrease in crosslink density of the rubber matrix. The k_1 and k_2 values are found to decrease with an increase in the crosslink density of the rubber matrix.

Table 4.2: Fitting parameters for 12 phr carbon black and 4 phr CNT samples with a different sulfur content

Amount of sulfur		k_1	m_1	R^2	k_2	m_2	R^2
12 phr CB	1 phr	1.527	0.989	0.970	58.31	0.0081	0.967
	3 phr	0.239	1.777	0.987	40.02	0.0354	0.979
	4 phr	0.039	2.583	0.999	6.07	0.1200	0.988
4 phr CNT	1 phr	5.06×10^{-7}	4.68	0.985	1.19	0.0733	0.985
	3 phr	1.41×10^{-7}	5.33	0.913	0.88	0.0975	0.996
	4 phr	7.08×10^{-8}	5.65	0.966	0.78	0.1123	0.974

4.3.2.3 Influence of process oil

To understand the effect of filler dispersion on the strain-dependent electrical conductivity, aromatic oils are used to assist the dispersion process. The filler concentration right at the percolation threshold (3.5 phr for CNT and 10.5 phr for carbon black) are selected to better visualize the piezoresistive properties. The addition of oil to the compounding process results in a stable electrically conducting percolated filler network and yields composites with higher electrical conductivity as seen in Figure 4.7. As depicted in Figure 4.7a, with an increase in oil content, a less change in relative resistance is observed for a given strain.

Therefore, the addition of plasticizer results in CNT composites with lower strain sensitivity but widens the strain sensing regime. In Figure 4.7c, the carbon black composites display less change with the incorporation of aromatic oil, which could be due to the amount of oil being less than the critical concentration required to effectively lubricate the polymer matrix.[167] With an addition of 5 phr oil, however, a higher elongation at break (stretching ability) is observed. Therefore, to visualize the effect of process oils in carbon black composites, a dosage of more than 5 phr is necessary.

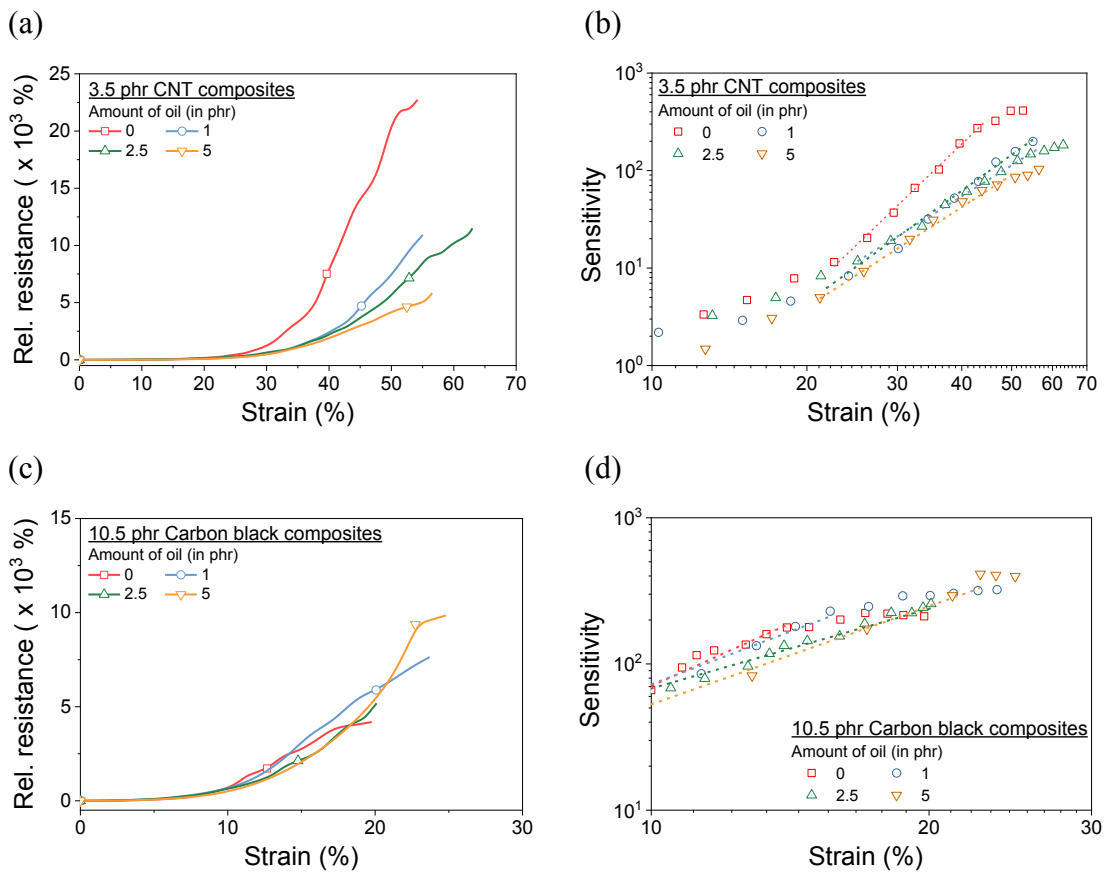


Figure 4.7: Relative resistance and (b) strain sensitivity with power law fit for 3.5 phr CNT composites with different process oil content. (c) Relative resistance and (d) strain sensitivity with power law fit for 10.5 phr carbon black composites with different process oil content.

The strain sensitivities are calculated for both the composites and presented in Figure 4.7b and Figure 4.7d. Equations Eq 4.3 and Eq 4.4 are utilized to describe and fit the sensitivity- strain relationship, the fitting parameters are given in Table 4.3. In CNT composites, the k_I values are found to increase; m_I values are found to decrease

with the increase in oil content, indicating lower sensitivity than the un-plasticized composites. For the carbon black composites, with respect to the un-plasticized sample, 5 phr oil filled composite displays higher k_1 , k_2 as well as lower m_1 , m_2 values, indicating a lower sensitivity. In this case, also the power law and exponential fits serve as a simple tool to describe and quantify the strain sensitivity of the samples.

Table 4.3: Fitting parameters for 3.5 phr CNT and 10.5 phr carbon black samples with different process oil content

Amount of oil		k_1	m_1	R^2	k_2	m_2	R^2
3.5 phr CNT	0 phr	9.4×10^{-6}	4.91	0.998	0.48	0.1497	0.994
	1 phr	5.1×10^{-5}	3.80	0.976	0.54	0.113	0.991
	2.5 phr	3.0×10^{-4}	3.41	0.998	0.96	0.098	0.987
	5 phr	1.5×10^{-4}	3.28	0.988	0.33	0.125	0.993
10.5 phr CB	0 phr	0.254	2.46	0.974	2.36	0.325	0.964
	1 phr	0.332	2.33	0.993	5.94	0.232	0.980
	2.5 phr	1.053	1.8	0.992	9.46	0.181	0.984
	5 phr	0.31	2.23	0.992	8.77	0.169	0.990

It is now clear that the sensitivity or the operating regime for a rubber-based strain sensor could be tailored easily by proper selection of filler type, filler amount, crosslinking degree and use of softening agent or plasticizers. From a sensor perspective, operating regimes of few materials are summarized in Table 4.4. The table provides an outlook over the strain sensitivity (low to high) and possible working strain range (from 10% to 500%) of the developed materials.

4.4 Cyclic piezoresistivity

In order to realize the materials as strain sensors for long-term use, the samples should be capable of recovering after each sensing activity. Being viscoelastic in nature, the recovery is always accompanied by a hysteresis in the stress-strain behavior. Therefore, to evaluate the strain-dependent performance under continuous loading and unloading conditions, cyclic tests are performed with the CB and CNT filled samples.

Table 4.4: Sensitivity rating for various elastomeric composites Low strain (L): 10-50% strain; Medium strain (M): 50-100% strain; High strain (H): > 100% strain.

Constant	Variable		Measurable strain with sensitivity		
			> 10	> 100	> 500
2 phr Sulfur	CB content	12 phr	L	M	M
		13 phr	L	M	H
		15 phr	H	-	-
2 phr Sulfur	CNT content	3.5 phr	L	L	-
		4 phr	L	M	-
		5 phr	L	M	H
		6 phr	L	M	H
12 phr CB	Sulfur content	1 phr	L	M	H
		2 phr	L	M	M
		3 phr	L	L	M
		4 phr	L	L	L
4 phr CNT	Sulfur content	1 phr	L	M	H
		2 phr	L	M	-
		3 phr	L	L	-
		4 phr	L	L	-
3.5 phr CNT	Oil content	1 phr	L	L	-
		2.5 phr	L	L	-
		5 phr	L	M	-
10.5 phr CB	Oil content	1 phr	L	L	-
		2.5 phr	L	L	-
		5 phr	L	L	-

In order to visualize the piezoresistive effect during loading and its recovery upon unloading, samples loaded with high amount of fillers, well above the percolation concentration, are chosen for the study. At a strain rate of 100 mm/min for 20 cycles, the samples were stretched up to 80 % for 13 phr CB and 50 % for 4 phr CNT filled samples. Irrespective of the type of filler, the samples exhibit a tendency to recover its actual conductivity within the given time (Figure 4.8) [32]. For 13 phr CB sample in

Figure 4.8a, a relative resistance change of $\sim 1500\%$ is observed at 80% strain. After a few initial cycles, the change in relative resistance is almost constant with the applied strain [32]. The composites display good recovery, and repeatability. An irrecoverable relative resistance change (resistance set) after 20 cycles was found to be $\sim 200\%$. In Figure 4.8b, the CNT samples display strong piezoresistive effect with relative resistance change of $\sim 3500\%$ at a strain of 50%. Also, in this case, the relative resistance change appeared constant and repeatable after initial few cycles. The relative resistance set after 20 cycles was $\sim 1000\%$, which is significantly higher than carbon black composites. Upon comparing the responses of CB and CNT composites, it is understood that CB samples can withstand the high strain and could serve as sensory materials for high strain applications. The CNT samples, on the other hand, are able to yield sharp responses at relatively lower strains. Both the materials display good recoverability and repeatability, which allows the possibility of use in sensory applications.

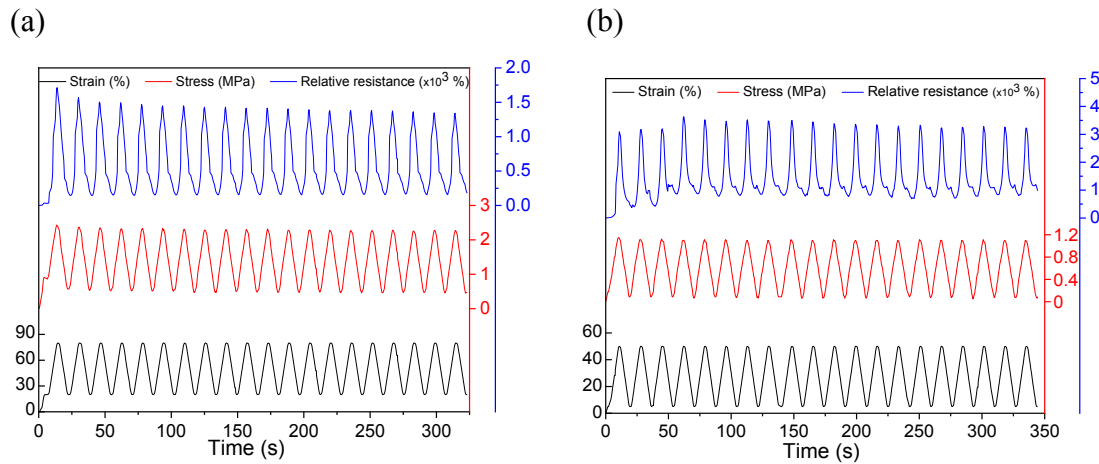


Figure 4.8: Several loading and unloading cycles test of (a) 13 phr carbon black and (b) 4 phr CNT filled composites

Chapter 5

Exploring the piezoresistive properties of SSBR composites under dynamic conditions

A part of the results from this chapter is published in
Rubber Chemistry and Technology, 91(4), **2018**, 651-667.

5.1 Introduction:

In the last section in chapter 4, cyclic tests displayed recoverable piezoresistive characteristics for the SSBR composites and therefore as a further attempt, the piezoresistive characteristics of the materials are studied under complex dynamic conditions. In this chapter, efforts have been laid to understand the relationship between dynamic mechanical properties and piezoresistive behavior. Such dynamic tests would be a challenge to the piezoresistive capabilities of the material because the rubber sample should respond and recover within the given deformation cycle.

As the percolation thresholds of carbon black and CNT are around 10.5 phr and 3 phr, respectively, the dynamic experiments were performed on samples containing filler concentrations higher than their respective percolation thresholds, to ensure high conductivity and strong piezoresistive response. Three different filler concentrations of CB and CNT were selected in such a way, that the dynamic piezoresistivity would cover a wide range of sensitivity. 12 phr CB and 3.5 phr CNT samples display the highest sensitivity, while 15 phr CB and 5 phr CNT exhibit the least. The influence of parameters such as filler content, test frequency, matrix crosslink density and test temperature on the piezoresistive behavior has been studied. The obtained information provided a deeper insight in visualizing the behavior of filler particles and filler network and their influence over the material's dynamic performance.

5.2 Introduction to dynamic tests

In general, a viscoelastic rubber sample responds to the sinusoidal stress with a sinusoidal strain, which is shifted in time and quantified as the characteristic phase shift of the material $\delta_{\sigma-\epsilon}$ [168]. For samples with a piezoresistive character, the dynamic strain will interfere with the filler network and cause a change in electrical resistance. It is believed that the stretching force would increase the interparticle distance between fillers and thereby the electrical resistance is increased [32, 169]. Consequently, when the strain is released, the interparticle distance becomes shorter,

recovering the electrical conductivity [32, 169]. Since the applied deformation is sinusoidal, the electrical resistance of the material is also expected to change in a sinusoidal manner, corresponding to the strain.

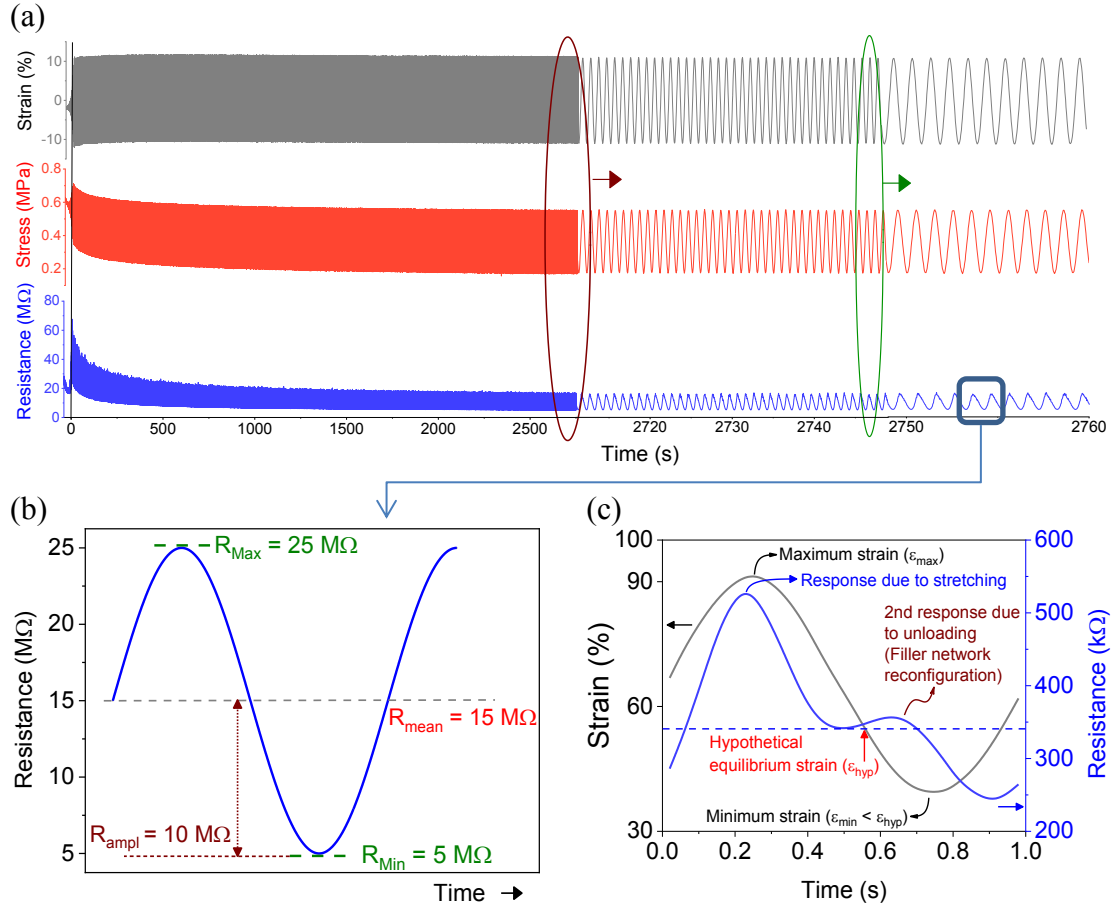


Figure 5.1: (a) Time sweep experiment of a 12 phr CB sample. (Smaller time frames are magnified and shown for better understanding) (b) calculation of mean resistance and dynamic resistance amplitude (c) strain and resistance signal for a 13phr CB sample at 25°C

Figure 5.1a depicts a time sweep experiment performed for a 12 phr CB sample. The raw data are plotted to get a first impression of the piezoresistive behavior as a function of time. Similar to the strain and stress curves, the electrical resistance profiles appear to be sinusoidal in nature. The resistance data comprise two important information as shown in Figure 5.1b. Firstly, the ‘mean electrical resistance’ (R_{mean}) is evaluated as the average from maximum and minimum of the electrical resistance signal, and calculated as per Eq.5.1, also be inferred as the offset of the electrical resistance signal from the x -axis. This quantity represents the actual or overall piezoresistance of the bulk sample. Secondly, the ‘dynamic electrical resistance

amplitude' (R_{ampl}) can be calculated from the difference between the maximum and minimum values as per Eq.5.2. This quantity represents the instantaneous piezoresistance change due to the dynamic strain [27, 155]. These two values together provides insight on the material's piezoresistive performance and its behavior under dynamic loading. In Figure 5.1a, the mean electrical resistance and the dynamic electrical resistance amplitude values of the material are found to decrease over time. Moreover, the recovery of the material is not monotonous during unloading and a second piezoresistive response is often observed as shown in Figure 5.1c (will be discussed later in sub-section 5.3.3).

$$\text{Mean electrical resistance } (R_{mean}) = \frac{R_{max} + R_{min}}{2} \quad \text{Eq.5.1}$$

$$\text{Dynamic electrical resistance amplitude } (R_{ampl}) = \frac{R_{max} - R_{min}}{2} \quad \text{Eq.5.2}$$

where R_{max} and R_{min} are the maximum and minimum values of the dynamic electrical resistance respectively.

5.2.1 Difference in relaxation under static and dynamic conditions

Normal quasi-static stress relaxation tests could be performed in universal testing machines (UTM) or with even simpler endurance testers. However, the distinctive advantage of using DMA to the study stress relaxation is the ability to understand the influence of dynamic forces and other dynamic parameters such as frequency and temperature on the uniaxial stress relaxation behavior. A comparative experiment is performed to highlight the influence of dynamic load on stress relaxation. Figure 5.2a compares the stress values obtained from a normal quasi-static stress relaxation experiment and the mean stress values calculated from a dynamic measurement. Figure 5.2b compares the resistance values obtained from the quasi-static stress relaxation experiment and the calculated mean electrical resistance values (as defined before) from the dynamic measurement. For the dynamic experiment, a dynamic strain of 30 % at 1 Hz is applied on a 60 % pre-strained sample at 35 °C (slightly higher than room temperature). For the quasi-static stress relaxation test, the stress and resistance are monitored by applying 60 % strain at 35 °C. In Figure 5.2, the electrical resistance appears to follow a similar relaxation profile like the stress decay,

under quasi-static as well as under dynamic conditions. Interestingly, the magnitude of the stress relaxation (the difference between initial and final value) without dynamic load is found to be less pronounced as compared with the mean stress profile (Figure 5.2a). Moreover, it is evident from the figures that the relaxation in terms of electrical resistance is much stronger than stress for the same sample. The sharp decrease in stress and resistance values under dynamic loading conditions could be caused by the fact that the dynamic oscillations alter the morphology or arrangement of the conducting filler particles, resulting in more conducting pathways.

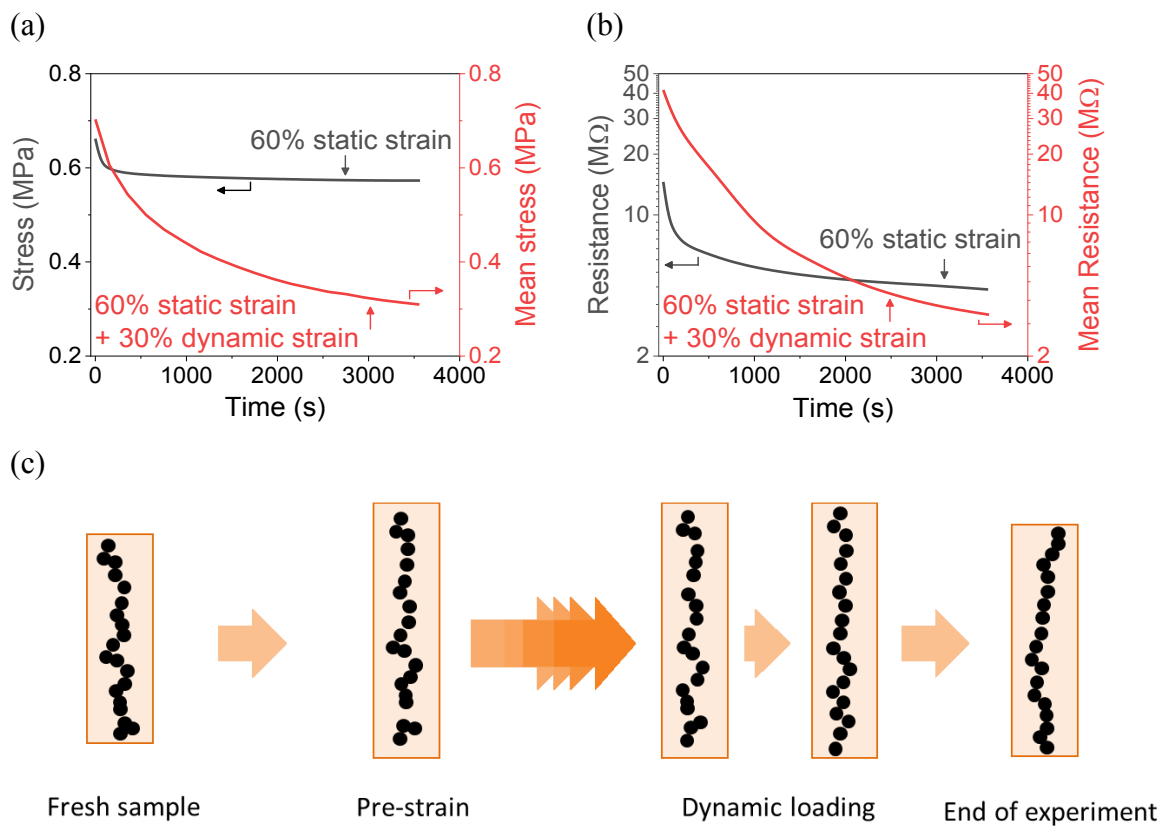


Figure 5.2: (a) Stress profile of 12 phr CB with and without dynamic load (without dynamic load refers to stress relaxation experiments) (b) Resistance profile of 12 phr CB with and without dynamic load (c) Deformation mechanism of conducting rubber sample during dynamic loading, the filler network become compact and coherent, resulting in higher conducting pathways.

A plausible, but still rough mechanism for the high changes in electrical resistance values during dynamic experiments is given in the scheme in Figure 5.2c. Since the samples are pre-strained, a pre-load forces the filler particles to align along the

stretched (longitudinal) direction. Additionally, the dynamic strain will destroy the larger filler clusters. So, in the dynamic experiment, the filler clusters are broken-down into smaller clusters and forced to orient along the longitudinal direction. These two effects together may reduce the interparticle distance between fillers over time and drive the particles to be aligned coherently, resulting in the formation of more conducting pathways in the filler network, which could be assumed as kind of ‘rearrangement’. As a consequence, the mean electrical resistance values are found to decrease. The tunneling theory [112, 134] also supports our mechanism, as in Eq 2.2 resistance is described as a function of interparticle distance $R \propto s$ and in Figure 5.2b, the decrease in electrical resistance with time, therefore, signifies that the interparticle distance between the conducting fillers is reducing with time.

5.2.2 Mean stress and mean electrical resistance

Mean stress values are calculated similarly to the mean electrical resistance from Figure 5.1a as per Eq.5.1 at regular time intervals and plotted in Figure 5.3a. It is obvious that the electrical resistance also exhibits an exponential decay pattern like the stress. Piezoresistivity arises due to changes in the filler network; therefore, focusing on the changes in electrical resistance is more relevant to this work, *i.e.* to visualize the filler networking and its behavior under various conditions. Figure 5.3b depicts the normalized curves, obtained as per Eq 5.3 and Eq 5.4. Such normalization would be helpful in comparing the piezoresistive performances of different samples at different experimental conditions.

$$\text{Relative stress } (\sigma/\sigma_0) = \sigma(t) / \sigma(0) \quad \text{Eq.5.3}$$

$$\text{Relative resistance } (R/R_0) = R(t) / R(0) \quad \text{Eq.5.4}$$

Where $\sigma(t)$ is the stress in the composite at given time t and $\sigma(0)$ is the stress value recorded at time $t = 0$ (*i.e.* the instance when the experiment starts and the static and dynamic load are applied on the sample as shown in Figure 5.1a). $R(t)$ is the electrical

resistance of the composite at given time t and $R(0)$ is the electrical resistance at time $t = 0$.

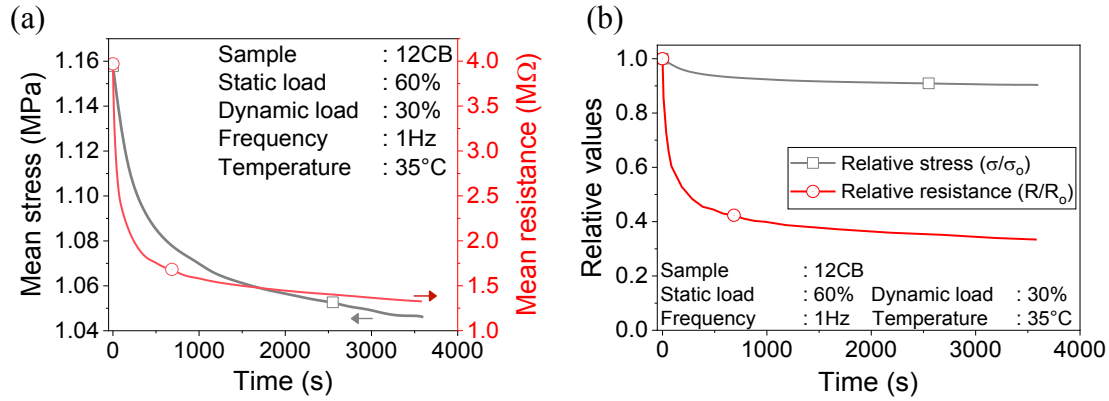


Figure 5.3: (a) Relaxation of mean stress and mean electrical resistance and (b) relative values of a 12phr CB filled sample during a time sweep experiment.

5.3 Time sweep measurements

5.3.1 Influence of the four major parameters (filler content, temperature, frequency and crosslink density) on mean resistance

The normalized piezoresistive changes (relative resistance) are studied at different experimental conditions and summarized in Figure 5.4. In Figure 5.4a, the maximum piezoresistive change is observed for 12-CB sample (magnitude of change in relative resistance from beginning [$t=0$] to the end of the experiment [$t=3600$]). This sample experiences a high rearrangement of the filler clusters due to the dynamic load, as per the rearrangement mechanism shown in Figure 5.2c. Due to the fact that the CB-filled samples exhibit an electrical percolation threshold of 10.5 phr [170], the 12CB sample is close to the percolation regime, displaying a high strain sensitivity. The 13CB and 15CB samples display less change because the conducting pathways are strongly established. This leads to lower sensitivity towards change in the resistance values with respect to the given dynamic strain [169, 170]. From Figure 5.4b, it could be noted that the change in electrical resistance is more pronounced at low temperatures. An explanation for this could be that at lower temperatures the rubber molecules are relatively stiffer and the applied force transfer to the particle network would take

place more promptly, which in turn destroys the filler-filler network and a high degree of rearrangement of the percolating network takes place.

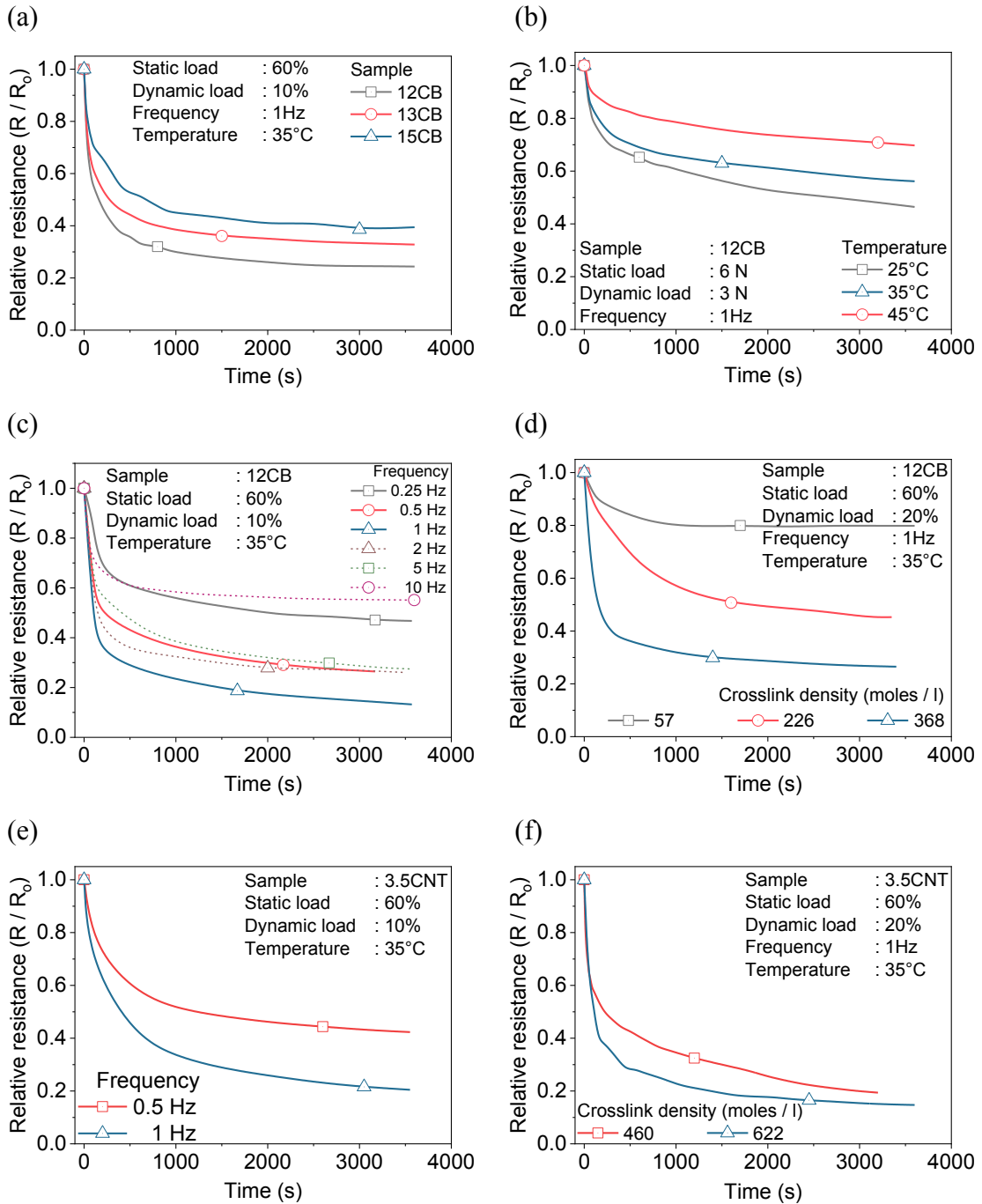


Figure 5.4: Relative resistance plots of (a) carbon black composites with different filler loading and 12phr CB samples at different (b) temperatures, (c) test frequencies and (d) crosslink densities and 3.5phr CNT samples (e) at low test frequencies and (f) with different crosslink densities.

Similar to temperature dependency, the relative resistance was also found to be dependent on test frequency. It could be noted in Figure 5.4c that at a frequency of

1 Hz, the change in relative resistance is the highest compared to the values obtained at higher or lower frequencies. It is assumed that the frequency of ~1 Hz is associated with the dynamics of destruction and reformation of conductive pathways of the filler network. At frequencies lower than 1 Hz, the breakdown of filler clusters would be minimal as they have sufficient time to re-orient and reconfigure during dynamic loading. For measurements greater than 1 Hz, the test frequency is higher than the time required for rearrangement. This is clearly obvious from the measurement at 10 HZ, where the least change is observed.

The crosslink density of the rubber has an impact on re-establishing the conducting pathways. The extent of relative resistance change due to rearrangement of the percolating network is found to be higher for the higher crosslinked sample as shown in Figure 5.4d. Samples with less crosslink density are already well percolated [170] and moreover, due to less matrix stiffness, the filler clusters would experience less destruction and therefore incur less rearrangement of the percolating network. When the carbon black was replaced by CNT, comparable effects are found, as obvious from Figure 5.4e&f. The rearrangement of the percolating network under dynamic conditions is found to be independent of the filler type or morphology (carbon black are particulate in nature and carbon nanotubes are fibrous having high aspect ratio).

5.3.2 Major parameters and electrical resistance amplitude

When the dynamic load is applied to the sample, they immediately disrupt the filler network and cause a proportionate change in electrical resistance. This instantaneous piezoresistive change could be measured from the amplitude of the obtained electrical resistance signal (R_{ampl}) as per Eq 5.2. The resistance amplitudes normalized by the initial value (at $t = 0$) are summarized for various CB and CNT samples in Figure 5.5. It could be noted from the figures that the dynamic resistance amplitudes reduce with time. Meaning, the temporal changes in the filler network become less with time. This further supports our proposed mechanism in Figure 5.2c. As the filler network has become more coherent due to rearrangement of the percolating network, it displays less instantaneous piezoresistive effect for the same dynamic strain.

Figure 5.5a display the resistance amplitude ratios for samples with different filler content. In the figure, 12CB sample displays the highest difference in resistance amplitudes. Earlier in Figure 5.4a, this sample displayed the highest change in mean resistance due to rearrangement of the percolating network. Therefore, as a consequence of the rearranged filler network, high reduction in instantaneous piezoresistivity is also observed. Figure 5.5b summarizes the resistance amplitude changes for 12 CB sample at different frequencies. The change in relative resistance amplitude values is found to show a maximum at a frequency of 1 Hz. At lower and higher frequencies, relatively less change is noticed. This concedes with the findings from Figure 5.4c, *i.e.*, where 1 Hz is identified as the critical frequency and a maximum rearrangement of the percolating network is observed.

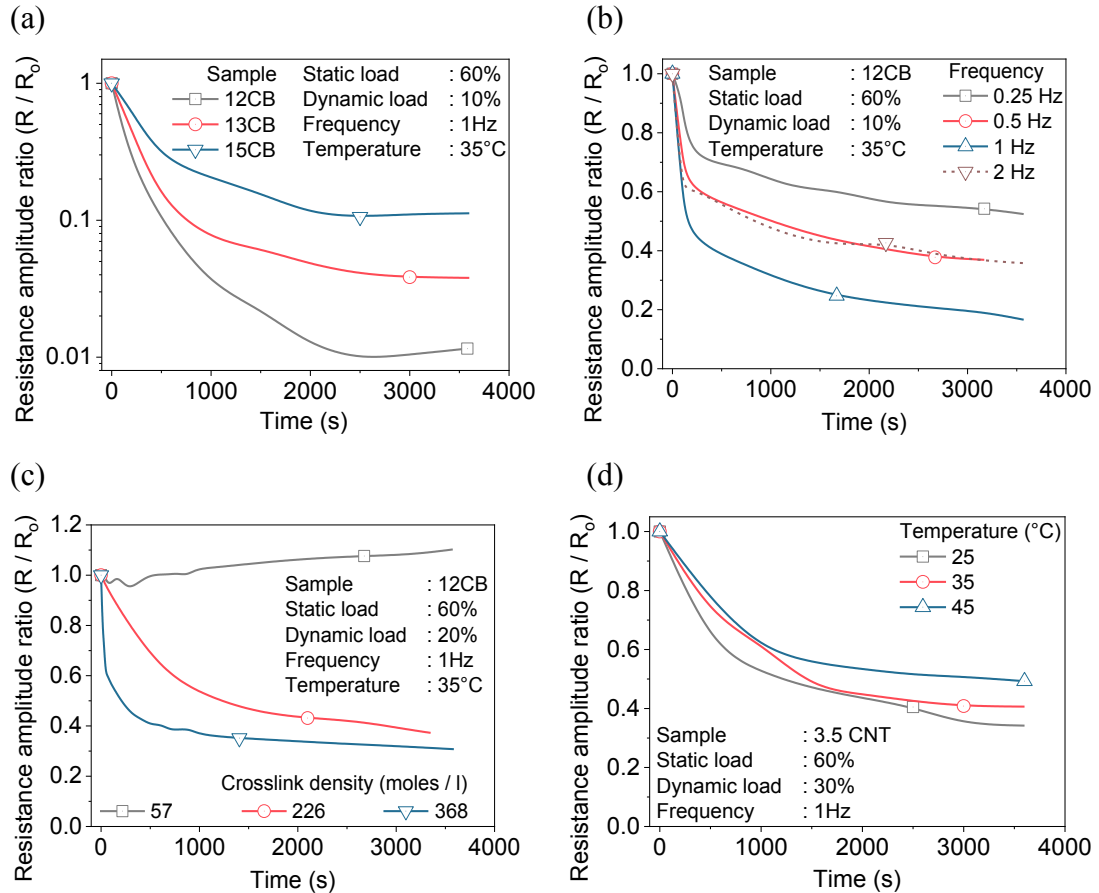


Figure 5.5: Dynamic resistance amplitude ratio of (a) different CB content, 12phr CB composites at different (b) frequencies, (c) crosslink-densities and (d) 3.5phr CNT composite at different temperatures

The resistance amplitude changes for 12 CB sample with different crosslink densities are summarized in Figure 5.5c. A higher change in dynamic resistance amplitude is observed for samples with higher crosslink density and correlates to the findings in Figure 5.4d. However, in the case of the least crosslinked sample, the dynamic amplitude is found to increase with time. Therefore, the filler clusters seem to undergo less rearrangement (of the percolating network) and rather experiences a higher destruction by the dynamic load. This could be the reason for the less change in mean resistance values observed earlier in Figure 5.4d for the least crosslinked sample. The influence of temperature on resistance amplitudes is summarized in Figure 5.5d. Increase in temperature reduces the extent of instantaneous piezoresistance change, which coincides well with the mean resistance changes observed earlier in Figure 5.4b for the CB samples. The extent of rearrangement of the percolating network is highest at 25 °C and likewise, the highest change in relative dynamic resistance amplitude is also being observed at 25 °C.

5.3.3 Analyzing the nature of the dynamic piezoresistive response

5.3.3.1 Causes for dynamic piezoresistive response

In course of the dynamic experiments, an atypical second response is observed in the resistance signals as shown in Figure 5.1c. Few publications report about such second peaks in piezoresistive behavior [35-38]. Kost *et al.* reasoned the cause of the second peaks could be due to orientational effects, *i.e.*, the filler network tends to orient along the longitudinal direction during loading, and while unloading the oriented filler network breaks down into a random network producing these second peaks[33]. Yamaguchi *et al.* stated that the time between loading and unloading is short and there is a competition between filler network destruction and reformation, *i.e.*, before complete network recovery, the subsequent loading cycle starts and destroys the network, which results in second peaks[35]. Zhang *et al.* reported that cyclic experiments are performed over a long time and the loading history from the previous cycles adds up; reflected as second peaks[171]. Yamaguchi *et al.* also reported that filler network destruction during loading could be much faster than the reformation during unloading and this dissimilarity causes the second peaks[35]. As pointed out

earlier, the second peaks are only observed during the unloading step and it is plausible that the peaks are an outcome of filler network reconfiguration.

Considering the explanations in the literature [35-38] and from our findings, we summarize the mechanism for the second peaks as follows: In course of the dynamic/cyclic experiment, the equilibrium of the filler network would be shifted to a hypothetical strain (ε_{hyp} , see in Figure 5.1c). The electrical resistance decreases smoothly until this point during unloading. When the strain is reduced further than the hypothetical equilibrium ($\varepsilon < \varepsilon_{hyp}$), an increase in electrical resistance is observed, indicating filler network reconfiguration. A maximum reconfiguration is observed when the strain reaches its minimum (ε_{min}). These intermediate reconfiguration processes are reflected as a second peak. A higher tendency for the filler network to reconfigure would be reflected as higher/taller second resistance peak. Figure 5.6 depicts the behavior of second peaks with respect to time for a 12-CB sample. The intensities of the second peaks are initially subtle but gets stronger with time. After a few cycles, the second peaks are found to be prominent and consistent. Therefore, these peaks are definitely a characteristic piezoresistive response of the material [37, 38].

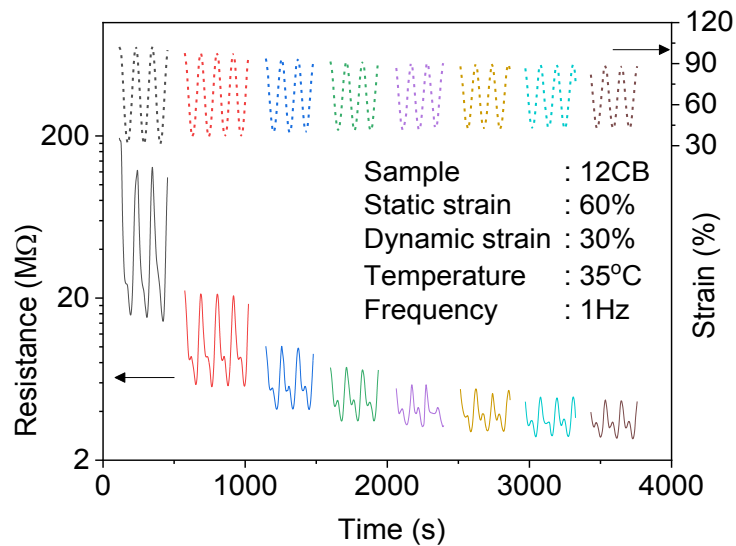


Figure 5.6: Evolution of the second peak with time for 12 phr CB sample.

5.3.3.2 Major parameters and second peaks

Figure 5.7a depicts the piezoresistive responses for samples with different filler content after 1 hour. As the amount of filler increases from 12 phr to 15 phr, the intensity of the second peaks becomes much stronger. So, the extent of filler network reconfiguration during unloading is higher as the amount of filler is increased. This effect could be attributed to the higher filler concentration, which reduces the free volume of the rubber matrix and imposes higher stress on the filler network during unloading. Figure 5.7b depicts the influence of temperature. The intensities of the second peaks are strong at room temperature and become subtle at higher temperatures. High temperatures encourage higher filler mobility and facilitate a smoother reconfiguration of the filler clusters, thereby eliminating the need for a forced network reconfiguration.

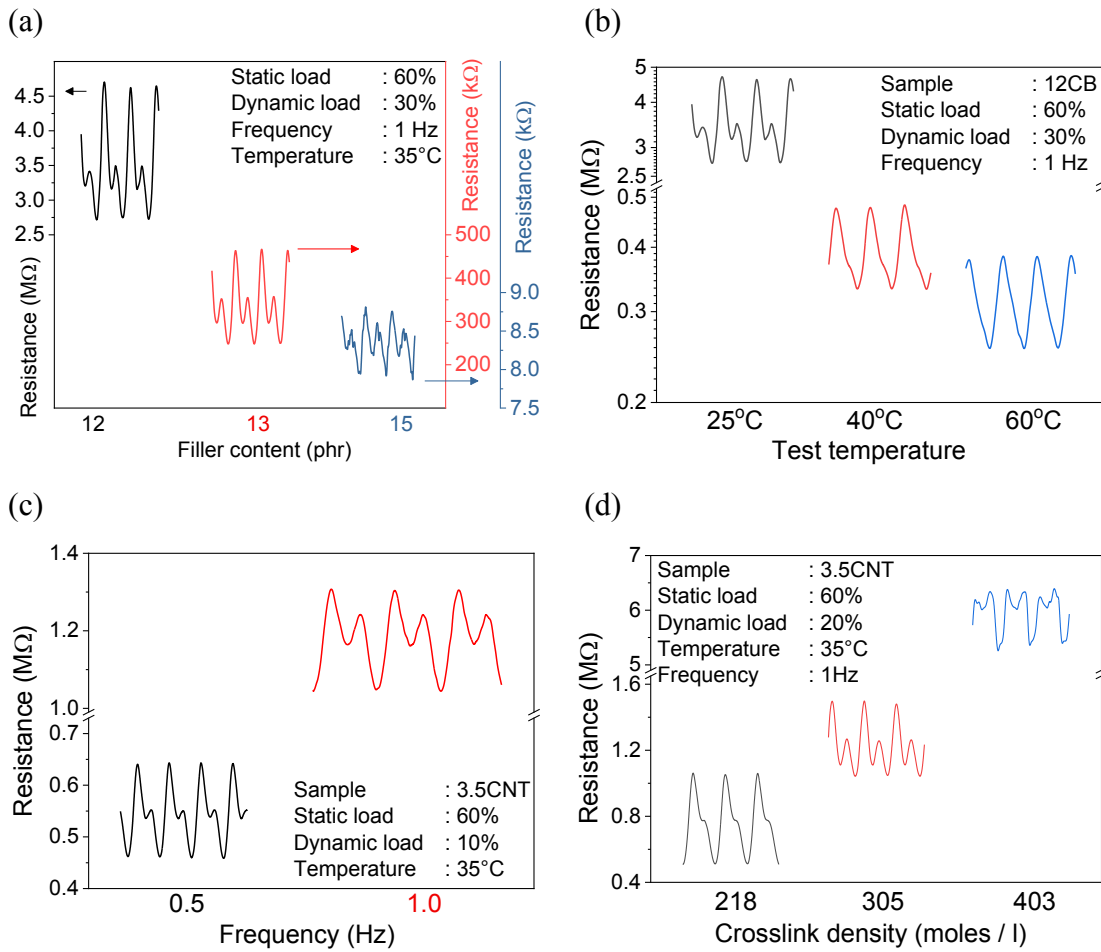


Figure 5.7: Second peaks summarized after 1 hour for (a) different CB content, (b) 12 phr CB at different temperatures, (c) 3.5 phr CNT sample at different frequencies and (d) 3.5 phr CNT sample with different crosslink densities.

In [Figure 5.7c](#) the CNT samples display second peaks even at 0.5 Hz. So, a time of 2 sec is not sufficient for the CNT clusters to smoothly reconfigure between the loading-unloading cycles. Therefore, during unloading, the filler clusters are subjected to a forced reconfiguration. The intensity of the second peak at 1 Hz is much stronger, indicating higher stress and higher reconfiguration than the low frequencies. In [Figure 5.7d](#) a smoother reconfiguration is facilitated by the less crosslinked 3.5 phr CNT samples, as obvious from the subtle second peaks. The intensities of second peaks are stronger and prominent with higher crosslinks, as a consequence of high degree of filler network reconfigurations.

5.4 Dynamic temperature sweep measurements

5.4.1 Influence of major parameters on mean and dynamic resistance

The change in electrical resistance is studied over different temperatures to further understand the dynamic piezoresistance. In these experiments, the temperature is gradually decreased from 60 °C to the glass transition temperature ($T_g \sim -15$ °C) of the rubber. The relative resistance values are calculated as per [Eq. 5.3](#) and summarized for various composites. [Figure 5.8a](#) shows the relative resistance values for different concentrations of carbon black. The mean resistance values are found to increase gradually with the decrease in temperature for all the samples. The sample with 12 phr of CB shows the highest dependence on temperature, it became insulating (*i.e.* the electrical resistance is higher than 300 MΩ and cannot be measured with our data recorder) at around 0 °C. The sample with 13phr of CB becomes non-conducting at less than -5 °C. In the case of 15 phr CB, the filler network is well percolated and therefore, the conducting pathways are stable enough to withstand high deformations near to T_g . At low temperatures, the rubber molecules have less mobility and once the filler-filler network is broken, the reformation process becomes more and more hindered. This irrecoverable damage results in a reduction in the effective number of conducting pathways and finally, attributes to a permanent non-conducting behavior. This was also realized when temperature scans were performed from T_g to high temperatures. The samples lost their conductivity immediately at the start of the experiment. Moreover, it takes a much longer time, *i.e.*, until a sufficiently high

temperature is reached by the sample to recover and become conducting again. This problem poses the difficulty to start the experiments from low temperature.

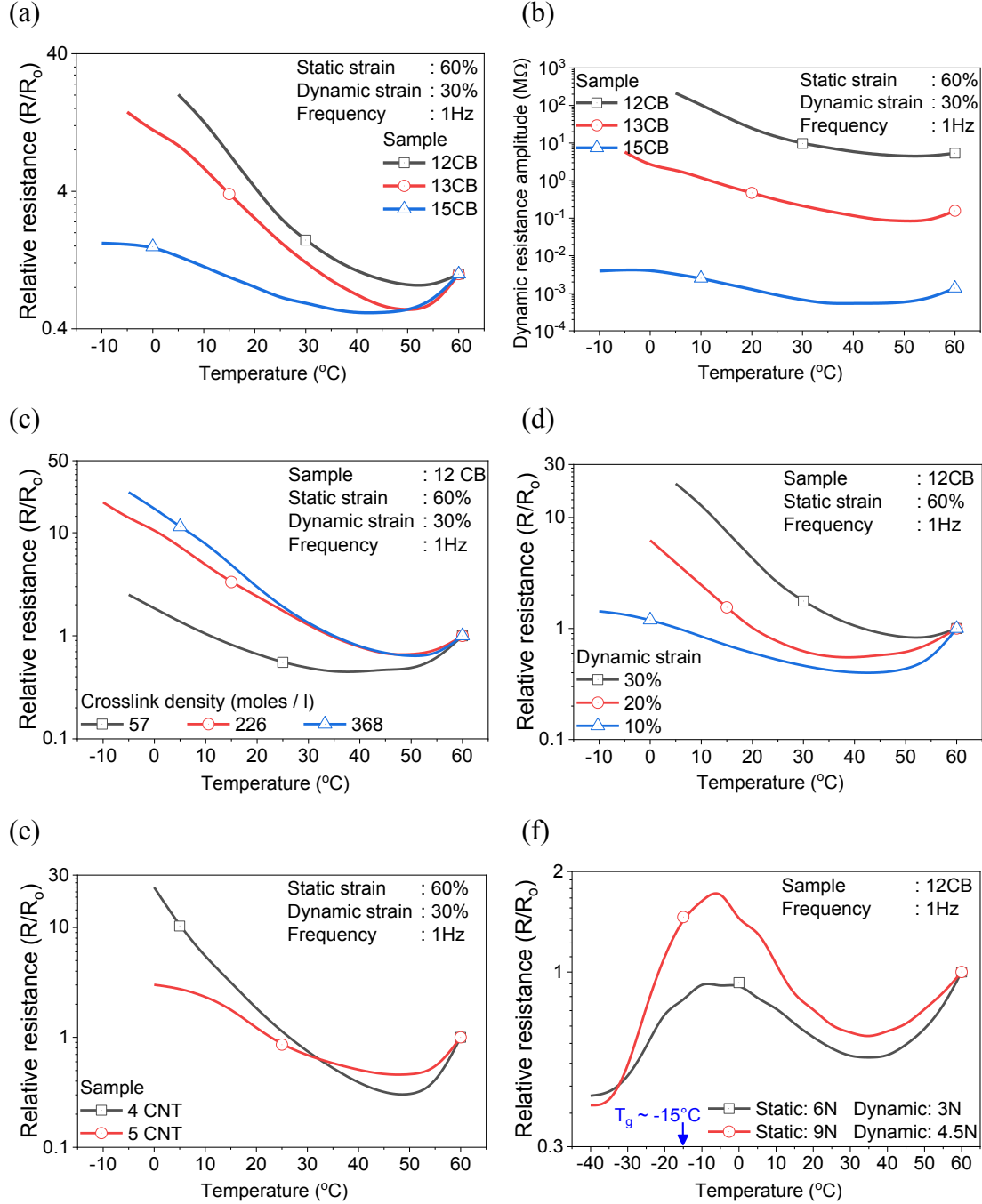


Figure 5.8: Change in (a) relative resistance and (b) dynamic resistance amplitude against temperature for different CB content. Change in relative resistance for 12phr CB sample (c) with different crosslink densities, (d) at different dynamic strains. (e) CNT samples with different filler levels and (f) 12CB sample tested with less force. [For all the cases, the temperature sweeps are performed from high (60°C) to low temperatures]

The instantaneous piezoresistance change (dynamic resistance amplitude) in [Figure 5.8b](#) is higher at low temperatures (in comparison to the values 60 °C). As mentioned earlier, the effective number of conducting pathways becomes lesser at low temperatures. Therefore, only a few remaining conducting pathways (that still exist at low temperatures) are expected to respond to the given dynamic load. Due to this fact, higher dynamic resistance amplitudes are observed for the same dynamic strain at much lower temperatures. This process continues up to a certain temperature where all the conducting pathways are destroyed, and the sample becomes insulating.

In [Figure 5.8c](#), the less cross-linked sample shows less dependence over temperature as it favors higher filler mobility. The 12 CB samples tested with constant static, but different dynamic strains are summarized in [Figure 5.8d](#). At a low dynamic strain of 10 %, the samples display less change in relative resistance (less than a value of 2) over the temperature range. Even for such a low dynamic strain, the sample displays piezoresistive characteristics near the T_g . The highest dependence is observed when 30 % dynamic strain is being imposed. The samples became non-conducting at 10 °C. It is imagined that high dynamic strain intensely destroys the filler network and results in non-conducting nature much earlier. CNT filled samples in [Figure 5.8e](#) also displays similar response like CB, *i.e.* highly filled CNT samples show less dependence on temperature signifying that the concept is applicable for both filler types. Since all the samples became non-conducting around T_g , an experiment is performed with relatively less force and depicted in [Figure 5.8f](#). The low force is to ensure that the filler network is not destroyed. This allows examining the piezoresistive properties of the samples at temperatures lower than T_g . The samples displayed a rearrangement of the percolating network from 60 °C down to 35 °C evidenced by the decreasing relative resistance values. Hereafter, the relative resistance values are found to increase gradually due to the obvious effects mentioned earlier. At temperatures lower than T_g , the relative resistance values are found to decrease significantly. This could be due to the high matrix stiffness and for the applied force; the samples would be sparingly stretched. This would cause a negligible change in the filler clusters and in-turn results in a less piezoresistive effect.

5.4.2 Major parameters and second peaks

The intensities of second peaks are compared in Figure 5.9a for a 12 phr CB sample to understand their behavior over temperature. The intensity of the second peaks is low at high temperatures and becomes stronger as temperature reduces. Distinct second peaks are observed below 20°C, signifying high reconfiguration in the system during the unloading cycles below room temperature.

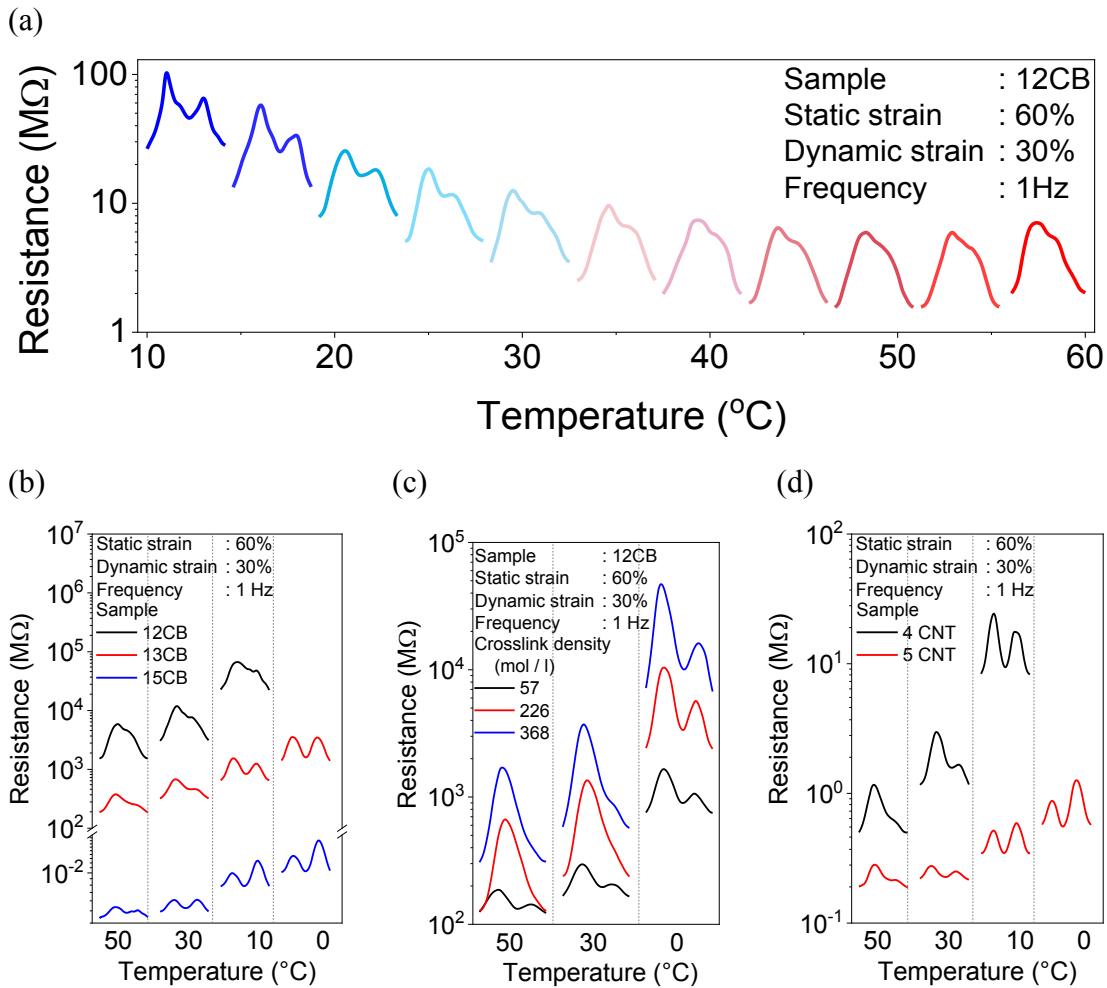


Figure 5.9: Dependence of the second peak on temperature for samples (a) with different concentrations of carbon black, (b) 12CB with different crosslink densities and (c) with different concentrations of CNT

Figure 5.9b depicts the resistance responses for samples with differing filler fractions. For the sample with 12 phr CB, the influence is subtle initially and becomes significant at ~10 °C. The 13 phr and 15 phr CB samples display second peaks even at high temperatures, which become stronger at 0 °C. It is interesting to note that at 0 °C,

the intensities of first and second peaks are almost similar in the case of 13 phr CB sample, while for 15 phr CB samples, the intensity of the second peak is even stronger than the primary signal. It turns out that the changes in the filler network in these samples during the loading process are considerably less than the changes happening in the filler network during unloading. This effect could be attributed to the high filler fraction, which reduces the free volume and results in higher stress in the rubber matrix during the unloading phase. [Figure 5.9c](#) depicts the dependence of a 12 phr CB sample with different crosslink densities. All the samples show a rather small effect at high temperatures and strong second peaks at low temperatures. Samples with higher crosslink densities show high resistance, high resistance amplitudes and higher influences of second peaks. This could be due to the crosslinks imposing hindrance to filler mobility and also decreasing the free volume, which in turn contributes to the aforementioned effects. Also, for the different CNT samples in [Figure 5.9d](#), small effects at high temperatures and significant peaks at low temperatures are clearly noticeable. Also, in this case, 5 phr CNT samples show stronger second peaks at low temperatures, similar to highly filled 15 phr CB samples. The second peaks are clearly a characteristic consequence of the piezoresistive effect, which is observed for both of the conducting fillers, vastly influenced by the filler fraction, matrix viscosity and temperature.

5.5 Dynamic strain sweep measurements

The non-linear dependence of the elastic modulus (E') over the strain amplitude for a viscoelastic material is well established and known as 'Payne effect' [172]. The same concept was extended to study the relationship between dynamic mechanical strain amplitude and electrical resistance. [Figure 5.10a](#) depicts the change in conductance over a dynamic strain sweep experiment. In this figure, the electrical conductance increases up to a certain strain, followed by a sharp decrease. The initial gain in conductance could be related to the very low strain amplitudes that facilitate possible filler network orientations (rearrangement of the percolating network) along the longitudinal direction and enhancing the number of effective conducting pathways.

When strain amplitudes exceed a critical limit, the filler network is destroyed; disrupting the percolated conducting pathways and causing a sharp decrease in

conductance. This critical strain is found to be around 5 % and 7 % for 12 phr and 13 phr CB respectively. Until this point, filler network formation predominates and beyond, the destruction process predominates. In Figure 5.10b the 12 CB sample display the same tendency even at a higher temperature. However, in this case, the critical strain is shifted to ~15 %; this could be due to the influence of the high temperature as a smooth rearrangement of the percolating network may be still possible at higher strains. It is well known that the critical strain of mechanical filler network breakdown (γ_c) is represented by the maxima in the plot of loss modulus (E'') against dynamic strain [173]. Interestingly, from Figure 5.10c&d can be observed that this critical strain of filler network breakdown coincides exactly with the critical strain observed in the case of electrical conductance.

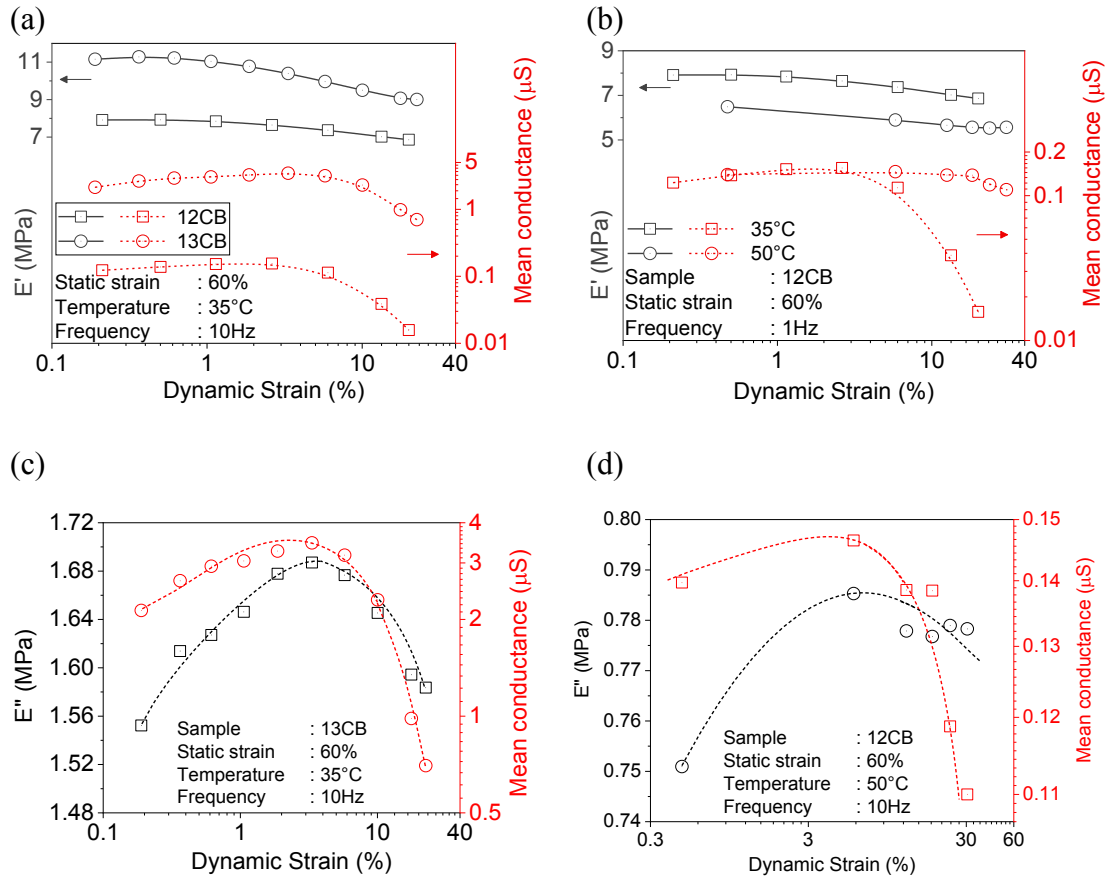


Figure 5.10: Dependence of elastic modulus (E') and mean conductance over dynamic strain for (a) different CB content and (b) 12 CB sample at 50 °C. Dependence of loss modulus (E'') and mean conductance over dynamic strain for (c) 13 CB sample at 35 °C and (d) 12 CB sample at 50 °C.

5.6 Hysteresis profiles under temperature sweep experiments

The dynamic loading data are plotted in the form of stress-strain or resistance-strain loops to understand the hysteresis of the material. In Figure 5.11a, the stress hysteresis shifts slightly as temperature reduces. Interestingly in Figure 5.11b, hysteresis is also observed in resistance, which shifts upwards as temperature decreases. The increase in resistance values at low temperatures could be ascribed to the earlier discussions from Figure 5.8. Interestingly, the change in shape of the hysteresis loops at lower temperatures is an effect related to the second peaks. The second peaks are initially subtle, therefore display smooth hysteresis profiles. With temperatures nearing T_g the effect of second peaks becomes prominent, reflecting as disfigured hysteresis curves.

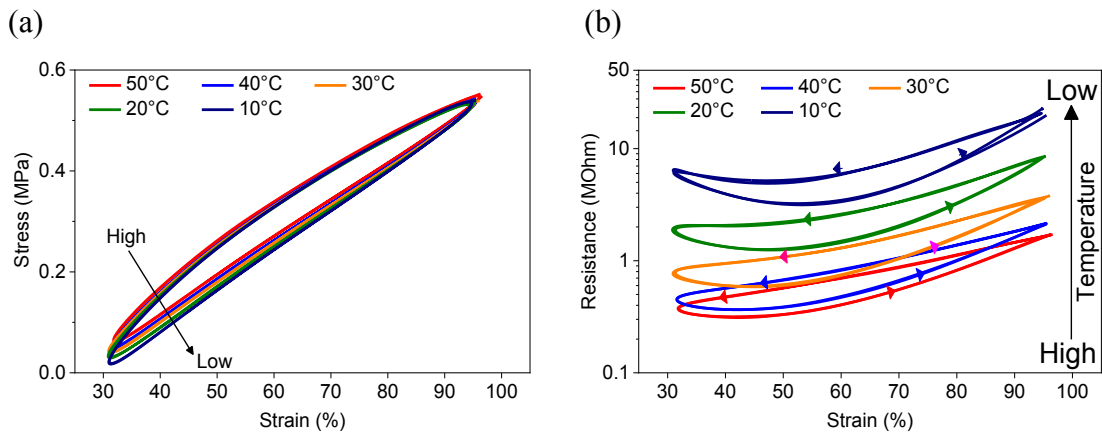


Figure 5.11: (a) Stress hysteresis profiles (b) Resistance hysteresis profiles of 12phr carbon black sample at different temperatures plotted from dynamic temperature sweep experiments.

Chapter 6

Predicting the mechanical performance and
filler network behavior using dynamic
piezoresistivity

6.1 Introduction

In chapter 5, the mean stress values and the mean electrical resistance values displayed relaxation behavior under time sweep experiments, which appeared similar in terms of magnitude. Exploiting this similarity, a correlation is established between mechanical stress relaxation and piezoresistance in this chapter. The relationship between stress and resistance was found to be valid at various conditions of frequency and temperature for samples with different filler content and matrix crosslink density. This allows an estimation of stress relaxation from the electrical resistance data, which could be a practical and viable new method for performance monitoring of elastomer materials.

When rubbers are subjected to dynamic strain, they display a short delay in responding to the applied load and are characterized as phase shift δ . The concept of phase shift ($\delta_{\sigma-\epsilon}$) between stress and strain was extended to electrical resistance and a characteristic piezoresistive phase shift between mechanical stress and electrical resistance ($\delta_{R-\sigma}$) was deduced with the help of Fourier transformation. The change in piezoresistive phase shift was studied at different experimental conditions. Finally, the behavior and characteristics of the second peaks are studied in detail by separating the first and second piezoresistive peaks that occur during loading and unloading respectively. The deduced individual peak amplitudes were also studied at various experimental conditions. To study the kinetics, the ratios of their amplitudes were compared during time and temperature sweep experiments.

6.2 Correlating stress and resistance relaxations

In Chapter 5, the mean stress values are found to display exponential relaxation behavior during the time sweep experiments. The Maxwell – Wiechert model [158], explained by Eq 3.3 would be able to perfectly define the stress relaxation behavior. Since the mean resistance values also exhibit a similar exponential decay, the same model could be utilized and Eq 6.1 presents the modified equation to define the piezoresistance relaxation behavior.

$$R(t) = R_f + \sum_{m=1}^3 r_m e^{-t/\tau_{r_m}} \quad \text{Eq. 6.1}$$

where $R(t)$ is the resistance of the sample at time t , R_f is the residual resistance, r_m are resistance relaxation coefficients, τ_r are the relaxation times for the resistance.

Fitting the same relaxation model for stress and piezoresistance allows us to study and correlate the mutual dependencies. For utilizing the piezoresistance data to predict the stress relaxation behavior, the similarity in stress and piezoresistance relaxation profiles is once again exploited. Since the relaxation profiles appear similar (an exponential decay) and the rubber matrix is also the same, we assume that the relaxation times for piezoresistive change and the stress relaxation would be similar.

Therefore, besides using the same model, the relaxation times obtained from the relative resistance fit ($\tau_{r_1} < \tau_{r_2} < \tau_{r_3}$) are utilized to fit the relative mean stress values.

6.2.1 Different filler loading

Figure 6.1a depicts the relative resistance plots of samples containing different concentrations of CB. It can be found that the stress relaxation and piezoresistance changes in the materials are following a similar trend and display relaxation curves during the time sweep experiment. The experimental data are fitted with Eq 6.1 and the fit parameters are summarized in Table 6.1. Figure 6.1b shows the relative mean stress values, fitted with Eq 3.3 by fixing the relaxation times to τ_{r_1} , τ_{r_2} , and τ_{r_3} obtained from the earlier resistance fit. R^2 values > 0.99 indicate that the stress relaxation behavior could be perfectly fitted and described by the same relaxation times. So, the assumption of a single relaxation time to define stress and piezoresistive relaxation holds true, *i.e.*, $\tau_{r_1} = \tau_{s_1} = \tau_1$; $\tau_{r_2} = \tau_{s_2} = \tau_2$; $\tau_{r_3} = \tau_{s_3} = \tau_3$. The deduced stress relaxation coefficients are also summarized in Table 6.1.

The fact that the materials having common relaxation times is certainly advantageous, as correlating the relaxation coefficients and residual values would now suffice to deduce a relationship between stress relaxation and the piezoresistive behavior of the material.

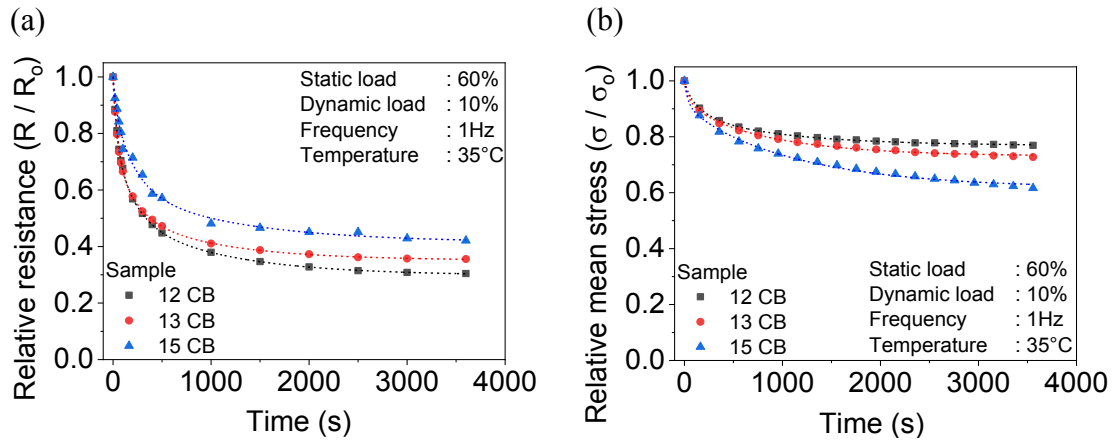


Figure 6.1: Relaxation profiles for samples with various carbon black loading (a) relative resistance and (b) relative mean stress. [Symbols represent the experimental data and dotted lines represent the fitted curves]

Table 6.1: Relative resistance and relative mean stress fit data for samples with different carbon black loading

Sample	Relative resistance			Relative mean stress		
	Coeff	Value	R^2	Coeff	Value	R^2
12 CB	R_f	0.29	0.999	σ_f	0.76	0.999
	r_1	0.22		s_1	0.03	
	r_2	0.26		s_2	0.09	
	r_3	0.21		s_3	0.1	
	τ_1 (s)	42		τ_1 (s)	42	
	τ_2 (s)	195		τ_2 (s)	195	
	τ_3 (s)	1010		τ_3 (s)	1010	
13 CB	R_f	0.35	0.999	σ_f	0.73	0.999
	r_1	0.24		s_1	0.06	
	r_2	0.23		s_2	0.04	
	r_3	0.17		s_3	0.16	
	τ_1 (s)	40		τ_1 (s)	40	
	τ_2 (s)	201		τ_2 (s)	201	
	τ_3 (s)	947		τ_3 (s)	947	
15 CB	R_f	0.41	0.999	σ_f	0.61	0.998
	r_1	0.1		s_1	0.08	
	r_2	0.28		s_2	0.02	
	r_3	0.19		s_3	0.27	
	τ_1 (s)	35		τ_1 (s)	35	
	τ_2 (s)	212		τ_2 (s)	212	
	τ_3 (s)	1183		τ_3 (s)	1183	

6.2.2 Major parameters and stress relaxation behavior

Before deducing a relationship between stress and piezoresistivity, it is vital to study the influence of critical parameters such as temperature, frequency and crosslink density on the relaxation behaviors. Therefore, the mean stress and resistance values for 12 phr CB samples tested at various experimental conditions are fitted and summarized in Figure 6.2a-f and Table 6.2.

Table 6.2: Relative resistance and relative mean stress fit data at various test conditions

	Temperature (°C)			Frequency (Hz)						Crosslink density (moles/l)		
	25	35	45	0.25	0.5	1	2	5	10	57	226	368
R_f	0.45	0.55	0.57	0.40	0.22	0.08	0.23	0.25	0.55	0.80	0.45	0.25
r_1	0.08	0.06	0.09	0.41	0.27	0.35	0.30	0.35	0.25	0.02	0.06	0.40
r_2	0.14	0.16	0.12	0.10	0.27	0.35	0.24	0.27	0.13	0.08	0.31	0.23
r_3	0.31	0.21	0.20	0.10	0.24	0.22	0.23	0.14	0.08	0.09	0.19	0.12
τ_1 (s)	31	25	58	139	76	71	30	2	28	3	3	1
τ_2 (s)	108	168	946	3072	76	71	284	145	202	181	551	173
τ_3 (s)	1805	2190	8826	3072	1712	2418	2226	1479	1193	345	985	1509
σ	0.76	0.88	0.83	0.80	0.59	0.30	0.72	0.85	0.84	0.81	0.90	0.89
s_1	0.02	0.02	0.00	0.04	0.05	0.09	0.03	0.02	0.07	0.00	0.03	0.01
s_2	0.04	0.00	0.01	0.08	0.05	0.09	0.08	0.03	0.02	0.00	0.02	0.06
s_3	0.17	0.09	0.14	0.08	0.33	0.53	0.16	0.09	0.07	0.20	0.04	0.04
R^2	0.997	0.991	0.986	0.994	0.995	0.985	0.999	0.999	0.999	0.92	0.996	0.999

Also, in this case, the relaxation times deduced from the relative resistance plots (fitted by Eq 6.1) are used to fit the stress relaxation curves (by Eq 3.3). The obtained R^2 values in Table 6.2 from the stress relaxation fit appear promising.

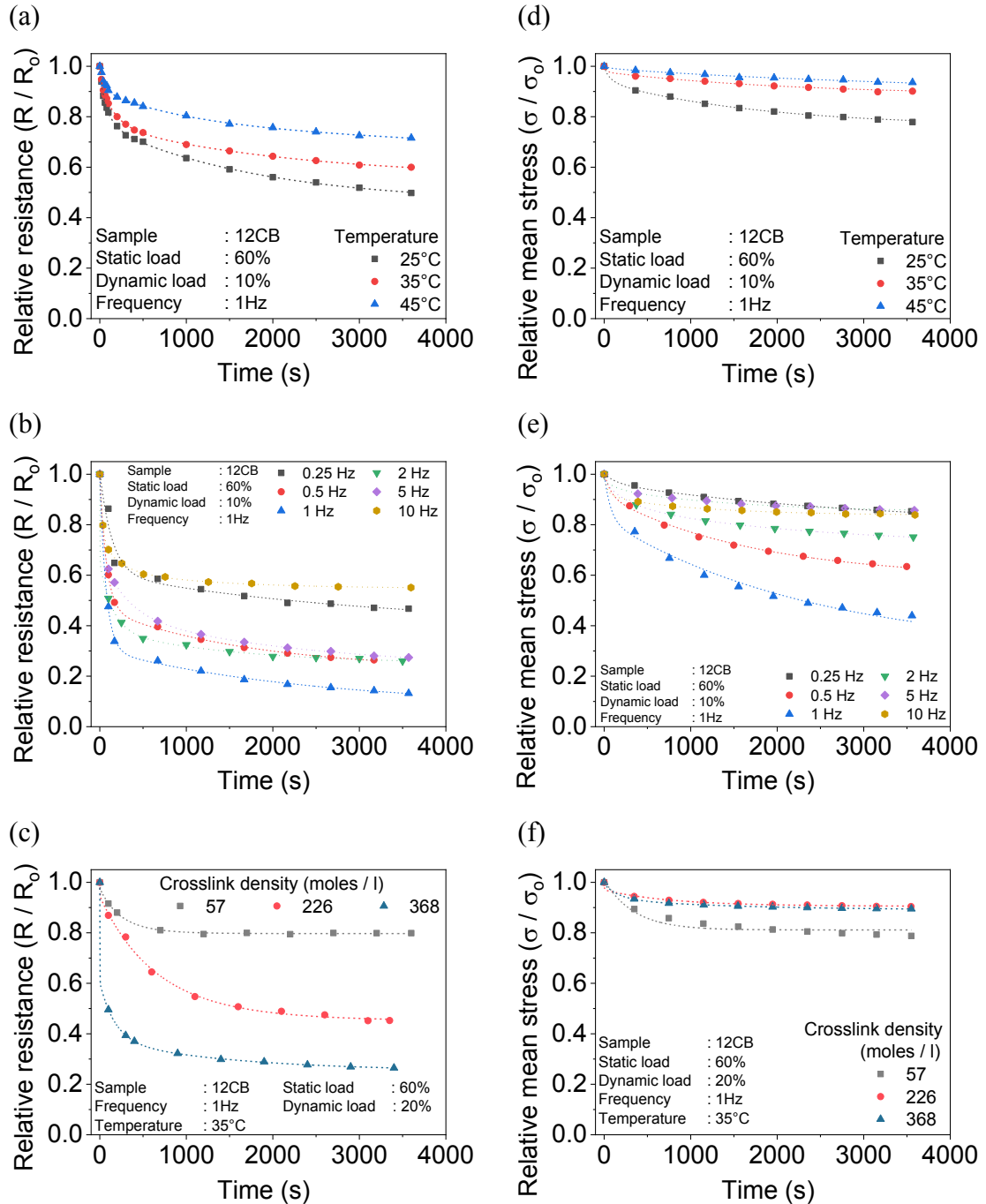


Figure 6.2: Relative resistance plots with fitting for 12CB samples tested at different (a) temperatures, (b) frequency and (c) crosslink density. Relative mean stress plots of the same samples at different (d) temperatures, (e) frequency and (f) crosslink density. [Symbols represent the experimental data and dotted lines represent the fit]

6.2.3 Correlating the relaxation parameters

The piezoresistance relaxation coefficients (r_1, r_2, r_3) and stress relaxation coefficients (s_1, s_2, s_3) from Table 6.1 and Table 6.2 are compared and summarized in a single plot in Figure 6.3. This would generate a master calibration curve and provides a general relationship between mean stress and mean resistance. As a simple generalization, a linear dependency is assumed between the values. The linear fit for the relaxation coefficients in Figure 6.3a yields a slope of ~ 0.5 with no intercept and the linear fit for the residual values in Figure 6.3b yields a slope of ~ 0.8 with an intercept at 0.4. A low R^2 value of around 0.7 is obtained, as the data cluster summarized here consists of results from different filler types and also from experiments that are performed under various conditions. However, when calibration curves are constructed for individual samples, the predicted stress relaxation would be more accurate and highly reliable.

By this approach, one could easily predict the stress relaxation, as the relaxation times are obtained directly from the resistance curves and the stress relaxation coefficients could be calculated from the calibration curves. Mostly rubber products serve in intricate areas, where the mechanical stress could not be measured or monitored in-line, but electrical resistance could be measured very easily using simple multi-meters. With a bridging relationship between the two, the mechanical stress could be very easily estimated. The advantage, in this case, is the elimination of any external/additional components, as the rubber product itself performs the role of a sensor.

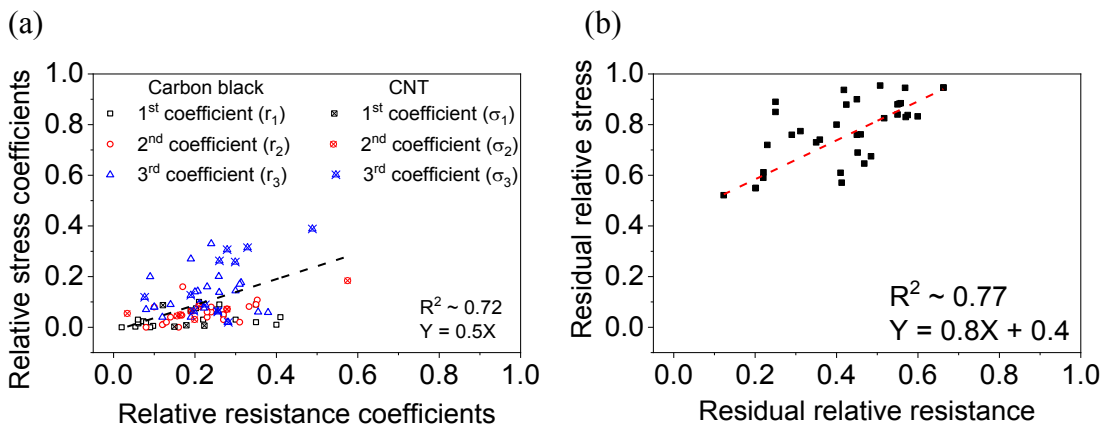


Figure 6.3: Summary of relaxation parameters of various carbon black and carbon nanotubes samples. (a) Coefficients of relative stress versus coefficients of relative resistance (b) residual values of relative stress versus residual values of relative resistance.

6.3 Evaluating the phase shifts (δ) between stress, strain, and resistance

Any viscoelastic material would display a delay in responding to the applied load and this delay is characterized as phase shift δ [156]. In dynamic experiments, this phase shift is calculated as the time lag between the stress and strain signals as shown in Figure 6.4. In the present case, the electrical resistance signals also exhibit a lag in responding to the strain and are quantified as ' $\delta_{R-\varepsilon}$ '.

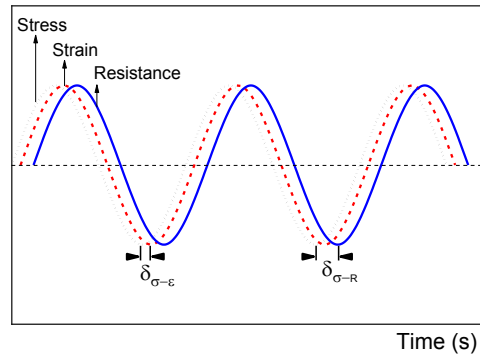


Figure 6.4: Phase shifts between strain, stress, and resistance

Since the electrical resistance signal comprises a second peak (Figure 6.5a), it is necessary to separate the second piezoresistive response which is merged with the main signal. Fourier transformation is a very effective tool to distinguish individual functions in a multi-sine signal. In the Fourier domain, each sine wave gives a peak and the peak intensity denotes the amplitude of the sine waves (Eq 6.2). Figure 6.5b depicts an example Fourier transformation data of the resistance signal for a 12 phr CB sample. Since our resistance curves are vertically shifted by a factor (mean resistance), there is a corresponding offset at 0 Hz.

$$F(f) = \begin{cases} A_n, & f = f_n \\ 0, & \text{otherwise} \end{cases} \quad \text{Eq. 6.2}$$

Where A_n is the amplitude of the sine wave and f_n is the frequency.

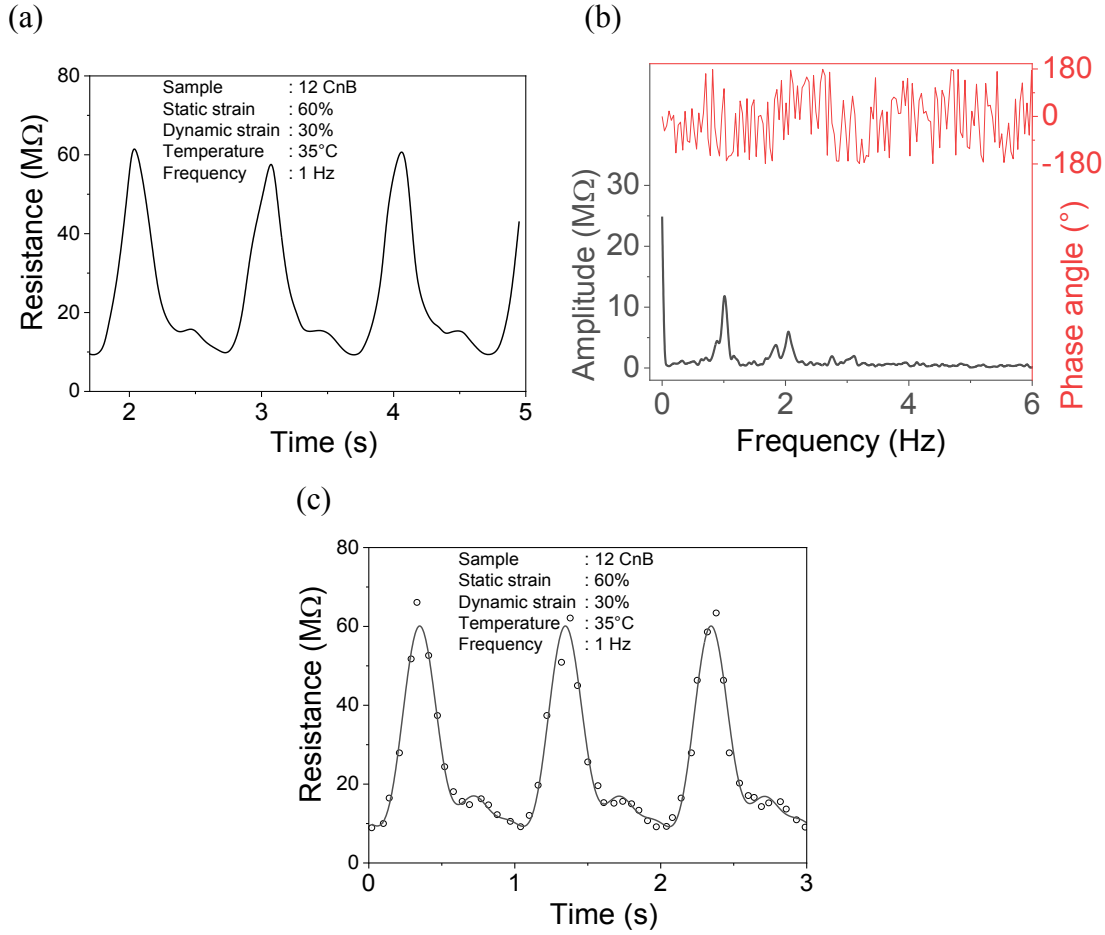


Figure 6.5: An example (a) resistance signal, (b) its Fourier transformed data and (c) the sine function fitting for a 12phr CB sample (Open circles: experimental data & solid line: Multi-sine fit).

The data from the Fourier transformation is then utilized to fit multiple sine curves as per Eq 6.3 to describe the whole resistance signal in good accordance as shown in Figure 6.5c. The resulting sine series can also be used to distinguish between the individual signals at various frequencies and their corresponding phase shifts.

$$f(t) = Y_o + \sum_{i=1}^n A_n \sin(2\pi f_n t + x_{s_n}) \quad \text{Eq. 6.3}$$

where Y_o is the vertical offset (mean resistance), A_n is the amplitude of the sine wave, f_n are the frequencies and x_s is the horizontal shift, n is number of secondary harmonics

The phase shifts between stress, strain, and resistance were calculated by two methods

1. Computing the difference in horizontal shift values (Δx_c) between stress, strain and primary electrical resistance signal obtained from the sine curves
2. Computing the difference in phase angle ($\Delta\theta$) between stress, strain, and electrical resistance obtained from the Fourier transformation data

Three different phase shift values are obtained from the above-mentioned calculations.

- (1) $\delta_{\sigma-\varepsilon}$: Phase shift between stress (σ) and strain (ε)
- (2) $\delta_{R-\varepsilon}$: Phase shift between electrical resistance (R) and strain (ε)
- (3) $\delta_{R-\sigma}$: Phase shift between electrical resistance (R) and stress (σ)

In general, for polymers, the tangent of phase shift (δ) is evaluated from the phase shift values. The term $\tan \delta$ or loss factor is also defined by the ratio of loss modulus (E'') to storage modulus (E') as shown in Eq. 2.6. It represents mechanical damping or internal friction in a viscoelastic system. A high $\tan \delta_{\sigma-\varepsilon}$ value is indicative of a material that has a high non-elastic component, while a low value indicates a material with more elastic nature. So, the tangent of the phase shift between electrical resistance and stress ($\tan \delta_{R-\sigma}$) is calculated and considered for further study.

6.3.1 Phase shift values during time sweep experiments

6.3.1.1 Filler content and phase shifts

Figure 6.6 depicts the changes in $\tan \delta$ for samples with different CB content. The observed $\tan \delta_{R-\varepsilon}$ values are found to be higher than $\tan \delta_{\sigma-\varepsilon}$ (Please note the different scaling in Figure 6.6). This is caused by the increase in $\delta_{R-\varepsilon}$ values and this time lag in resistance could be inferred as the time required for the stress to be transferred from the polymer matrix to the filler network. It is well known that when filled rubbers composites are stretched, the rubber matrix would initially respond to the force and then the load would be transferred to the fillers [122, 174, 175]. Few experimental works have also reported a time lag between loading and response for various

polymer composites [27, 165, 176]. Moreover, according to the tunneling theory, only a change in the filler network could cause the change in the resistance values [177, 178]. Therefore, an increase in resistance corresponds to the moment when the distance between the filler clusters or filler network has increased. Hence, the characteristic phase shifts we observe between the stress and electrical resistance signals represent the time required by the load to cause a change in the filler network, *i.e.* the reaction time of the filler clusters or the filler network. The observed $\delta_{R-\varepsilon} > \delta_{\sigma-\varepsilon}$ values confirm that the filler network needs a much longer time than the rubber matrix to respond to the applied strain.

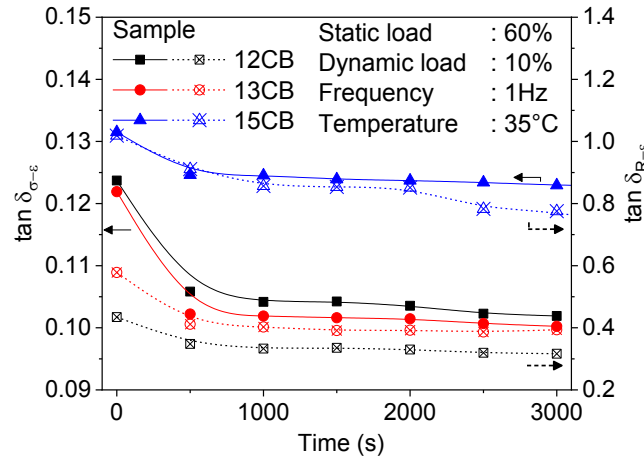


Figure 6.6: $\tan \delta$ plots from a time sweep experiment performed for samples containing different CB loading [Filled symbols and solid line: $\tan \delta_{\sigma-\varepsilon}$ and open crossed symbols and dash line: $\tan \delta_{R-\varepsilon}$]

Sample with 13 phr and 15 phr of CB shows higher $\tan \delta_{R-\varepsilon}$ values than 12 phr CB samples. Since the filler network is well established at higher CB loading, a much longer time is necessary for the same dynamic strain to disrupt the percolated filler network and display a change in resistance. Interestingly, the $\tan \delta$ change profiles for stress-strain and resistance-strain look very similar, an initial decrease followed by steady values. The $\tan \delta_{R-\varepsilon} / \tan \delta_{\sigma-\varepsilon}$ ratio is found to be approx. 3.0, 4.0 and 5.0 for 12 phr CB, 13 phr CB and 15 phr CB samples respectively. For further understanding, the piezoresistive phase shift values, the $\tan \delta_{\sigma-R}$ values are calculated and summarized for samples with 12 phr of CB under different conditions. Moreover, in Figure 6.6, the $\tan \delta$ values became constant after 1000s for the 12 CB samples. Therefore, the $\tan \delta$ values calculated at 3500s are compared in Figure 6.7.

6.3.1.2 Major parameters and phase shifts

The time sweep experiments performed at different temperatures under identical loading conditions are depicted in Figure 6.7a. The $\tan \delta_{\sigma-R}$ values are not affected much by temperature. However, samples tested at a higher temperature display slightly lower $\tan \delta_{\sigma-R}$ values. This means that the transfer of load to the filler network is faster at a higher temperature; this could be due to the lower matrix viscosity as well as the higher filler dynamics.

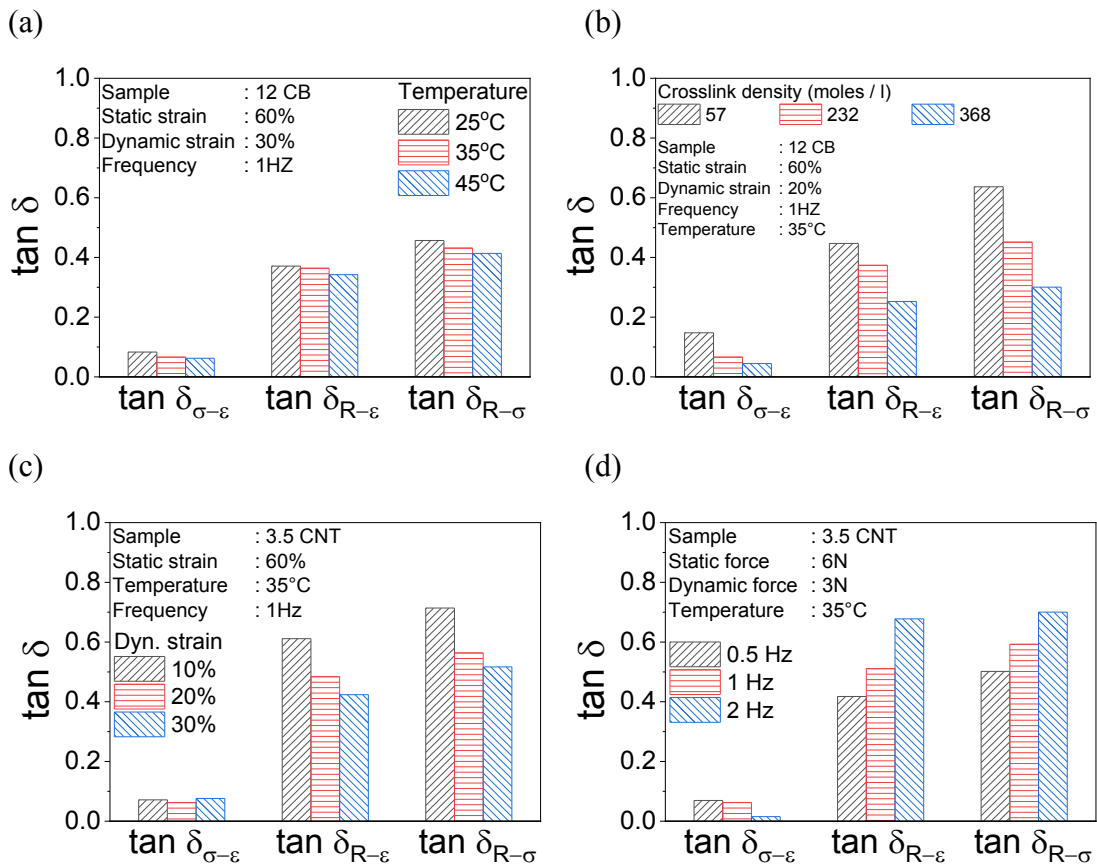


Figure 6.7: $\tan \delta$ values summarized after 1 hour from time sweep experiments for (a) 12 CB samples at different temperatures, (b) 12 CB samples with different crosslink density, (c) 3.5 CNT sample at different dynamic strain and (d) 3.5 CNT sample at different frequencies

In Figure 6.7b, 12 phr carbon black samples differing in their crosslink densities are tested under identical loading conditions. The sample with the highest crosslink density shows the least $\tan \delta_{\sigma-R}$ value. Low $\tan \delta_{\sigma-R}$ values indicate an early disruption of the filler network. This could be attributed to the higher stiffness of the rubber

matrix, which transfers the load to the filler network much faster and causing an early disruption of the percolated filler network. Therefore, with low matrix crosslinking, the rubber takes a relatively long time to transfer the load to the fillers, giving more time before disrupting them.

Figure 6.7c depicts the change in $\tan \delta_{\sigma-R}$ values for 3.5 CNT samples with different dynamic strains. The $\tan \delta_{\sigma-R}$ value is the least for 30% dynamic strain, which indicates an earlier disruption of the percolated filler network. Therefore, higher dynamic strains transfer the load to the filler network more rapidly, which reflects as lower piezoresistive phase shifts ($\delta_{\sigma-R}$). Figure 6.7d summarizes the $\tan \delta$ values of 3.5 CNT samples measured at different frequencies. With an increase in frequency, higher $\tan \delta_{\sigma-R}$ values are observed, signifying that the filler network is disrupted much earlier at lower frequencies. Interestingly, in all the time sweep measurements, the $\tan \delta$ values display a relationship as per Eq 6.4

$$\tan \delta_{\sigma-R} = \tan \delta_{\sigma-\varepsilon} + \tan \delta_{R-\varepsilon} \quad \text{Eq. 6.4}$$

6.3.2 Phase shifts during temperature sweep experiments

To get a clearer insight on the behavior of piezoresistive phase shift ($\delta_{\sigma-R}$), the changes in $\tan \delta$ values are studied during temperature sweep measurements. Figure 6.8a depicts the $\tan \delta$ values for samples with different carbon black content during temperature sweep measurements. The $\tan \delta_{\sigma-R}$ values are found to be constant up to 20°C and a slight increase was observed at 10°C. At much lower temperatures, the sample became non-conducting and therefore it is difficult to deduce the phase shift values. The $\tan \delta_{\sigma-R}$ values for 13 CB samples are found to be higher than 12 CB; similar to Figure 6.6 (from the time sweep experiments). At high filler concentrations, the filler network is strongly percolated. Therefore, relatively longer times are required to disrupt the conducting pathways and cause a change in the electrical resistance, resulting as higher $\tan \delta_{\sigma-R}$ values. In Figure 6.8b the 12 CB sample is tested with low and high dynamic strain. With low dynamic strain, the $\tan \delta_{\sigma-R}$ values are found to be nearly constant. With higher dynamic strain, the stress transfer to the

filler network will be rapid and would easily disrupt the percolated filler network, resulting in lower phase shift (or lower $\tan \delta_{\sigma-R}$) values.

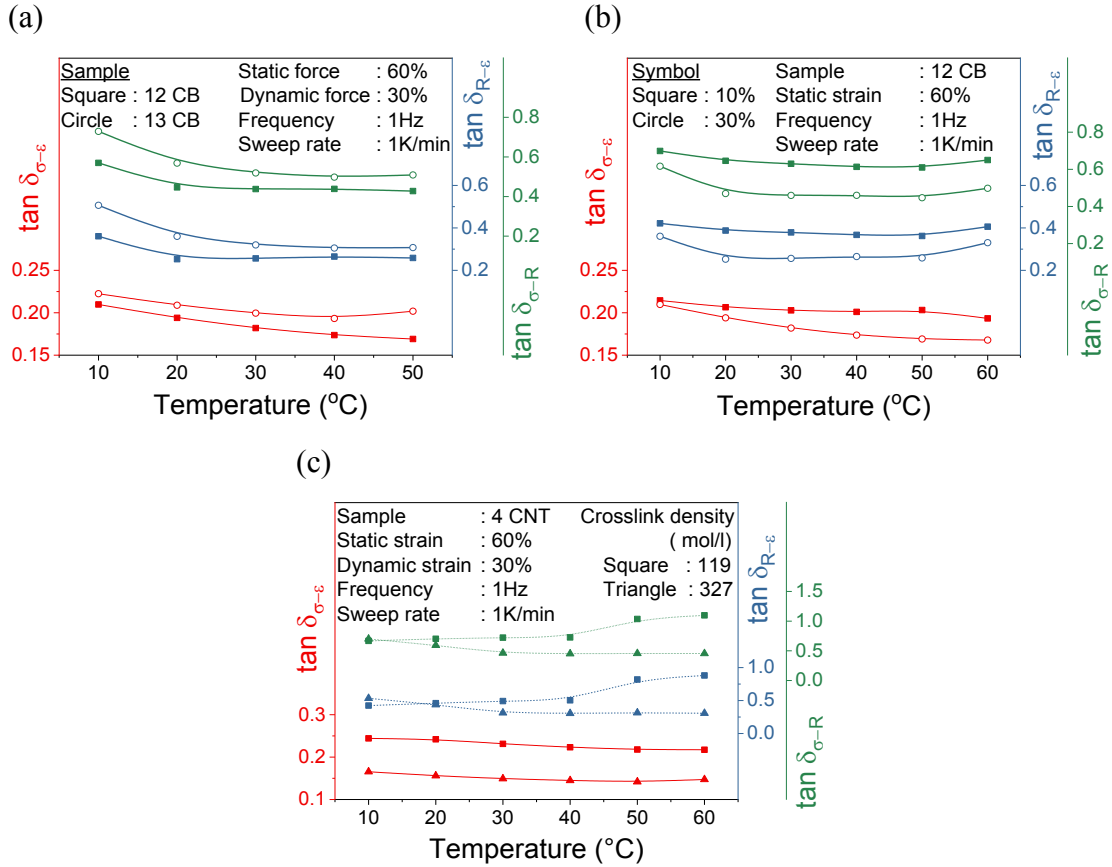


Figure 6.8: $\tan \delta$ plots for temperature sweep experiments performed for (a) samples with different CB content, (b) 12 phr CB samples at different dynamic strain and (c) 3.5 phr CNT sample with different crosslink density

In Figure 6.8c, the $\tan \delta$ values of 4 phr CNT sample with different crosslink densities are given. Similar to Figure 6.7 the samples with a higher crosslink density display lower $\tan \delta_{\sigma-R}$ values over the entire temperature range indicating their reaction times are less, *i.e.* the filler network would be disrupted earlier. However, for the less crosslinked sample, the $\tan \delta_{\sigma-R}$ value at 60°C is much higher and is found to decrease gradually with temperature. This indicates that the reaction time of the filler network is much larger at high temperatures. As these temperature sweep experiments have been performed with high static and dynamic strain, it limited the temperature scan window as the samples become non-conducting at 0 °C. To get a deeper insight into

the phase shift values at T_g and beyond, the $\tan \delta$ values are summarized from experiments that are performed with much lower force in Figure 6.9.

Figure 6.9a depicts the dependence of $\tan \delta$ for samples with different carbon black content. As observed in Figure 6.8, the $\tan \delta_{\sigma-R}$ values are found to increase with a decrease in temperature. Up to $\sim 10^\circ\text{C}$, the changes in $\tan \delta_{\sigma-R}$ values are found to be very low (~ 0.1). When the temperature is further reduced towards T_g , the $\tan \delta_{\sigma-R}$ values are found to increase sharply. This would imply that the reaction time of the filler network has increased, *i.e.* the filler network needs a longer time to be disrupted at low temperatures. As discussed in chapter 5, Figure 5.8f, due to the milder force and high stiffness at low temperatures, the rubber experiences relatively less stretch. As the strain is less, the piezoresistive effect is also less. Therefore, corresponding to the (less) strain at low temperatures, the filler particles show longer response times (larger $\delta_{\sigma-R}$) and ultimately reflects as much higher $\tan \delta_{\sigma-R}$. Figure 6.9b depicts the change in $\tan \delta$ values for samples under different loads. With higher dynamic force, the stress transfer to the filler network will be rapid and would easily disrupt the percolated filler network, resulting in lower phase shift ($\delta_{\sigma-R}$) values; similar to Figure 6.8b. Slightly lower $\tan \delta_{\sigma-R}$ values are therefore observed for the samples tested with higher dynamic force and also, a significant increase in $\tan \delta_{\sigma-R}$ is observed around T_g .

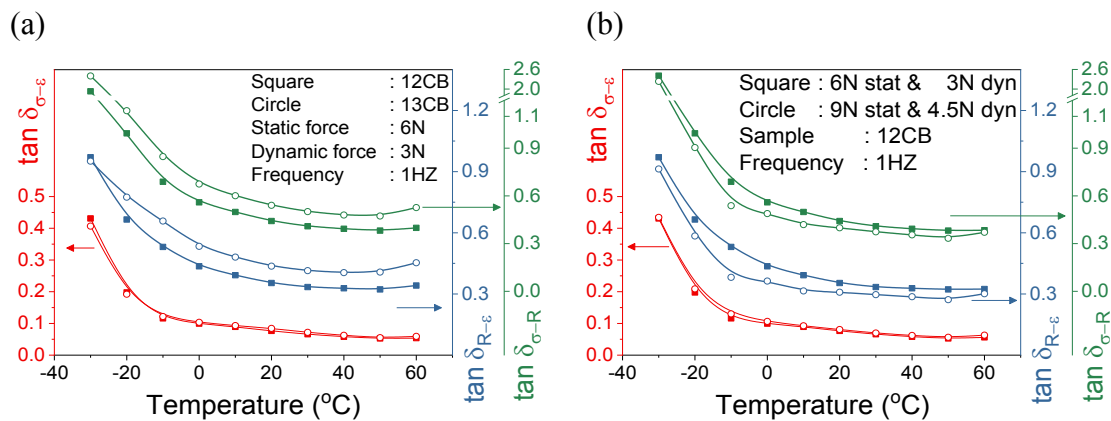


Figure 6.9: $\tan \delta$ plots for temperature sweep experiments performed for (a) samples with different carbon black concentrations (b) 12 phr CB samples at different loading conditions

6.4 Relation between second peaks and viscoelastic properties of the polymer

To understand the intensity and kinetics of the second peaks (Figure 5.1c), the amplitudes A_1 and A_2 , from the Fourier transformation data and the sine series are studied. It has been observed that the value A_1 corresponds to the piezoresistive effect that happens during loading and the value A_2 corresponds to the second piezoresistive peak that occurs during unloading. When there are no second peaks, then $A_2 = 0$; when there are subtle second peaks or traces of second peaks, then $A_2 \ll A_1$; when the second peaks are prominent, then $A_2 < A_1$ and when the second peaks are strong, then $A_2 \geq A_1$. To understand the behavior of the second peaks, the peaks intensities A_1 and A_2 are initially summarized for various samples under a time sweep experiment in Figure 6.10.

6.4.1 Time sweep measurements

Figure 6.10a summarizes the peak amplitudes A_1 and A_2 for samples with different CB content. The samples with the lowest amount of CB display higher A_1 and A_2 values, due to the reasons explained in Chapter 5, Figure 5.5. The amplitude ratios of A_2 / A_1 are almost constant and found to be around 0.2 and 0.25 for 12 CB and 13 CB respectively. Due to the stronger second peaks in 15 CB samples an amplitude ratio of ~ 1.2 is obtained, which means $A_2 > A_1$ and is also evident in Figure 6.10a. The amplitude ratios indicate the extent of reconfiguration or struggle that filler network experiences during unloading. Therefore, high A_2 / A_1 ratios observed for 15 CB denotes a high degree of filler network reconfiguration. In Figure 6.10b the 12 CB sample is tested with two different loads. With a lower force, the amplitudes of the first and second peaks are less. The amplitude A_2 is subtle for low force ($A_2 \ll A_1$) and becomes prominent ($A_2 < A_1$) at higher dynamic forces. The amplitude ratios A_2 / A_1 are found to be around 0.15 and 0.25 for 3N and 4.5N respectively, indicating a high degree of reconfiguration with a higher force.

In Figure 6.10c the peak amplitudes of 12 phr CB samples are summarized at various temperatures. At higher temperature, the peak amplitudes are found to reduce with time due to rearrangement of the percolated filler network (discussed in detail in

Chapter 5, Figure 5.5). The peak amplitudes of A_2 are found to be almost similar at 35 °C and 45 °C. However, significantly higher A_2 are observed at 25 °C due to a higher degree of reconfiguration during the unloading cycles. The amplitude ratios A_2 / A_1 are found to be around 0.23, 0.20 and 0.16 at 25 °C, 35 °C and 45 °C respectively. In Figure 6.10d the A_1 and A_2 values are summarized for 12 phr CB samples with different crosslink densities. The amplitude A_2 is subtle for samples with less crosslink density and yields A_2 / A_1 ratios of ~ 0.25 . With higher crosslink density, the ratio of A_2 / A_1 is found to be around 0.5, indicating stronger filler cluster reconfigurations. Therefore, a hindrance to the filler network mobility compels for an intermediate reconfiguration process (during unloading) and results in stronger second peaks.

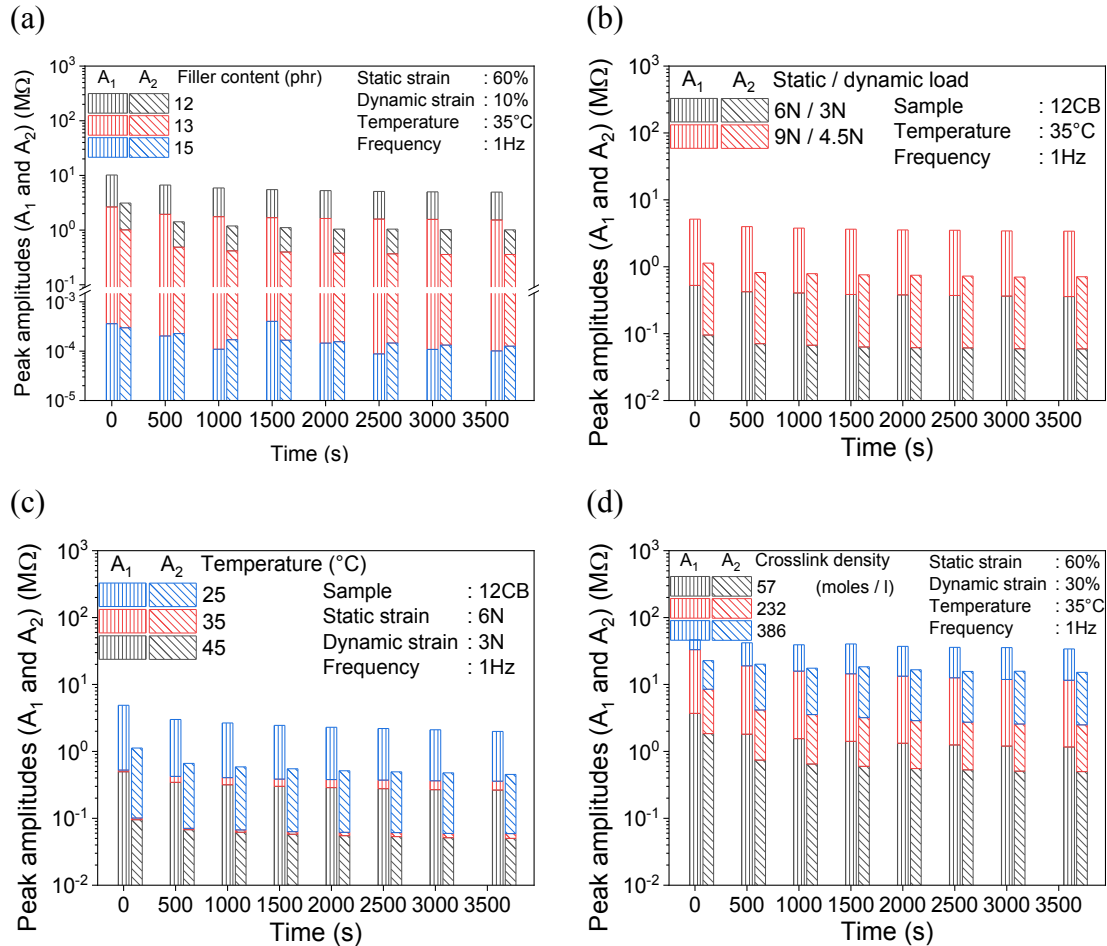


Figure 6.10: Peak amplitudes (A_1 and A_2) summarized for (a) samples with different filler content and 12 phr CB sample at different (b) loads, (c) temperature and (d) crosslink density.

6.4.2 Temperature sweep measurements

To get a deeper insight into the behavior of the second peaks, the amplitudes A_1 and A_2 studied in temperature sweep experiments and given in Figure 6.11. In Figure 6.11a, the amplitudes A_1 and A_2 are summarized for samples with different filler content. In concurrence to the facts explained in Figure 5.8f, the amplitudes vary in three stages, a decrease from 60 °C to 30 °C due to rearrangement of the percolating network effects, then increase from 30 °C to 0 °C due to reduction in number of percolated filler clusters and again decrease from 0 °C to -30 °C due to low piezoresistive effect. The amplitude ratios A_2/A_1 that denotes the degree of reconfiguration are calculated from Figure 6.11a and summarized in Figure 6.11c. Unlike time sweep experiments, the peak amplitude varies with respect to temperature. The amplitude ratios indicate that the second peaks are initially subtle at 60 °C and becomes prominent with a reduction in temperature. The lower amplitude ratios at -30 °C could be associated with the less piezoresistive change pertaining to the matrix stiffness. The larger A_2/A_1 values for 13 CB indicate a high degree of reconfiguration than the 12CB samples, which concedes with the findings and discussions in Chapter 5, Figure 5.9b. Also, interestingly, the maximum effect from second peaks is observed for both the samples at T_g (temperature corresponding to the maximum of $\tan \delta_{\sigma-\epsilon}$)

Figure 6.11b summarizes the peak amplitudes for 12 phr CB samples tested with different loads. As expected, the peak amplitudes are larger for samples tested with higher dynamic force and the three-stage change in peak amplitudes is more clearly observed with the high dynamic load. The peak amplitude ratios are calculated and summarized in Figure 6.11d. From 60 °C to 30 °C, the A_2/A_1 values display no change irrespective of the dynamic load and subsequently, the sharp increase is observed. The larger amplitude ratios at 4.5 N indicate that samples endure a high degree of reconfiguration. At T_g the maximum effect is observed and the amplitude $A_2 \geq A_1$ for the higher dynamic load. Therefore, at T_g , the sample experiences more filler network destruction during to unloading. For comparison purpose, the mechanical $\tan \delta_{\sigma-\epsilon}$ is also plotted in Figure 6.11c&d. Since the piezoresistive $\tan \delta_{\sigma-R}$ Aligns well with the mechanical $\tan \delta_{\sigma-\epsilon}$, this method could also be an alternative approach to identify the glass transition temperature (T_g) of rubber composites.

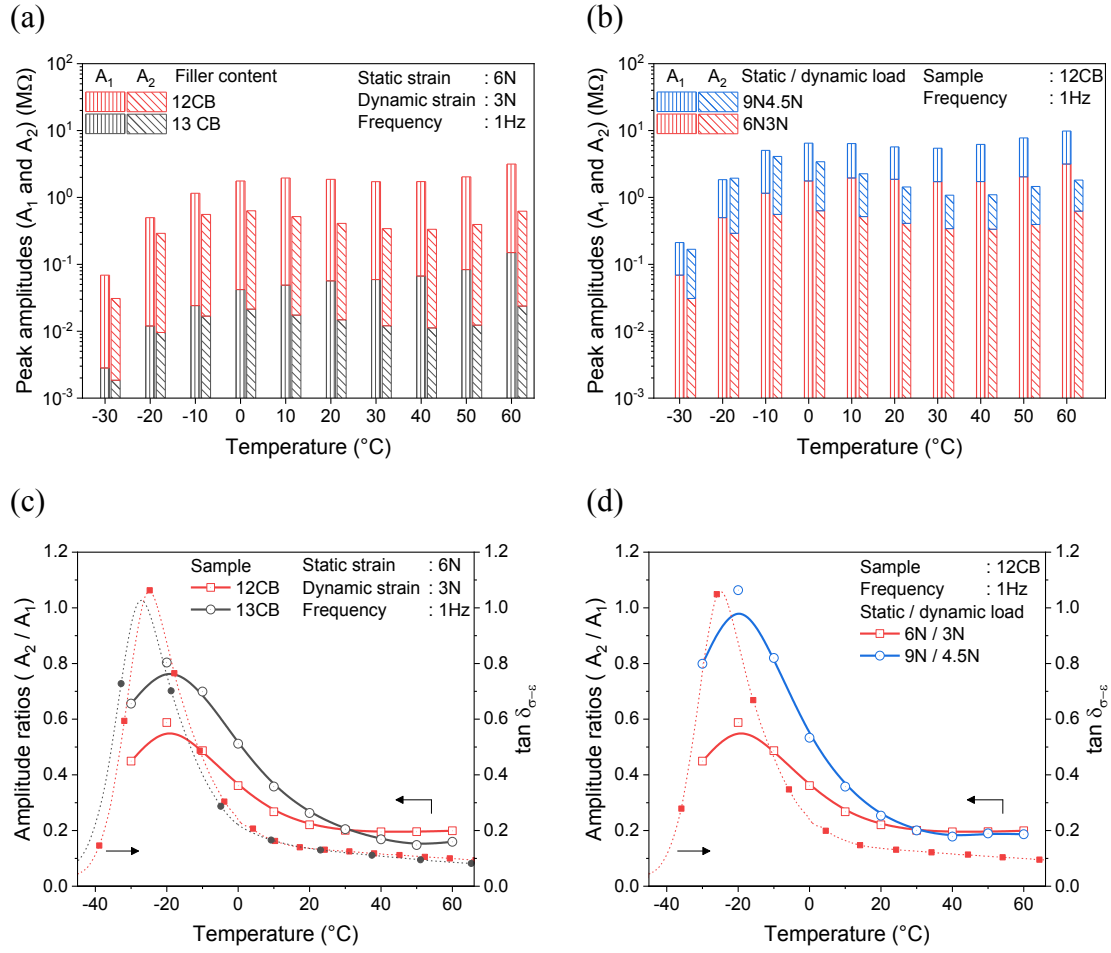


Figure 6.11: Peak amplitudes (A_1 and A_2) summarized for (a) samples with different filler content and (b) 12 phr CB sample at different loads. Amplitude ratios A_2 / A_1 summarized for (c) samples with different filler content and (d) 12 phr CB sample at different loads

Chapter 7

Investigating the potentials of dynamic
piezoresistivity for commercial applications

7.1 Introduction

The possibilities of utilizing the developed concept for commercial use and the scope for further studies are discussed in this chapter. In the earlier chapters, the piezoresistive behavior of SSBR is studied in detail under quasi-static and dynamic conditions. The utilized conducting fillers, carbon black and multi-walled carbon nanotubes are special in terms of their exceptional physical properties. So, it is vital to assess the piezoresistive behavior for conventional fillers, in order to ensure the applicability of the concept for daily use rubber products. Three different general purpose or conventional carbon blacks (CCB) are chosen based on their application. Intermediate super abrasive furnace (ISAF) carbon blacks (N220) grades are commonly used in truck and high-performance tire treads. They are known to offer good tear and abrasion resistance to the rubber compound. The N330 high abrasive furnace (HAF) black is one of the popularly used fillers for passenger car tire treads, solid tires, and conveyor belts. The N660 semi-reinforcing general-purpose furnace (GPF) blacks are best suitable for tire sidewalls and products such as O-rings, inner-tubes, body mounts, and cables. The three different carbon blacks are also expected to display very different dynamic piezoresistive effect. As piezoresistance behavior has been extensively studied for SSBR, two further rubbers that are generally used in tire industries, namely NR and BR are filled with conductive carbon black (Printex XE-2b) and assessed for their dynamic piezoresistive capabilities. At last, few interesting further studies that can be extended from the current work are highlighted with examples.

7.2 Piezoresistive behavior of SSBR with conventional carbon blacks

7.2.1 Time sweep

Figure 7.1 summarizes the relative resistance and relative mean stress values extracted from the dynamic time sweep experiment for SSBR samples filled with 60 phr of conventional carbon blacks (CCB). In Figure 7.1a three different types of carbon blacks are compared. The resistance relaxation profiles indicate that the degree of

conducting network is stronger for N660 blacks, while N220 blacks display the least tendency to rearrange the filler network.

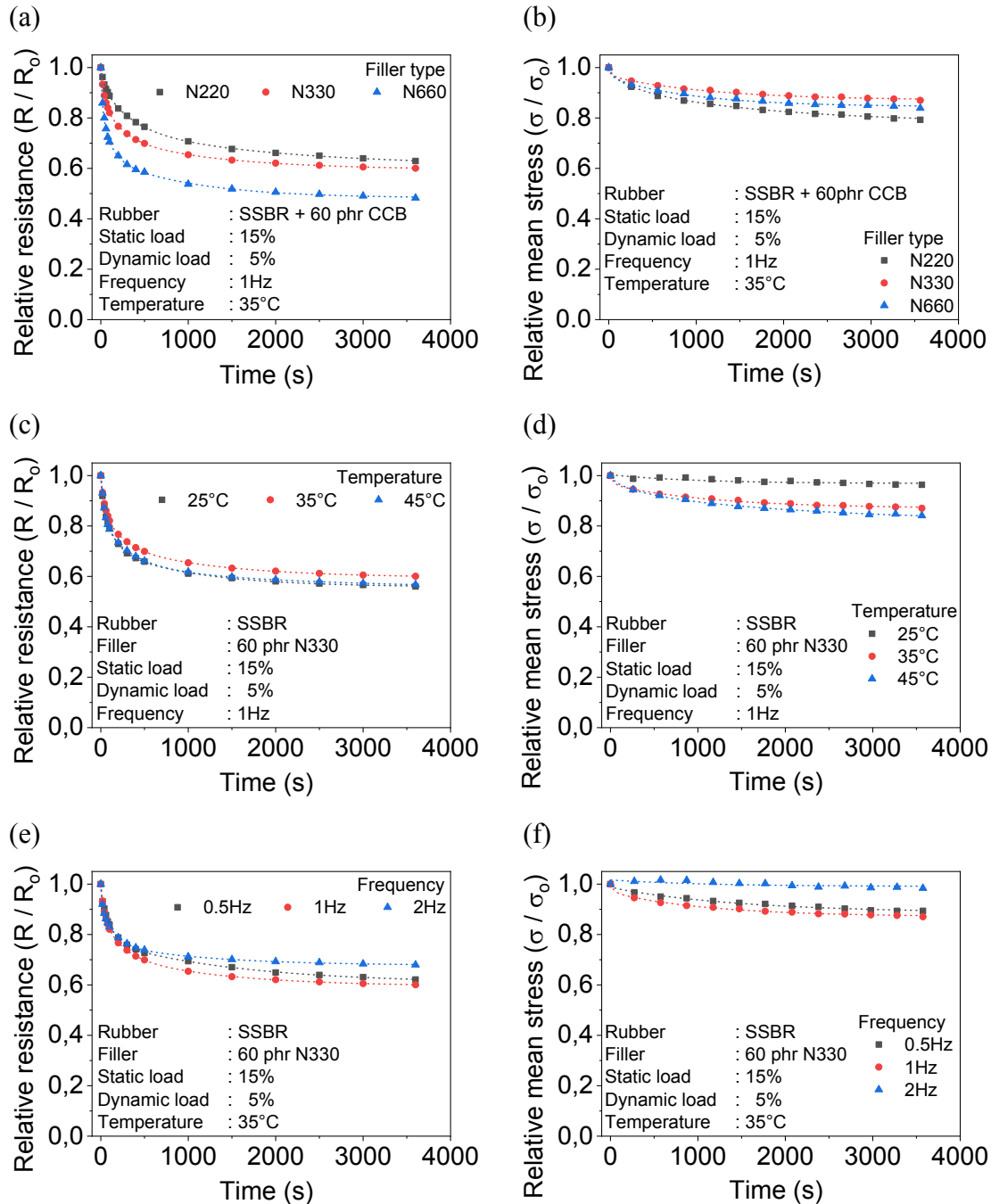


Figure 7.1: (a) relative resistance and (b) relative mean stress plots with fitting for SSBR samples with different types of CCB.(c) relative resistance and (d) relative mean stress plots with fitting for SSBR samples with N330 CCB at different temperature.(e) relative resistance and (f) relative mean stress plots with fitting for SSBR samples with N330 CCB at different frequency. [Symbols represent the experimental data and dotted lines represent the fit]

During dynamic loading and unloading cycle, the fillers particles are forced to rearrange, and the particles are undergoing a kind of flocculation process to form a stronger filler-filler network. Most probably, the lower structure of the N660 (less aspect ratio, more spherical in nature) facilitates easy orientation of the filler particles and promotes flocculation behavior. Figure 7.1c compares samples of SSBR filled with 60 phr of N330, tested at three different temperatures and no significant changes in filler network behavior is observed. Figure 7.1e compares N330 samples tested at different frequencies. The mean resistance profiles of N330 blacks are very similar to the conductive carbon blacks, as seen in Chapter 5, Figure 5.4. The sample at 1 Hz displays maximum reorientation of the fillers towards a more percolating filler-filler network. Therefore, the piezoresistive behavior of SSBR composites is found to be similar for samples with conventional carbon blacks and conductive carbon blacks.

Table 7.1: Relative resistance and relative mean stress fit data for SSBR filled with 60 phr of different CCB & SSBR filled with 60phr N330 at different conditions

	Filler type			Temperature (°C)			Frequency (Hz)		
	N220	N330	N660	25°C	35°C	45°C	0.5 Hz	1 Hz	2 Hz
R_f	0.608	0.595	0.482	0.558	0.594	0.550	0.606	0.594	0.677
r_1	0.062	0.117	0.167	0.087	0.118	0.191	0.045	0.116	0.084
r_2	0.172	0.152	0.186	0.199	0.150	0.172	0.181	0.152	0.152
r_3	0.157	0.136	0.164	0.156	0.138	0.090	0.168	0.137	0.087
τ_1 (s)	37	36	21	25	37	47	12	36	17
τ_2 (s)	315	209	112	131	208	350	116	208	143
τ_3 (s)	1833	1190	988	998	1190	2213	1524	1190	1159
σ_f	0.778	0.871	0.845	0.969	0.870	0.816	0.886	0.870	0.991
s_1	0.027	0.033	0.029	0.002	0.036	0.020	0.012	0.030	0.000
s_2	0.054	0.002	0.012	0.000	0.001	0.042	0.003	0.007	0.000
s_3	0.142	0.095	0.115	0.035	0.094	0.122	0.100	0.094	0.026
R^2	0.997	0.989	0.993	0.882	0.990	0.998	0.990	0.989	0.853

The relative mean resistance profiles are fitted with Eq 6.1 and their corresponding mean stress values in Figure 7.1b, d, f are fitted with Eq 3.3. Also, in this case, the relaxation times obtained from relative resistance plots are utilized to define the stress relaxation behavior and the fit parameters are summarized in Table 7.1. The relaxation times of stress and resistance agree well, evidenced by the R^2 values. Therefore, it is possible to establish a relationship between stress relaxation and piezoresistance changes by easily correlating the relaxation coefficients. So, prediction of stress relaxation behavior from electrical resistance is also possible for SSBR filled with conventional carbon black, provided they display piezoresistive characteristics.

Second peaks are also observed for the conventional carbon blacks during the time sweep measurements similar to conducting carbon blacks seen in Chapter 5, Figure 5.6. Fourier transformation is utilized to define the dynamic resistance profiles of the material. The peak amplitude ratios (A_2 / A_1) became constant after 500 s and are found to be ~ 4 for N220, ~ 2 for N330 and ~ 4.5 for N660 carbon blacks. Such high amplitude ratios indicate the formation of strong second peaks during unloading and this could be due to the dense filler network (60 phr of filler) that obscures the filler mobility. Therefore, the samples experience a high degree of reconfiguration during unloading, *i.e.* the changes happening in the filler network during unloading is rather more than those happening during loading/stretching.

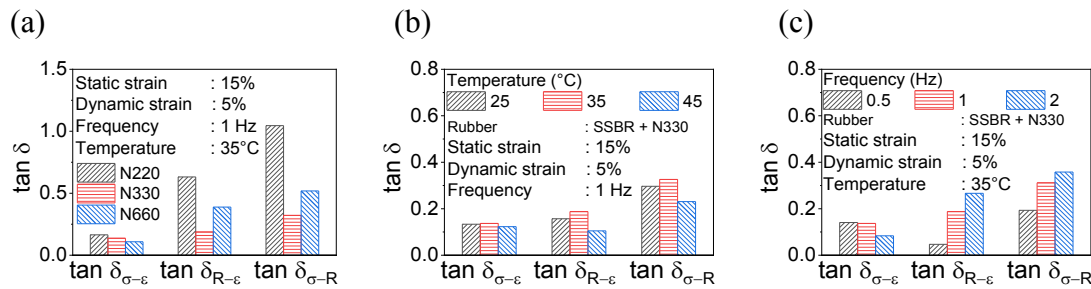


Figure 7.2: $\tan \delta$ values summarized after 1 hour from time sweep experiments for (a) SSBR with different CCB and SSBR/N330 samples at different (b) temperatures and (c) frequencies

The $\tan \delta_{\sigma-R}$ values are evaluated to understand the response times of the conventional blacks. In Figure 7.2a, the N330 blacks display the least response time (least $\delta_{\sigma-R}$

value), while N220 display the highest. Therefore, out of the three samples, the N220 filler network would need more time to be disrupted. In Figure 7.2b, for the same loading conditions, the N330 blacks display the lowest response time at 45 °C, similar to conducting carbon blacks in Chapter 6, Figure 6.7. In Figure 7.2c, the N330 blacks display the least response time at 0.5 Hz also similar to the conducting carbon blacks in Chapter 6, Figure 6.7.

7.2.2 Temperature sweep

Figure 7.3a depicts the $\tan \delta$ values for samples with different carbon blacks during temperature sweep measurement. The $\tan \delta_{\sigma-R}$ values are found to decrease up to 20°C and then increase gradually until T_g ; similar to the conducting carbon blacks shown in Chapter 6, Figure 6.8. The N220 black displays higher $\tan \delta_{\sigma-R}$ than N330 black. This would imply that N220 filler network is more stable and displays higher reaction time over the whole temperature regime. The higher $\tan \delta_{\sigma-R}$ values displayed by the N220 blacks could be associated with their high reinforcing nature and low particle size. The amplitude ratios in Figure 7.3b indicate that the second peaks are prominent for both the blacks even at 60 °C and become much stronger at low temperatures. The maximum effect from the second peaks is observed at 0 °C, while the sample has its T_g at around -25 °C. The peak amplitude ratios are significantly larger for N220 samples, similar to the time sweep measurements and emphasize that the degree of reconfiguration is substantially higher during the unloading cycles.

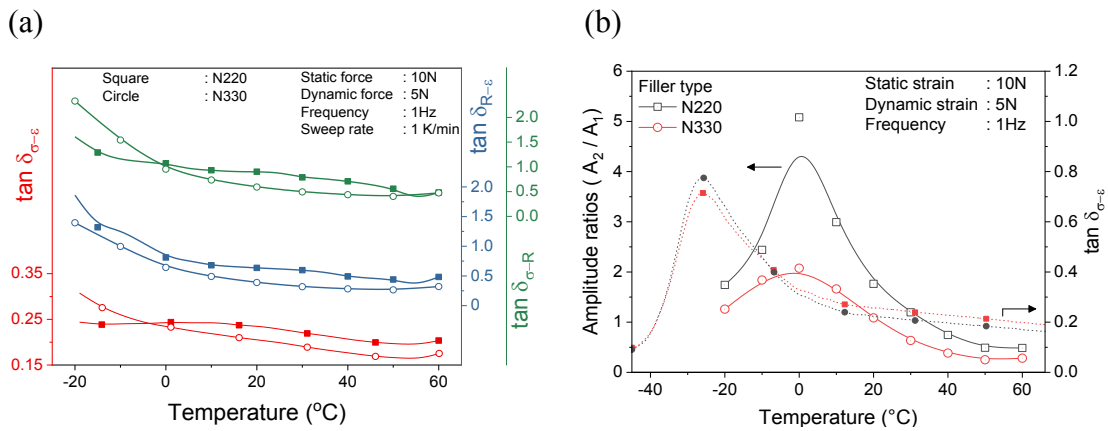


Figure 7.3: (a) $\tan \delta$ and (b) resistance amplitude ratios (A_2/A_1) for SSBR with different types of carbon blacks.

7.2.3 Strain sweep

In Figure 7.4, the electrical conductivity increases until the critical strain due to rearrangement of the percolating network and then decreases sharply due to network destruction, similar to the conducting carbon blacks in Chapter 5, Figure 5.10. The critical strain in terms of electrical conductivity is found to be around 4 % for both the conventional carbon blacks.

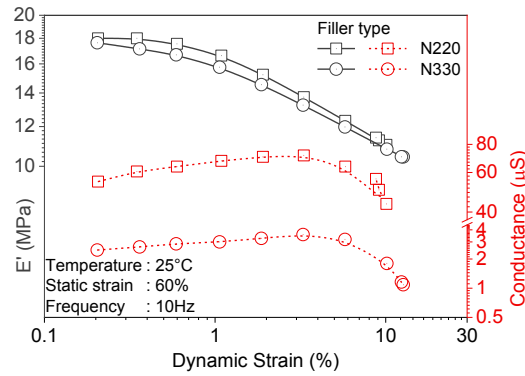


Figure 7.4: Dependence of mean conductance and elastic modulus (E') on the dynamic strain for different carbon blacks

7.2.4 Summary

Utilizing mean resistance values to predict stress relaxation is found to be effective for conventional fillers as well, offering the possibility to use this concept for carbon black filled rubber samples that display piezoresistive characteristics. The amplitude ratios (A_2/A_1) prove that the double peaks are a definite piezoresistive response and are independent of the nature or type of filler. The piezoresistive phase shift values ($\tan \delta_{\sigma-R}$) at different experimental conditions for conducting carbon blacks, CNT and conventional carbon blacks display similar trend, which highlights the fact that behavior of the filler network is identical for all filler types. This is further affirmed by the resemblance in the strain sweep profiles of the conventional carbon blacks and conducting carbon black.

7.3 Piezoresistive behavior of NR, BR, and SSBR with conducting carbon blacks

7.3.1 Time sweep measurements

The dynamic piezoresistive behavior of SSBR has been studied in-depth with conducting carbon black (CB) and also their piezoresistive capabilities are tested with few conventional carbon blacks. To assess the dynamic piezoresistive capabilities of other rubbers, samples of NR, SSBR, and BR filled with 12 phr of CB are studied.

Figure 7.5a depicts the relative resistance changes for different filled rubbers. SSBR displays a remarkable change in the resistance during repeated cyclic deformation, while BR undergoes through such process in a relatively lesser extent. The relative resistance profiles are fitted with Eq 6.1 and their corresponding mean stress values in Figure 7.5b are fitted with Eq 3.3. Also, in this case, the relaxation times obtained from relative resistance plots are utilized to define the stress relaxation behavior and the fit parameters are summarized in Table 7.2. High R^2 values in the table indicate that prediction of stress relaxation behavior from piezoresistance data is, therefore, possible for other rubbers as well.

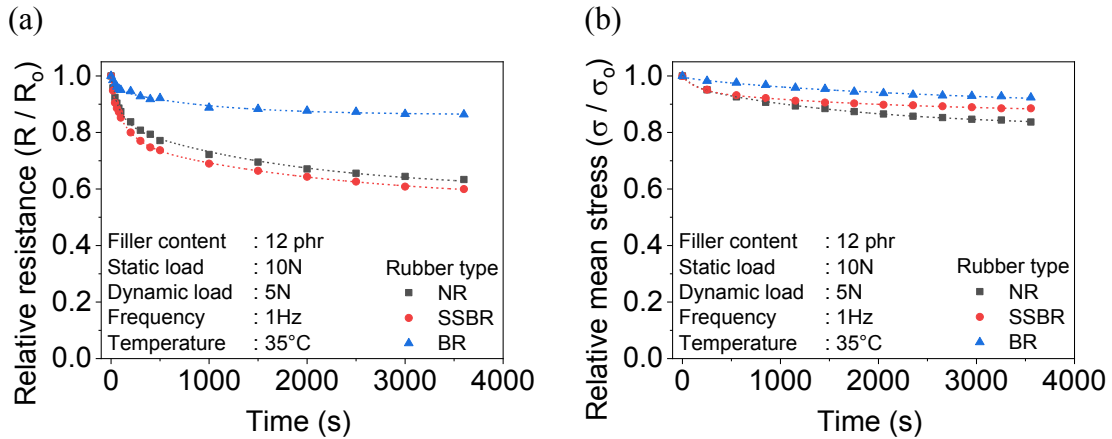


Figure 7.5: (a) relative resistance and (b) relative mean stress plots with fitting for different rubbers. [Symbols represent the experimental data and dotted lines represent the fit]

Second peaks are also observed in all the rubbers during time sweep measurements as shown in Chapter 5, Figure 5.6. Therefore, they are definitely a unique piezoresistive response from the conducting fillers and are independent of the rubber matrix. So,

Fourier transformation is utilized to define the resistance profiles of the material. The peak amplitude ratios (A_2/A_1) are found to be ~ 0.2 for all rubber types, meaning the second peaks are subtle.

Table 7.2: Relative resistance and relative mean stress fit data for different rubbers

Sample	Relative resistance			Relative mean stress		
	Coeff	Value	R^2	Coeff	Value	R^2
NR	R_f	0.59	0.999	σ_f	0.82	0.999
	r_1	0.03		s_1	0.00	
	r_2	0.13		s_2	0.04	
	r_3	0.23		s_3	0.15	
	τ_1 (s)	25		τ_1 (s)	25	
	τ_2 (s)	107		τ_2 (s)	107	
	τ_3 (s)	1805		τ_3 (s)	1805	
SSBR	R_f	0.55	0.999	σ_f	0.87	0.995
	r_1	0.06		s_1	0.00	
	r_2	0.15		s_2	0.05	
	r_3	0.21		s_3	0.08	
	τ_1 (s)	31		τ_1 (s)	31	
	τ_2 (s)	168		τ_2 (s)	168	
	τ_3 (s)	2189		τ_3 (s)	2189	
BR	R_f	0.85	0.999	σ_f	0.83	0.998
	r_1	0.04		s_1	0.00	
	r_2	0.08		s_2	0.03	
	r_3	0.01		s_3	0.14	
	τ_1 (s)	58		τ_1 (s)	58	
	τ_2 (s)	946		τ_2 (s)	946	
	τ_3 (s)	8825		τ_3 (s)	8825	

The $\tan \delta_{\sigma-R}$ values are evaluated to examine the response times of the different rubbers. Interestingly, in Figure 7.6, different rubbers display different response times (evidenced from the different $\tan \delta_{\sigma-R}$), signifying the influence of rubber matrix on the response time of the fillers. NR displays the least $\tan \delta_{\sigma-R}$ value, while SSBR displays the highest and BR displays an intermediate value. This could be due to differences in interactions between the rubber matrices and the carbon black. Therefore, for the same load, the filler network in NR would be disrupted first, followed by BR and SBR.

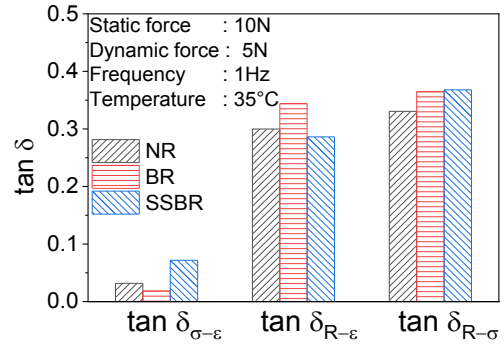


Figure 7.6: $\tan \delta$ values summarized after 1 hour from time sweep experiments for different rubbers

7.3.2 Summary

The amplitude ratios (A_2/A_1) prove that the double peaks are definite and unique piezoresistive response of the filler network and are independent of the matrix rubber. Utilizing piezoresistance data to predict stress relaxation prove to be effective also for different rubber matrices, emphasizing the applicability of the concept for all rubber types. The piezoresistive phase shift values ($\delta_{\sigma-R}$) offered a new possibility to understand the influence of rubber matrix on the response time of the fillers.

7.4 Scope for further research

7.4.1 Possible extensions of the current work

In continuation to sub-section 7.2 on SSBR composites with conventional carbon blacks [Figure 7.1](#), further studies could be done to generate a calibration chart for individual grades of conventional carbon black or targeting a specific rubber product that displays piezoresistive characteristics. This would offer a much easier and simpler route to determine the product performance by monitoring the resistance changes. Perform additional experiments to generate a fingerprint chart by identifying the distinguishable effects from individual grades of carbon blacks. Thereby, the type of carbon black could be identified in the future by comparing the properties with the fingerprint charts.

In continuation to sub-section 7.3, the temperature sweep and strain sweep experiments could be performed for different rubbers filled with CB, CNT or even conventional carbon blacks. This would offer much deeper insight on the role of matrix rubber on the dynamic piezoresistive response of the material, thereby, the rubber matrix dependent filler network behavior could be evaluated.

7.4 2 Dynamic piezoresistive studies under compression force

SSBR rubbers showed dynamic piezoresistive capabilities under compression force as well. Figure 7.7 depicts the change in mean resistance values for a 12 phr CB filled SSBR sample tested under compression strain. The findings are promising and open vast research possibilities to understand the dynamic piezoresistance of rubbers under compression force. This would relate well to rubber products such as seals, O-rings, gaskets, etc. and monitoring the stress relaxation behavior through piezoresistance would ensure more safety as any failure could be detected and avoided in time.

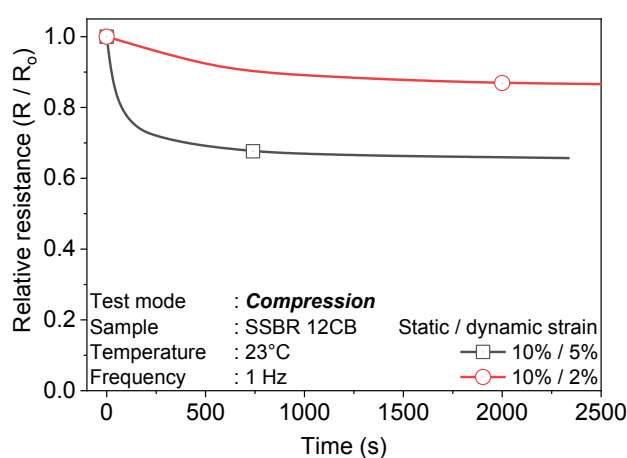


Figure 7.7: Mean resistance values for 12CB sample tested in compression mode

7.4.3 Dynamic piezoresistive studies with graphene nanoplatelets and Ionic liquids

This work covers particulate CB fillers and fibrous CNT fillers (as have high aspect ratios). Therefore, it would be highly encouraging to explore the dynamic piezoresistivity of conducting layered fillers. Graphenes and few of their allotropes are also promising alternative fillers that impart conductivity in rubbers [4, 151].

Understanding their deformation behavior of such filler morphology under dynamic conditions is also necessary. Additionally, composites could also be prepared with the assistance of ionic liquids, as they are known to offer further improvements in the electrical conductivity [179, 180].

7.4.4 Studying carbon black and silica hybrid filler systems

Carbon blacks are often used with other fillers, and a most common co-filler is silica. Assessing the dynamic piezoresistive characteristics of such dual filler composites would yield an overall insight on the filler network. Even though silica and rubber are non-conducting by nature, the piezoresistive effect could be achieved through the carbon blacks.

7.4.5 Studying the interparticle distance using tunneling theory

Piezoresistivity could also serve as a very powerful tool to evaluate the interparticle distance between fillers inside the rubber matrix. Rubber is a highly insulating medium and the electrical conduction could only happen through the 3D percolated filler network. The tunneling theory Eq. 2.2 states in simple terms that the electrical conductivity is directly related to the interparticle distance between fillers ($\sigma \propto <d>$) [26, 145]. Few works have done such studies on polymer composites and this could be attempted for rubbers as well, to understand the filler networking behavior [134, 145, 178].

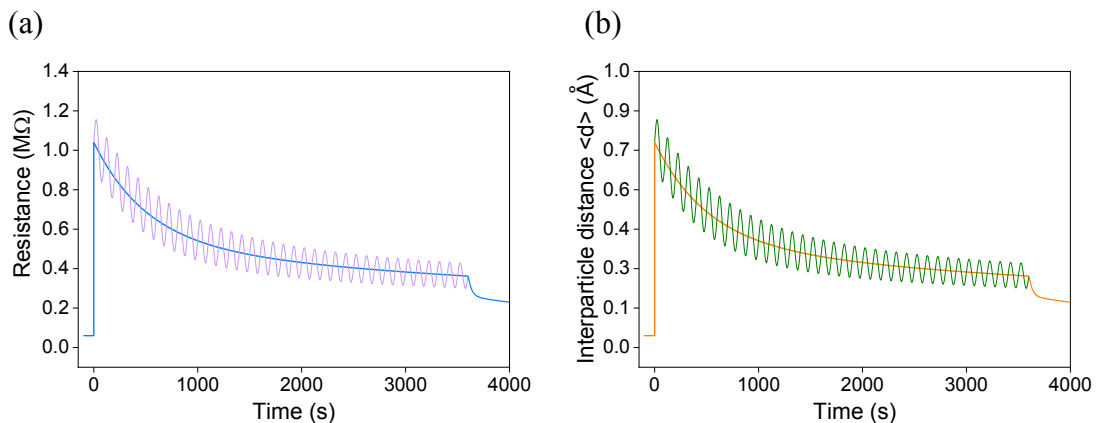


Figure 7.8: (a) Changes in resistance of a rubber sample during the dynamic experiment and (b) corresponding changes in interparticle distance for the sample calculated using tunneling theory

There would be two interparticle distances for a sample as shown in [Figure 7.8](#). First would be the interparticle distance deduced from the mean resistance values. Since the mean resistance values represent the actual resistance of the bulk of the material, the interparticle distance calculated from these values would refer to the actual state of the filler particles. It could be understood as the average of all the interparticle distances. Secondly, the dynamic load also affects the interparticle distances. It instantaneously increases the interparticle distances during loading and recovers the same during unloading. Therefore, the dynamic change in the interparticle distance could be calculated directly from the dynamic resistance amplitude values. This value would yield the maximum change in interparticle distance caused by the dynamic load.

Conclusions

In this work, piezoresistive rubber samples were developed using conventional carbon blacks, conductive carbon blacks and multiwalled carbon nanotubes as fillers with few commercial rubbers, namely SSBR, NR and BR. With the help of a dynamic mechanical analyzer and utilizing the concept of piezoresistivity, the behavior of filler network inside the rubbers was studied in detail under dynamic loading conditions. Fine tuning the piezoresistive behavior *i.e.* the strain sensitivity was achieved easily by playing with different material parameters like type of the conducting fillers, the volume fraction of the conducting fillers, process oil dosage and crosslink density of the rubber matrix. The strain-dependent electrical conductivity of the crosslinked elastomer matrix was found to be strongly dependent on the filler dispersion, filler-filler network and the structure of the filler. Rubber composites that respond to strains as low as ~ 10 % strain or highly robust characteristics (that seldom responded to mechanical strain) were developed by tweaking the compound formulation. The most strain sensitive region under uniaxial tension mode was fitted with empirical equations and this work can pave the way in designing sensors with various sensitivities that could be operated at different strain regimes. By optimizing rubber materials with the above-mentioned critical parameters, one can use such material as a “sensor” for various applications.

During cyclic deformation, the filler-filler network was found to disrupt and recover harmoniously corresponding to the applied strain. The magnitude of electrical resistance change was found to decrease for the first few cycles due to rearrangement of the filler network, after which a stable response was observed. This recoverability during cyclic measurement motivated to study the piezoresistive behavior of these materials under more complex dynamic loading conditions. As a result, first ever attempt to study the dynamic piezoresistive behavior of conductive rubber composite was conducted within this work.

During time sweep measurements, the percolated filler network was found to rearrange inside the rubber matrix, aided by the dynamic strain. This apparently reflected as decrease in electrical resistance and a possible mechanism was proposed for this behavior. The nature and behavior of the second resistance response which arise during unloading was keenly studied during time and temperature sweep

measurements and was ascribed to the reconfiguration of filler network. A higher compulsion to reconfigure reflected as stronger second peaks, while the effect was found to be maximum near the glass transition temperature T_g , due to limited mobility of the filler network. The influence of critical parameters on the piezoresistive behavior such as dynamic load, frequency, temperature, and crosslink density was considered throughout the study. Each parameter had their own signature effect on the piezoresistive response and the findings offered a preliminary understanding of the filler network behavior inside the rubber matrix at various dynamic loading conditions. In general, situations that ease the filler mobility such as high temperature, low frequency, and low crosslink density resulted in a lower degree of rearrangement of the percolating filler network.

A correlation was established between mechanical stress relaxation and piezoresistivity. Therefore, by knowing the electrical resistance changes of the rubber sample, it's corresponding mechanical stress could be estimated. The changes in electrical resistance in a rubber product could therefore be easily monitored. This technique would help in avoiding unexpected or premature failure of rubber components. It is generally difficult to predict the stress relaxation in a rubber product and especially when they serve in intricate areas. Moreover, current stress detection mechanisms are expensive and are also non-rubber products leading to compatibility issues. So, it would be certainly advantageous when the rubber product itself plays the role of a sensor.

The piezoresistive phase shift value ($\delta_{\sigma-R}$) gives a clear picture of the responsiveness of the filler network. Time sweep measurements at various conditions conveyed that after a few cycles, the filler network would display constant $\delta_{\sigma-R}$ values, whereas during temperature sweep, the values were found to be larger at low temperatures. From temperature sweep experiments, it could be said that below T_g , the applied force hardly affects the filler network, *i.e.*, the filler network takes more time to respond and it is the polymer matrix that responds instantly and plays also a major role.

The amplitude ratios of the first and second electrical resistance peaks (dynamic resistance response) from time and temperature sweep measurements evidenced that

second peaks are a prominent piezoresistive response of the material. The amplitude ratios (A_2/A_1) were found to be constant during time sweep experiments. High temperature, low frequency, and low crosslink density displayed minimal influences on second peaks as these conditions favor smooth reconfiguration of the filler network during unloading. During temperature sweep, the peak ratios were smaller at high temperatures and found to increase at low temperatures, with the maximum effect occurring near the T_g . This signified that the filler network suffered a higher extent of reconfiguration at low temperatures and especially more at T_g .

Possibilities of utilizing the concept of piezoresistivity for real-time use are discussed by studying the piezoresistive behavior of SSBR filled with conventional carbon blacks and three different rubber matrices filled with conductive carbon blacks. A correlation exists between stress relaxation and piezoresistance change for the conventional carbon blacks as well. Second peaks were observed even at high temperatures due to the higher filler loading, which became much stronger at lower temperatures. The strain sweep profiles of the conventional blacks appeared similar to the conductive carbon black. Therefore, irrespective of the filler type, they display similar behavior, meaning they share the same mechanism. Therefore, the concept is applicable for conventional carbon blacks, provided they display piezoresistive characteristics.

Apart from SSBR, NR and BR are commonly used rubbers in the tire industry. Therefore, the dynamic piezoresistivity is tested on these rubbers as well. All the rubbers offer the possibility to correlate stress relaxation with the piezoresistivity. Second peaks, an imperative effect that occurs during unloading were observed for all the rubbers, highlighting the effect being a prominent piezoresistive response from the filler network. Interestingly, different rubbers displayed different response times (predicted from the $\tan \delta_{\sigma-R}$ values), signifying the role played by rubber-filler interactions on the piezoresistive properties.

To conclude, the rubber polymer network is intrinsically a highly insulating medium and the electrical conductivity of a rubber composite containing electrically conductive fillers is tracked back to the formation of a 3D percolated filler network.

In this case, the electrical conductivity is directly related to the interparticle distance between fillers ($\sigma \propto \langle d \rangle$) [145]. In the course of dynamic-mechanical deformations of the conductive rubber composites, eventual structural changes of the filler network could therefore be correlated and interpreted from the recorded electrical resistance data. Hence, this study not just portrayed the piezoresistive characteristics under dynamic conditions; but projects the changes occurring in the filler network.

The information will be helpful in understanding the behavior of filler particles and filler network in rubber products that are constantly experiencing dynamic forces such as tires, conveyor belts, dynamic seals, shafts, dampers, etc. Moreover, piezoresistivity is an effect generally displayed by all conducting filler, *e.g.* Graphite, Graphenes, conventional carbon blacks, etc., provided, the filler concentration is more than the electrical percolation threshold. Therefore, this concept is widely applicable for most of the rubber products.

An example from recent tire research is shown in [Figure 8.1](#) to highlight the importance of rubber based sensors. Tire manufacturers are trying to incorporate sensors into tires for developing smart adaptable tires for the future [181]. One main disadvantage of such sensing elements is that they are usually non-rubber objects, sometimes resulting in incompatibility. Therefore in such areas, rubber sensors developed from present work pose advantage in innumerable ways, such as: cost-effectiveness, perfect compatibility with the tire rubber, synchronous deformation of the sensor element with the tire deformation, and many more.



[Figure 8.1: Sensor embedded in tire-tread to detect tire pressure and sense road conditions \[181\].](#) Reproduced from Continental Tires – Press release August 12, 2017.

References

-
- [1] M. H. Polley, and B. B. S. T. Boonstra, "Carbon Blacks for Highly Conductive Rubber," *Rubber Chemistry and Technology*, vol. 30, no. 1, pp. 170-179, 1957.
- [2] J.-S. Noh, "Conductive Elastomers for Stretchable Electronics, Sensors and Energy Harvesters," *Polymers*, vol. 8, no. 4, pp. 123, 2016.
- [3] P. K. Pramanik, D. Khastgir, S. K. De *et al.*, "Pressure-sensitive electrically conductive nitrile rubber composites filled with particulate carbon black and short carbon fibre," *Journal of Materials Science*, vol. 25, no. 9, pp. 3848-3853, 1990.
- [4] C. Tang, N. Chen, and X. Hu, "Conducting Polymer Nanocomposites: Recent Developments and Future Prospects," *Conducting Polymer Hybrids*, V. Kumar, S. Kalia and H. C. Swart, eds., pp. 1-44, Cham: Springer International Publishing, 2017.
- [5] S. De, P. E. Lyons, S. Sorel *et al.*, "Transparent, flexible, and highly conductive thin films based on polymer-nanotube composites," *ACS Nano*, vol. 3, no. 3, pp. 714-20, Mar 24, 2009.
- [6] M.-C. Choi, Y. Kim, and C.-S. Ha, "Polymers for flexible displays: From material selection to device applications," *Progress in Polymer Science*, vol. 33, no. 6, pp. 581-630, 2008.
- [7] P. J. Skabara, and N. J. Findlay, "Polymer Electronics. Oxford Master Series in Physics 22. By Mark Geoghegan and Georges Hadziioannou," *Angewandte Chemie International Edition*, vol. 53, no. 13, pp. 3310-3310, 2014.
- [8] M. Bartsch, H. Kempa, M. Otto *et al.*, "Device and circuit simulation of printed polymer electronics," *Organic Electronics*, vol. 8, no. 4, pp. 431-438, 2007.
- [9] S. Cao, S. Pyatt, C. J. Anthony *et al.*, "Flexible Bond Wire Capacitive Strain Sensor for Vehicle Tyres," *Sensors (Basel)*, vol. 16, no. 6, Jun 21, 2016.
- [10] G. Erdogan, L. Alexander, and R. Rajamani, "A novel wireless piezoelectric tire sensor for the estimation of slip angle," *Measurement Science and Technology*, vol. 21, no. 1, pp. 015201, 2009.
- [11] K. Subramaniam, A. Das, and G. Heinrich, "Development of conducting polychloroprene rubber using imidazolium based ionic liquid modified multi-walled carbon nanotubes," *Composites Science and Technology*, vol. 71, no. 11, pp. 1441-1449, 2011.
- [12] Rajesh, T. Ahuja, and D. Kumar, "Recent progress in the development of nano-structured conducting polymers/nanocomposites for sensor applications," *Sensors and Actuators B: Chemical*, vol. 136, no. 1, pp. 275-286, 2009.
- [13] M. Kazemian Abyaneh, S. Ekar, and S. K. Kulkarni, "Piezoresistivity and Mechanical Behavior of Metal-polymer Composites under Uniaxial Pressure," *Journal of Materials Science Research*, vol. 1, no. 3, 2012.
- [14] F. Lux, "Models proposed to explain the electrical conductivity of mixtures made of conductive and insulating materials," *Journal of Materials Science*, vol. 28, no. 2, pp. 285-301, January 01, 1993.
- [15] D. Bulgin, "Electrically Conductive Rubber," *Rubber Chemistry and Technology*, vol. 19, no. 3, pp. 667-695, 1946/09/01, 1946.
- [16] M. Knite, V. Teteris, A. Kiploka *et al.*, "Polyisoprene-carbon black nanocomposites as tensile strain and pressure sensor materials," *Sensors and Actuators A: Physical*, vol. 110, no. 1-3, pp. 142-149, 2004.

- [17] M. Knite, K. Ozols, G. Sakale *et al.*, "Polyisoprene and high structure carbon nanoparticle composite for sensing organic solvent vapours," *Sensors and Actuators B: Chemical*, vol. 126, no. 1, pp. 209-213, 2007.
- [18] B. Kumar, M. Castro, and J. F. Feller, "Poly(lactic acid)-multi-wall carbon nanotube conductive biopolymer nanocomposite vapour sensors," *Sensors and Actuators B: Chemical*, vol. 161, no. 1, pp. 621-628, 2012.
- [19] A. Talaie, J. Y. Lee, H. Eisazadeh *et al.*, "Towards a conducting polymer-based electronic nose and electronic tongue," *Iranian Polymer Journal*, vol. 9, no. 1, pp. 3-10, Jan, 2000.
- [20] C. Gau, H. S. Ko, and H. T. Chen, "Piezoresistive characteristics of MWNT nanocomposites and fabrication as a polymer pressure sensor," *Nanotechnology*, vol. 20, no. 18, pp. 185503, May 6, 2009.
- [21] C. Yong Ryu, S. Hoon Nam, and S. Kim, "Conductive rubber electrode for wearable health monitoring," *Conf Proc IEEE Eng Med Biol Soc*, vol. 4, pp. 3479-81, 2005.
- [22] J. A. Rogers, T. Someya, and Y. Huang, "Materials and Mechanics for Stretchable Electronics," *Science*, vol. 327, no. 5973, pp. 1603-1607, 2010.
- [23] M. Izadi, F. Danafar, and M. Z. A. Ab Kadir, "Natural Rubber- Carbon Nanotubes Composites, Recent Advances and Challenges for Electrical Applications," *2016 Ieee International Conference on Automatic Control and Intelligent Systems (I2casis)*, pp. 61-65, 2016.
- [24] M. G. Siswanto, N. P. Bo, Parangtopo *et al.*, "Electrical Conductivity and ESR Studies of Carbon-Black-Loaded Natural Rubber," *Rubber Chemistry and Technology*, vol. 61, no. 2, pp. 269-280, 1988.
- [25] N. C. Das, T. K. Chaki, and D. Khastgir, "Effect of axial stretching on electrical resistivity of short carbon fibre and carbon black filled conductive rubber composites," *Polymer International*, vol. 51, no. 2, pp. 156-163, 2002.
- [26] Alamusi, N. Hu, H. Fukunaga *et al.*, "Piezoresistive strain sensors made from carbon nanotubes based polymer nanocomposites," *Sensors (Basel)*, vol. 11, no. 11, pp. 10691-723, 2011.
- [27] A. Vega, J. Sumfleth, H. Wittich *et al.*, "Time and temperature dependent piezoresistance of carbon nanofiller/polymer composites under dynamic load," *Journal of Materials Science*, vol. 47, no. 6, pp. 2648-2657, 2011.
- [28] W. Obitayo, and T. Liu, "A Review: Carbon Nanotube-Based Piezoresistive Strain Sensors," *Journal of Sensors*, vol. 2012, pp. 1-15, 2012.
- [29] N. T. Selvan, S. B. Eshwaran, A. Das *et al.*, "Piezoresistive natural rubber-multiwall carbon nanotube nanocomposite for sensor applications," *Sensors and Actuators a-Physical*, vol. 239, pp. 102-113, Mar 1, 2016.
- [30] D. Sethi, R. Ram, and D. Khastgir, "Electrical conductivity and dynamic mechanical properties of silicon rubber-based conducting composites: effect of cyclic deformation, pressure and temperature," *Polymer International*, vol. 66, no. 9, pp. 1295-1305, 2017.
- [31] T. Villmow, A. John, P. Pötschke *et al.*, "Polymer/carbon nanotube composites for liquid sensing: Selectivity against different solvents," *Polymer*, vol. 53, no. 14, pp. 2908-2918, 2012.
- [32] T. S. Natarajan, S. B. Eshwaran, K. W. Stöckelhuber *et al.*, "Strong Strain Sensing Performance of Natural Rubber Nanocomposites," *ACS Appl Mater Interfaces*, vol. 9, no. 5, pp. 4860-4872, Feb 08, 2017.

- [33] J. Kost, M. Narkis, and A. Foux, "Resistivity behavior of carbon-black-filled silicone rubber in cyclic loading experiments," *Journal of Applied Polymer Science*, vol. 29, no. 12, pp. 3937-3946, 1984.
- [34] G. Georgousis, K. Roumpos, E. Kontou *et al.*, "Strain and damage monitoring in SBR nanocomposites under cyclic loading," *Composites Part B: Engineering*, vol. 131, no. Supplement C, pp. 50-61, 2017/12/15/, 2017.
- [35] K. Yamaguchi, J. J. C. Busfield, and A. G. Thomas, "Electrical and mechanical behavior of filled elastomers. I. The effect of strain," *Journal of Polymer Science Part B: Polymer Physics*, vol. 41, no. 17, pp. 2079-2089, 2003.
- [36] J. J. C. Busfield, A. G. Thomas, and K. Yamaguchi, "Electrical and mechanical behavior of filled elastomers 2: The effect of swelling and temperature," *Journal of Polymer Science Part B: Polymer Physics*, vol. 42, no. 11, pp. 2161-2167, 2004.
- [37] J. J. C. Busfield, A. G. Thomas, and K. Yamaguchi, "Electrical and mechanical behavior of filled rubber. III. Dynamic loading and the rate of recovery," *Journal of Polymer Science Part B: Polymer Physics*, vol. 43, no. 13, pp. 1649-1661, 2005.
- [38] P. Ciselli, L. Lu, J. J. C. Busfield *et al.*, "Piezoresistive polymer composites based on EPDM and MWNTs for strain sensing applications," *E-Polymers*, vol. 14, pp. 13, Feb 17, 2010.
- [39] S. Sokolov, "Calculation of the stress-strain state of pneumatic tires by the finite element method," *Journal of Machinery Manufacture and Reliability*, vol. 36, no. 1, pp. 45-49, 2007.
- [40] X. Yang, "Finite element analysis and experimental investigation of tyre characteristics for developing strain-based intelligent tyre system," School of Mechanical Engineering, University of Birmingham, 2011.
- [41] R. Matsuzaki, T. Keating, A. Todoroki *et al.*, "Rubber-based strain sensor fabricated using photolithography for intelligent tires," *Sensors and Actuators A: Physical*, vol. 148, no. 1, pp. 1-9, 2008.
- [42] E. Trueman, Great Britan GB5757, 1882.
- [43] E. Bormann, *High tension rubber insulated cable* US2096840, 1937.
- [44] M. J. Granier, "Propriétés conductrices du caoutchouc fortement chargé en noir de fumée," *Comptes rendus hebdomadaires des séances de l'Académie des sciences*, vol. 196, 1933.
- [45] T. L. Shepherd, *Improvements in and relating to the production of rubber threads, filaments and the like and fabrics made therewith* U.K. GB467083 (A), 1937.
- [46] B. C. Borel and Société d'Exploitation des Câbles Electriques Système Berthoud, *Process for the protection of metals against electrolytic corrosion, and means for carrying out such process*, U.K. GB447064 (A), 1936.
- [47] L. E. C. Company, *Improvements in or relating to rubber compositions having electrical conducting properties* U.K. GB526894 (A), 1940.
- [48] Standard Telephones Cables Ltd, Thomas Robertson Scott, John Krauss Webb *et al.*, *Improvements in insulated electric cables*, U.K. GB527734 (A), 1940.
- [49] B. J. Habgood, and J. R. S. Waring, "Electrically Conducting Neoprene and Rubber," *Rubber Chemistry and Technology*, vol. 15, no. 1, pp. 146-157, 1942/03/01, 1942.
- [50] U. S. R. Company, *Improvements in a pneumatic tyre and method of making same*, UK GB544757, 1940.

- [51] N. T. H. Maatschappij, *Improved manufacture of electric conducting and resistance material* Great Britan GB236880, 1925.
- [52] H. D.-e. K. NV, *The manufacture of electrical conductors*, Great Britan GB396891, 1933.
- [53] C. R. Boggs, *High tension rubber insulation*, U.S. US2074826 (A), to SIMPLEX WIRE & CABLE COMPANY, USPTO, 1937.
- [54] C. Gummiwerk, *Improvements in and relating to card-clothing for carding engines*, GB467141, 1937.
- [55] G. Co., *Improvements in or relating to composite resilient materials* GB518490, 1940.
- [56] A. R. Thomas;, and H. I. Company, *Improvements in or relating to electro-deposition of metals and metal alloys* GB534818, 1941.
- [57] E. M. Abdel-Bary, M. Amin, and H. H. Hassan, "Factors affecting electrical conductivity of carbon black-loaded rubber. II. Effect of concentration and type of carbon black on electrical conductivity of SBR," *Journal of Polymer Science: Polymer Chemistry Edition*, vol. 17, no. 7, pp. 2163-2172, 1979.
- [58] Z. H. Li, J. Zhang, and S. J. Chen, "Effects of carbon blacks with various structures on vulcanization and reinforcement of filled ethylene-propylene-diene rubber," *Express Polymer Letters*, vol. 2, no. 10, pp. 695-704, 2008.
- [59] B. B. S. T. Boonstra, and E. M. Dannenberg, "Electrical Conductivity of Rubber-Carbon Black Vulcanizates," *Industrial & Engineering Chemistry*, vol. 46, no. 1, pp. 218-227, 1954/01/01, 1954.
- [60] S. Iijima, "Helical Microtubules of Graphitic Carbon," *Nature*, vol. 354, no. 6348, pp. 56-58, Nov 7, 1991.
- [61] K. S. Novoselov, A. K. Geim, S. V. Morozov *et al.*, "Electric Field Effect in Atomically Thin Carbon Films," *Science*, vol. 306, no. 5696, pp. 666-669, 2004.
- [62] A. A. Athawale, and A. M. Joshi, "Electronic Applications of Ethylene Propylene Diene Monomer Rubber and Its Composites," *Flexible and Stretchable Electronic Composites*, D. Ponnamma, K. K. Sadasivuni, C. Wan *et al.*, eds., pp. 305-333, Cham: Springer International Publishing, 2016.
- [63] B. P. Kapgate, and C. Das, "Electronic Applications of Chloroprene Rubber and Its Composites," *Flexible and Stretchable Electronic Composites*, D. Ponnamma, K. K. Sadasivuni, C. Wan *et al.*, eds., pp. 279-304, Cham: Springer International Publishing, 2016.
- [64] K. K. Sadasivuni, D. Ponnamma, J.-J. Cabibihan *et al.*, "Electronic Applications of Polydimethylsiloxane and Its Composites," *Flexible and Stretchable Electronic Composites*, D. Ponnamma, K. K. Sadasivuni, C. Wan *et al.*, eds., pp. 199-228, Cham: Springer International Publishing, 2016.
- [65] D. Ponnamma, K. K. Sadasivuni, K. T. Varughese *et al.*, "Natural Polyisoprene Composites and Their Electronic Applications," *Flexible and Stretchable Electronic Composites*, D. Ponnamma, K. K. Sadasivuni, C. Wan *et al.*, eds., pp. 1-35, Cham: Springer International Publishing, 2016.
- [66] M. T. Sebastian, and J. Chameswary, "Poly(Isobutylene-co-Isoprene) Composites for Flexible Electronic Applications," *Flexible and Stretchable Electronic Composites*, D. Ponnamma, K. K. Sadasivuni, C. Wan *et al.*, eds., pp. 335-364, Cham: Springer International Publishing, 2016.
- [67] R. Stephen, and S. Thomas, "Electronic Applications of Styrene-Butadiene Rubber and Its Composites," *Flexible and Stretchable Electronic Composites*,

- D. Ponnammma, K. K. Sadasivuni, C. Wan *et al.*, eds., pp. 261-277, Cham: Springer International Publishing, 2016.
- [68] V. I. Roldughin, and V. V. Vysotskii, "Percolation properties of metal-filled polymer films, structure and mechanisms of conductivity," *Progress in Organic Coatings*, vol. 39, no. 2-4, pp. 81-100, 2000.
- [69] Y. P. Mamunya, V. V. Davydenko, P. Pissis *et al.*, "Electrical and thermal conductivity of polymers filled with metal powders," *European Polymer Journal*, vol. 38, no. 9, pp. 1887-1897, 2002.
- [70] S. P. Lacour, J. Jones, Z. Suo *et al.*, "Design and Performance of Thin Metal Film Interconnects for Skin-Like Electronic Circuits," *IEEE Electron Device Letters*, vol. 25, no. 4, pp. 179-181, 2004.
- [71] G. Chen, "Preparation of a poly(vinyl chloride)/layered double hydroxide nanocomposite with a reduced heavy-metal thermal stabilizer," *Journal of Applied Polymer Science*, vol. 106, no. 2, pp. 817-820, 2007.
- [72] S. P. Lacour, S. Benmerah, E. Tarte *et al.*, "Flexible and stretchable micro-electrodes for in vitro and in vivo neural interfaces," *Medical & Biological Engineering & Computing*, vol. 48, no. 10, pp. 945-954, October 01, 2010.
- [73] R. Pelrine, R. D. Kornbluh, Q. Pei *et al.*, "Dielectric elastomer artificial muscle actuators: toward biomimetic motion." p. 12.
- [74] R. Shankar, T. K. Ghosh, and R. J. Spontak, "Dielectric elastomers as next-generation polymeric actuators," *Soft Matter*, vol. 3, no. 9, pp. 1116-1129, 2007.
- [75] P. Brochu, and Q. Pei, "Advances in Dielectric Elastomers for Actuators and Artificial Muscles," *Macromolecular Rapid Communications*, vol. 31, no. 1, pp. 10-36, 2010.
- [76] R. J. Full, and K. Meijer, "Artificial muscles versus natural actuators from frogs to flies." p. 8.
- [77] R. F. Service, "Electronic Textiles Charge Ahead," *Science*, vol. 301, no. 5635, pp. 909-911, 2003.
- [78] K. W. Oh, H. J. Park, and S. H. Kim, "Stretchable conductive fabric for electrotherapy," *Journal of Applied Polymer Science*, vol. 88, no. 5, pp. 1225-1229, 2003.
- [79] W. A. Daoud, J. H. Xin, and Y. S. Szeto, "Polyethylenedioxythiophene coatings for humidity, temperature and strain sensing polyamide fibers," *Sensors and Actuators B: Chemical*, vol. 109, no. 2, pp. 329-333, 2005/09/14/, 2005.
- [80] C. Pang, C. Lee, and K.-Y. Suh, "Recent advances in flexible sensors for wearable and implantable devices," *Journal of Applied Polymer Science*, vol. 130, no. 3, pp. 1429-1441, 2013.
- [81] L. Hu, M. Pasta, F. L. Mantia *et al.*, "Stretchable, porous, and conductive energy textiles," *Nano Lett*, vol. 10, no. 2, pp. 708-14, Feb 10, 2010.
- [82] K. Takei, T. Takahashi, J. C. Ho *et al.*, "Nanowire active-matrix circuitry for low-voltage macroscale artificial skin," vol. 9, pp. 821, 09/12/online, 2010.
- [83] S. Wagner, S. P. Lacour, J. Jones *et al.*, "Electronic skin: architecture and components," *Physica E: Low-dimensional Systems and Nanostructures*, vol. 25, no. 2, pp. 326-334, 2004/11/01/, 2004.
- [84] S. C. B. Mannsfeld, B. C. K. Tee, R. M. Stoltenberg *et al.*, "Highly sensitive flexible pressure sensors with microstructured rubber dielectric layers," vol. 9, pp. 859, 09/12/online, 2010.

- [85] A. Russo, B. Y. Ahn, J. J. Adams *et al.*, “Pen-on-Paper Flexible Electronics,” *Advanced Materials*, vol. 23, no. 30, pp. 3426-3430, 2011.
- [86] J. A. Rogers, Z. Bao, K. Baldwin *et al.*, “Paper-like electronic displays: Large-area rubber-stamped plastic sheets of electronics and microencapsulated electrophoretic inks,” *Proceedings of the National Academy of Sciences*, vol. 98, no. 9, pp. 4835-4840, April 24, 2001, 2001.
- [87] D.-H. Kim, Y.-S. Kim, J. Wu *et al.*, “Ultrathin Silicon Circuits With Strain-Isolation Layers and Mesh Layouts for High-Performance Electronics on Fabric, Vinyl, Leather, and Paper,” *Advanced Materials*, vol. 21, no. 36, pp. 3703-3707, 2009.
- [88] E. Biddiss, and T. Chau, “Dielectric elastomers as actuators for upper limb prosthetics: Challenges and opportunities,” *Medical Engineering & Physics*, vol. 30, no. 4, pp. 403-418, 2008/05/01/, 2008.
- [89] M. Jin-Hee, B. Dong Hyun, C. Yoon Young *et al.*, “Wearable polyimide–PDMS electrodes for intrabody communication,” *Journal of Micromechanics and Microengineering*, vol. 20, no. 2, pp. 025032, 2010.
- [90] R. Carta, P. Jourand, B. Hermans *et al.*, “Design and implementation of advanced systems in a flexible-stretchable technology for biomedical applications,” *Sensors and Actuators A: Physical*, vol. 156, no. 1, pp. 79-87, 2009/11/01/, 2009.
- [91] O. Graudejus, B. Morrison, C. Goletiani *et al.*, “Encapsulating Elastically Stretchable Neural Interfaces: Yield, Resolution, and Recording/Stimulation of Neural Activity,” *Advanced Functional Materials*, vol. 22, no. 3, pp. 640-651, 2012.
- [92] L. Johnson, F. K. Perkins, T. O’Hearn *et al.*, “Electrical stimulation of isolated retina with microwire glass electrodes,” *Journal of Neuroscience Methods*, vol. 137, no. 2, pp. 265-273, 2004/08/30/, 2004.
- [93] N. Paine, J. S. Mehling, J. Holley *et al.*, “Actuator Control for the NASA-JSC Valkyrie Humanoid Robot: A Decoupled Dynamics Approach for Torque Control of Series Elastic Robots,” *Journal of Field Robotics*, vol. 32, no. 3, pp. 378-396, 2015.
- [94] J. C. Nawroth, H. Lee, A. W. Feinberg *et al.*, “A tissue-engineered jellyfish with biomimetic propulsion,” *Nat Biotech*, vol. 30, no. 8, pp. 792-797, 08/print, 2012.
- [95] E. Buselli, A. M. Smith, L. M. Grover *et al.*, “Development and characterization of a bio-hybrid skin-like stretchable electrode,” *Microelectronic Engineering*, vol. 88, no. 8, pp. 1676-1680, 2011/08/01/, 2011.
- [96] K. Gabor, L. Patrick, and W. Michael, “An arm wrestling robot driven by dielectric elastomer actuators,” *Smart Materials and Structures*, vol. 16, no. 2, pp. S306, 2007.
- [97] D.-H. Kim, J. Xiao, J. Song *et al.*, “Stretchable, Curvilinear Electronics Based on Inorganic Materials,” *Advanced Materials*, vol. 22, no. 19, pp. 2108-2124, 2010.
- [98] D.-H. Kim, J.-H. Ahn, W. M. Choi *et al.*, “Stretchable and Foldable Silicon Integrated Circuits,” *Science*, vol. 320, no. 5875, pp. 507-511, 2008.
- [99] D.-H. Kim, J. Song, W. M. Choi *et al.*, “Materials and noncoplanar mesh designs for integrated circuits with linear elastic responses to extreme mechanical deformations,” *Proceedings of the National Academy of Sciences*, vol. 105, no. 48, pp. 18675-18680, December 2, 2008, 2008.

- [100] P. J. Hung, K. Jeong, G. L. Liu *et al.*, "Microfabricated suspensions for electrical connections on the tunable elastomer membrane," *Applied Physics Letters*, vol. 85, no. 24, pp. 6051-6053, 2004.
- [101] T. Someya, Y. Kato, T. Sekitani *et al.*, "Conformable, flexible, large-area networks of pressure and thermal sensors with organic transistor active matrixes," *Proceedings of the National Academy of Sciences of the United States of America*, vol. 102, no. 35, pp. 12321-12325, August 30, 2005, 2005.
- [102] S. K. Lee, B. J. Kim, H. Jang *et al.*, "Stretchable graphene transistors with printed dielectrics and gate electrodes," *Nano Lett*, vol. 11, no. 11, pp. 4642-6, Nov 09, 2011.
- [103] Z. Yu, X. Niu, Z. Liu *et al.*, "Intrinsically Stretchable Polymer Light-Emitting Devices Using Carbon Nanotube-Polymer Composite Electrodes," *Advanced Materials*, vol. 23, no. 34, pp. 3989-3994, 2011.
- [104] Z. Fan, H. Razavi, J.-w. Do *et al.*, "Three-dimensional nanopillar-array photovoltaics on low-cost and flexible substrates," vol. 8, pp. 648, 07/05/online, 2009.
- [105] M. Kaltenbrunner, G. Kettlgruber, C. Siket *et al.*, "Arrays of Ultracompliant Electrochemical Dry Gel Cells for Stretchable Electronics," *Advanced Materials*, vol. 22, no. 18, pp. 2065-2067, 2010.
- [106] J. Lee, J. Wu, M. Shi *et al.*, "Stretchable GaAs Photovoltaics with Designs That Enable High Areal Coverage," *Advanced Materials*, vol. 23, no. 8, pp. 986-991, 2011.
- [107] D. McCoul, W. Hu, M. Gao *et al.*, "Recent Advances in Stretchable and Transparent Electronic Materials," *Advanced Electronic Materials*, vol. 2, no. 5, pp. 1500407-n/a, 2016.
- [108] S. R. Broadbent, and J. M. Hammersley, "Percolation processes," *Mathematical Proceedings of the Cambridge Philosophical Society*, vol. 53, no. 03, pp. 629, 07//, 2008.
- [109] D. Stauffer, "Scaling Theory of Percolation Clusters," *Physics Reports-Review Section of Physics Letters*, vol. 54, no. 1, pp. 1-74, 1979.
- [110] S. Kirkpatrick, "Percolation and Conduction," *Reviews of Modern Physics*, vol. 45, no. 4, pp. 574-588, 10/01/, 1973.
- [111] R. Zallen, "The Percolation Model," *The Physics of Amorphous Solids*, pp. 135-204: Wiley-VCH Verlag GmbH & Co. KGaA, 2005.
- [112] S. Vionnet-Menot, C. Grimaldi, T. Maeder *et al.*, "Tunneling-percolation origin of nonuniversality: Theory and experiments," *Physical Review B*, vol. 71, no. 6, pp. 064201, 02/16/, 2005.
- [113] W. Bauhofer, and J. Z. Kovacs, "A review and analysis of electrical percolation in carbon nanotube polymer composites," *Composites Science and Technology*, vol. 69, no. 10, pp. 1486-1498, 2009/08/01/, 2009.
- [114] P.-G. Ren, Y.-Y. Di, Q. Zhang *et al.*, "Composites of Ultrahigh-Molecular-Weight Polyethylene with Graphene Sheets and/or MWCNTs with Segregated Network Structure: Preparation and Properties," *Macromolecular Materials and Engineering*, vol. 297, no. 5, pp. 437-443, 2012.
- [115] G. C. Long, C. Y. Tang, K. W. Wong *et al.*, "Resolving the dilemma of gaining conductivity but losing environmental friendliness in producing polystyrene/graphene composites via optimizing the matrix-filler structure," *Green Chemistry*, vol. 15, no. 3, pp. 821-828, 2013.

- [116] O. Regev, P. N. B. ElKati, J. Loos *et al.*, "Preparation of Conductive Nanotube–Polymer Composites Using Latex Technology," *Advanced Materials*, vol. 16, no. 3, pp. 248-251, 2004.
- [117] N. Hu, Z. Masuda, C. Yan *et al.*, "The electrical properties of polymer nanocomposites with carbon nanotube fillers," *Nanotechnology*, vol. 19, no. 21, pp. 215701, May 28, 2008.
- [118] D. Stauffer, and A. Aharony, *Introduction to Percolation Theory*: Taylor & Francis, 1992.
- [119] X. Zeng, X. Xu, P. M. Shenai *et al.*, "Characteristics of the Electrical Percolation in Carbon Nanotubes/Polymer Nanocomposites," *The Journal of Physical Chemistry C*, vol. 115, no. 44, pp. 21685-21690, 2011.
- [120] H. Tang, X. Chen, and Y. Luo, "Electrical and dynamic mechanical behavior of carbon black filled polymer composites," *European Polymer Journal*, vol. 32, no. 8, pp. 963-966, 1996/08/01/, 1996.
- [121] A. Mierczynska, M. Mayne-L'Hermite, G. Boiteux *et al.*, "Electrical and mechanical properties of carbon nanotube/ultrahigh-molecular-weight polyethylene composites prepared by a filler prelocalization method," *Journal of Applied Polymer Science*, vol. 105, no. 1, pp. 158-168, 2007.
- [122] P. M. Ajayan, and J. M. Tour, "Materials Science: Nanotube composites," *Nature*, vol. 447, no. 7148, pp. 1066-1068, 06/28/print, 2007.
- [123] K. D. Ausman, R. Piner, O. Lourie *et al.*, "Organic Solvent Dispersions of Single-Walled Carbon Nanotubes: Toward Solutions of Pristine Nanotubes," *The Journal of Physical Chemistry B*, vol. 104, no. 38, pp. 8911-8915, 2000/09/01, 2000.
- [124] K. Balasubramanian, and M. Burghard, "Chemically Functionalized Carbon Nanotubes," *Small*, vol. 1, no. 2, pp. 180-192, 2005.
- [125] N. Grossiord, J. Loos, O. Regev *et al.*, "Toolbox for Dispersing Carbon Nanotubes into Polymers To Get Conductive Nanocomposites," *Chemistry of Materials*, vol. 18, no. 5, pp. 1089-1099, 2006/03/01, 2006.
- [126] K. Subramaniam, A. Das, F. Simon *et al.*, "Networking of ionic liquid modified CNTs in SSBR," *European Polymer Journal*, vol. 49, no. 2, pp. 345-352, 2013.
- [127] Y. Zhan, M. Lavorgna, G. Buonocore *et al.*, "Enhancing electrical conductivity of rubber composites by constructing interconnected network of self-assembled graphene with latex mixing," *Journal of Materials Chemistry*, vol. 22, no. 21, pp. 10464, 2012.
- [128] L. Bokobza, M. Rahmani, C. Belin *et al.*, "Blends of carbon blacks and multiwall carbon nanotubes as reinforcing fillers for hydrocarbon rubbers," *Journal of Polymer Science Part B: Polymer Physics*, vol. 46, no. 18, pp. 1939-1951, 2008.
- [129] A. Das, K. W. Stöckelhuber, R. Jurk *et al.*, "Modified and unmodified multiwalled carbon nanotubes in high performance solution-styrene–butadiene and butadiene rubber blends," *Polymer*, vol. 49, no. 24, pp. 5276-5283, 2008.
- [130] K. P. Sau, T. K. Chaki, and D. Khastgir, "Electrical and mechanical properties of conducting carbon black filled composites based on rubber and rubber blends," *Journal of Applied Polymer Science*, vol. 71, no. 6, pp. 887-895, 1999.
- [131] W.-T. Park, "Piezoresistivity," *Encyclopedia of Nanotechnology*, B. Bhushan, ed., pp. 2111-2117, Dordrecht: Springer Netherlands, 2012.

- [132] W. Thomson, "On the Electro-Dynamic Qualities of Metals:--Effects of Magnetization on the Electric Conductivity of Nickel and of Iron," *Proceedings of the Royal Society of London*, vol. 8, no. 0, pp. 546-550, January 1, 1856, 1856.
- [133] J. W. Cookson, "Theory of the Piezo-Resistive Effect," *Physical Review*, vol. 47, no. 2, pp. 194-195, 01/15/, 1935.
- [134] N. Hu, Y. Karube, C. Yan *et al.*, "Tunneling effect in a polymer/carbon nanotube nanocomposite strain sensor," *Acta Materialia*, vol. 56, no. 13, pp. 2929-2936, Aug, 2008.
- [135] X.-W. Zhang, Y. Pan, Q. Zheng *et al.*, "Time dependence of piezoresistance for the conductor-filled polymer composites," *Journal of Polymer Science Part B: Polymer Physics*, vol. 38, no. 21, pp. 2739-2749, 2000.
- [136] T. Villmow, S. Pegel, A. John *et al.*, "Liquid sensing: smart polymer/CNT composites," *Materials Today*, vol. 14, no. 7-8, pp. 340-345, 2011.
- [137] H. H. Hassan, S. A. Khairy, S. B. El-Guiziri *et al.*, "Influence of static and cyclic compression on the electrical conductivity of FEF black-loaded rubbers," *Polymer Bulletin*, vol. 22, no. 5-6, pp. 621-627, 1989.
- [138] S. A. Mansour, "Effect of extensional cyclic strain on the mechanical and physico-mechanical properties of PVC-NBR/graphite composites," *eXPRESS Polymer Letters*, vol. 2, no. 12, pp. 836-845, 2008.
- [139] R. Zhang, H. Deng, R. Valenca *et al.*, "Strain sensing behaviour of elastomeric composite films containing carbon nanotubes under cyclic loading," *Composites Science and Technology*, vol. 74, pp. 1-5, Jan 24, 2013.
- [140] S. Li, Y. Wang, H. Cao *et al.*, "Flexible Tactile Sensor Based on Conductive Rubber and Sensing Mechanism," *Sensors & Transducers Journal*, vol. 150, no. 3, pp. 12-17, 2013.
- [141] M. Taya, W. J. Kim, and K. Ono, "Piezoresistivity of a short fiber/elastomer matrix composite," *Mechanics of Materials*, vol. 28, no. 1-4, pp. 53-59, 1998.
- [142] M. Lucci, P. Regoliosi, F. Brunetti *et al.*, "Carbon nanotubes films for sensing applications: From piezoresistive sensor to gas sensing," *Nonequilibrium Carrier Dynamics in Semiconductors Proceedings*, vol. 110, pp. 191-194, 2006.
- [143] L. Chen, G. H. Chen, and L. Lu, "Piezoresistive Behavior Study on Finger-Sensing Silicone Rubber/Graphite Nanosheet Nanocomposites," *Advanced Functional Materials*, vol. 17, no. 6, pp. 898-904, 2007.
- [144] Z.-M. Dang, M.-J. Jiang, D. Xie *et al.*, "Supersensitive linear piezoresistive property in carbon nanotubes/silicone rubber nanocomposites," *Journal of Applied Physics*, vol. 104, no. 2, pp. 024114, 2008.
- [145] B. Hu, N. Hu, Y. Li *et al.*, "Multi-scale numerical simulations on piezoresistivity of CNT/polymer nanocomposites," *Nanoscale Res Lett*, vol. 7, no. 1, pp. 402, 2012.
- [146] K. Ke, P. Pötschke, N. Wiegand *et al.*, "Tuning the Network Structure in Poly(vinylidene fluoride)/Carbon Nanotube Nanocomposites Using Carbon Black: Toward Improvements of Conductivity and Piezoresistive Sensitivity," *ACS Appl Mater Interfaces*, vol. 8, no. 22, pp. 14190-9, Jun 08, 2016.
- [147] J. R. Bautista-Quijano, P. Pötschke, H. Brunig *et al.*, "Strain sensing, electrical and mechanical properties of polycarbonate/multiwall carbon nanotube monofilament fibers fabricated by melt spinning," *Polymer*, vol. 82, pp. 181-189, Jan 15, 2016.

- [148] X. H. Liu, C. H. Lu, X. D. Wu *et al.*, "Self-healing strain sensors based on nanostructured supramolecular conductive elastomers," *J. Mater. Chem. A*, vol. 5, no. 20, pp. 9824-9832, May 28, 2017.
- [149] S. Tadakaluru, W. Thongsuwan, and P. Singjai, "Stretchable and flexible high-strain sensors made using carbon nanotubes and graphite films on natural rubber," *Sensors (Basel)*, vol. 14, no. 1, pp. 868-76, Jan 6, 2014.
- [150] P. Bifulco, D. Esposito, G. D. Gargiulo *et al.*, "A stretchable, conductive rubber sensor to detect muscle contraction for prosthetic hand control," pp. 173-176, 2017.
- [151] Y. Lin, S. Q. Liu, S. Chen *et al.*, "A highly stretchable and sensitive strain sensor based on graphene-elastomer composites with a novel double-interconnected network," *Journal of Materials Chemistry C*, vol. 4, no. 26, pp. 6345-6352, 2016.
- [152] T. Yamada, Y. Hayamizu, Y. Yamamoto *et al.*, "A stretchable carbon nanotube strain sensor for human-motion detection," *Nat Nanotechnol*, vol. 6, no. 5, pp. 296-301, May, 2011.
- [153] J. H. Kim, J. Y. Hwang, H. R. Hwang *et al.*, "Simple and cost-effective method of highly conductive and elastic carbon nanotube/polydimethylsiloxane composite for wearable electronics," *Sci Rep*, vol. 8, no. 1, pp. 1375, Jan 22, 2018.
- [154] A. Voet, A. K. Sircar, and T. J. Mullens, "Electrical Properties of Stretched Carbon Black Loaded Vulcanizates," *Rubber Chemistry and Technology*, vol. 42, no. 3, pp. 874-891, 1969.
- [155] S. V. Anand, and D. Roy Mahapatra, "Quasi-static and dynamic strain sensing using carbon nanotube/epoxy nanocomposite thin films," *Smart Materials and Structures*, vol. 18, no. 4, pp. 045013, 2009.
- [156] C. G. Robertson, "Dynamic Mechanical Properties," *Encyclopedia of Polymeric Nanomaterials*, S. Kobayashi and K. Müllen, eds., pp. 1-9, Berlin, Heidelberg: Springer Berlin Heidelberg, 2021.
- [157] S. Wiessner, "Rheological Behavior and Rubber Processing," *Encyclopedia of Polymeric Nanomaterials*, S. Kobayashi and K. Müllen, eds., pp. 1-10, Berlin, Heidelberg: Springer Berlin Heidelberg, 2021.
- [158] R. P. Rudra, "A Curve-Fitting Program to Stress-Relaxation Data," *Canadian Agricultural Engineering*, vol. 29, no. 2, pp. 209-211, Jul, 1987.
- [159] S. B. Eshwaran, D. Basu, S. R. Vaikuntam *et al.*, "Exploring the Role of Stearic Acid in Modified Zinc Aluminum Layered Double Hydroxides and Their Acrylonitrile Butadiene Rubber Nanocomposites," *Journal of Applied Polymer Science*, vol. 132, no. 9, Mar 5, 2015.
- [160] V. S. Raman, A. Das, K. W. Stöckelhuber *et al.*, "Improvement of mechanical performance of solution styrene butadiene rubber by controlling the concentration and the size of in situ derived sol-gel silica particles," *RSC Advances*, vol. 6, no. 40, pp. 33643-33655, 2016.
- [161] B. Basterra-Beroiz, R. Rommel, F. Kayser *et al.*, "NEW INSIGHTS INTO RUBBER NETWORK STRUCTURE BY A COMBINATION OF EXPERIMENTAL TECHNIQUES," *Rubber Chemistry and Technology*, vol. 90, no. 2, pp. 347-366, 2017.
- [162] H. H. Le, Z. Ali, M. Uthardt *et al.*, "Effect of the cross-linking process on the electrical resistivity and shape-memory behavior of cross-linked carbon black filled ethylene-octene copolymer," *Journal of Applied Polymer Science*, vol. 120, no. 4, pp. 2138-2145, 2011.

- [163] D. S. McLachlan, M. Blaszkiewicz, and R. E. Newnham, "Electrical-Resistivity of Composites," *Journal of the American Ceramic Society*, vol. 73, no. 8, pp. 2187-2203, Aug, 1990.
- [164] F. Semeriyonov, A. Chervanyov, R. Jurk *et al.*, "Non-monotonic dependence of the conductivity of carbon nanotube-filled elastomers subjected to uniaxial compression/decompression," *Journal of Applied Physics*, vol. 113, no. 10, pp. 103706, 2013.
- [165] D. Qian, E. C. Dickey, R. Andrews *et al.*, "Load transfer and deformation mechanisms in carbon nanotube-polystyrene composites," *Applied Physics Letters*, vol. 76, no. 20, pp. 2868-2870, 2000.
- [166] J. Kost, M. Narkis, and A. Foux, "Effects of axial stretching on the resistivity of carbon black filled silicone rubber," *Polymer Engineering and Science*, vol. 23, no. 10, pp. 567-571, 1983.
- [167] A. Petchkaew, K. Sahakaro, W. K. Dierkes *et al.*, "Petroleum-based Safe Process Oils in NR and NR/SBR Blends: Part III. Effects of Oil Types and Contents on the Properties of Carbon Black Filled Compounds," *KGK*, vol. 9, pp. 6, 2015.
- [168] J. D. Ferry, and H. S. Myers, "Viscoelastic Properties of Polymers," *Journal of The Electrochemical Society*, vol. 108, no. 7, pp. 142C, 1961.
- [169] N. T. Selvan, S. B. Eshwaran, A. Das *et al.*, "Piezoresistive natural rubber-multiwall carbon nanotube nanocomposite for sensor applications," *Sensors and Actuators A: Physical*, vol. 239, pp. 102-113, 3/1/, 2016.
- [170] E. S. Bhagavatheswaran, S. R. Vaikuntam, K. W. Stöckelhuber *et al.*, "High-performance elastomeric strain sensors based on nanostructured carbon fillers for potential tire applications," *Materials Today Communications*, vol. 14, pp. 240-248, 3//, 2018.
- [171] R. Zhang, H. Deng, R. Valenca *et al.*, "Strain sensing behaviour of elastomeric composite films containing carbon nanotubes under cyclic loading," *Composites Science and Technology*, vol. 74, pp. 1-5, 2013.
- [172] A. R. Payne, "The dynamic properties of carbon black-loaded natural rubber vulcanizates. Part I," *Journal of Applied Polymer Science*, vol. 6, no. 19, pp. 57-63, 1962.
- [173] G. Heinrich, M. Klüppel, and T. A. Vilgis, "Reinforcement of elastomers," *Current Opinion in Solid State and Materials Science*, vol. 6, no. 3, pp. 195-203, 2002/06/01/, 2002.
- [174] K. Muniandy, H. Ismail, and N. Othman, "Effects of partial replacement of rattan powder by commercial fillers on the properties of natural rubber composites," *BioResources*, vol. 7, no. 4, pp. 4640-4657, 2012.
- [175] J. S. Bergström, and M. C. Boyce, "Mechanical Behavior of Particle Filled Elastomers," *Rubber Chemistry and Technology*, vol. 72, no. 4, pp. 633-656, 1999.
- [176] L. S. Schadler, S. C. Giannaris, and P. M. Ajayan, "Load transfer in carbon nanotube epoxy composites," *Applied Physics Letters*, vol. 73, no. 26, pp. 3842-3844, 1998.
- [177] J. G. Simmons, "Generalized Formula for the Electric Tunnel Effect between Similar Electrodes Separated by a Thin Insulating Film," *Journal of Applied Physics*, vol. 34, no. 6, pp. 1793-1803, 1963.
- [178] A. B. Oskouyi, U. Sundararaj, and P. Mertiny, "Tunneling Conductivity and Piezoresistivity of Composites Containing Randomly Dispersed Conductive

- Nano-Platelets,” *Materials (Basel)*, vol. 7, no. 4, pp. 2501-2521, Mar 28, 2014.
- [179] T. Sekitani, Y. Noguchi, K. Hata *et al.*, “A rubberlike stretchable active matrix using elastic conductors,” *Science*, vol. 321, no. 5895, pp. 1468-72, Sep 12, 2008.
- [180] K. Subramaniam, A. Das, and G. Heinrich, “Highly conducting polychloroprene Composites based on multi-walled Carbon Nanotubes and 1-butyl 3-Methyl imidazolium bis(trifluoromethylsulphonyl)imide,” *Kgk-Kautschuk Gummi Kunststoffe*, vol. 65, no. 7-8, pp. 44-46, Jul-Aug, 2012.
- [181] K. Engelhart, "Continental presents two new tire technology concepts for greater safety and comfort," Continental Tires - Press Release, 2017.

List of figures

Figure 1.1: (a) Change in electrical resistance of CNT filled NR and SBR samples upon mechanical stretching [29]. (b) Change in electrical resistance of carbon black filled silicone rubber samples at different temperatures[30](Reproduced with permissions from John Wiley and Sons). (c) Change in electrical resistance of CNT filled polycarbonate samples upon exposure to various solvents [31] (Reproduced with permissions from Elsevier).	3
Figure 1.2: Electrically conducting NR samples filled with (a) CNT and (b) CB samples to yield non-reliable electrical hysteresis behavior under cyclic loading [32].....	3
Figure 1.3: Appearance of second piezoresistive response in course of cyclic loading experiment [37] (Reproduced with permissions from John Wiley and Sons).	4
Figure 2.1: Schematic representation of the dependence of electrical conductivity on filler volume fraction.	12
Figure 2.2: (a) Influence of filler aspect ratio on electrical conductivity [32] [reproduced with permissions from ACS] and (b) Influence of CNT aspect ratio on the percolation threshold [117] [reproduced with permissions from IOP Science]	14
Figure 2.3: Effect of filler dispersion (a) Improvement in electrical conductivity due to latex mixing [127] (Reproduced with permissions from Royal Society of Chemistry). (b) Improvement in electrical conductivity due to pre-dispersion of CNT in ethanol [129] (Reproduced with permissions from Elsevier).	16
Figure 2.4 : (a) Concentration of CNT within the NR phase and (b) magnified image as highlighted by a blue box. (c) Reduction in the percolation concentration of graphene. [All images are reproduced from [151] with permissions from Royal Society of Chemistry].	19
Figure 2.5: (a) Schematic representation of storage modulus (E') and loss modulus (E'') and (b) an example temperature sweep curve of unfilled SSBR.....	22
Figure 2.6: (a) An example stress relaxation curve and (b) Stress relaxation curve indicated with the relaxation parameters namely relaxation coefficient and relaxation time. (Inset: Representation of the Maxwell Model with combinations of springs and dashpots)	23
Figure 3.1: Chemical structure of SSBR.....	25
Figure 3.2 Chemical structure of NR.....	25
Figure 3.3 Chemical structure of BR	26
Figure 3.4: TEM Picture of Printex (12 Phr) inside the SSBR matrix	27
Figure 3.5: (a) Haake Rheomix 3000 with large mixing chamber (360 cm ³) with pictures of the rotors and the masticated rubber. (b) Haake Rheomix 600 with the small mixing chamber (85cm ³)	29
Figure 3.6: Two-roll mill	29
Figure 3.7: Heated press utilized to prepare the samples.....	30
Figure 3.8: A view of the utilized rubber process analyzer	33

Figure 3.9: Schematic representation of the experimental setup of the piezoresistance measurement device	35
Figure 3.10: In-house built piezoresistance measurement device with a magnified view of the sample clamps (left).....	35
Figure 3.11: Schematic view (left) and experimental setup (right) of the dynamic mechanical analyzer coupled with the in-house built device. [Picture in the orange box on the right depicts the clamping mechanism inside the DMA chamber and image inside the red box on the right depicts a sample data displayed in the computer].....	36
Figure 3.12: An example stress relaxation curve depicting the three characteristic relaxation times $\tau s1$, $\tau s2$ and $\tau s3$	39
Figure 4.1:(a) Dependence of conductance on the filler content (b) plot of log conductance against log $(P-P_c)$ with the linear scaling law fit [109, 118]. [P is the filler volume fraction and P_c is the filler volume fraction at percolation threshold]	42
Figure 4.2: Electrical conductance of the rubber composite as a function of sulfur content for (a) carbon blacks and (b) CNT. The plot of $\log \sigma$ against $\log (P-P_c)$ (with the linear fit) for different sulfur contents of (c) carbon black and (d) CNT filled composites.	43
Figure 4.3: (a) Variation in Shore A hardness with respect to plasticizer content and (b) dependence of electrical conductance with respect to the hardness of the composites	44
Figure 4.4: Change in (a) resistance and (b) relative resistance with an inset depicting changes in the low strain regime for various carbon black composites. Change in (c) resistance and (d) relative resistance with an inset depicting changes in the low strain regime for various CNT composites.	45
Figure 4.5: Strain sensitivity plots of (a) carbon black composites & (b) CNT composites.....	47
Figure 4.6: Log-log representation of the strain sensitivity with the power law fits for (a) carbon black and (b) CNT composites respectively.	49
Figure 4.7: Relative resistance and (b) strain sensitivity with power law fit for 3.5 phr CNT composites with different process oil content. (c) Relative resistance and (d) strain sensitivity with power law fit for 10.5 phr carbon black composites with different process oil content.	51
Figure 4.8: Several loading and unloading cycles test of (a) 13 phr carbon black and (b) 4 phr CNT filled composites.....	54
Figure 5.1: (a) Time sweep experiment of a 12 phr CB sample. (Smaller time frames are magnified and shown for better understanding) (b) calculation of mean resistance and dynamic resistance amplitude (c) strain and resistance signal for a 13phr CB sample at 25°C	56
Figure 5.2: (a) Stress profile of 12 phr CB with and without dynamic load (without dynamic load refers to stress relaxation experiments) (b) Resistance profile of 12 phr CB with and without dynamic load (c) Deformation mechanism of conducting rubber sample during dynamic loading, the filler network become compact and coherent, resulting in higher conducting pathways.	58
Figure 5.3: (a) Relaxation of mean stress and mean electrical resistance and (b) relative values of a 12phr CB filled sample during a time sweep experiment.....	60

Figure 5.4: Relative resistance plots of (a) carbon black composites with different filler loading and 12phr CB samples at different (b) temperatures, (c) test frequencies and (d) crosslink densities and 3.5phr CNT samples (e) at low test frequencies and (f) with different crosslink densities.	61
Figure 5.5: Dynamic resistance amplitude ratio of (a) different CB content, 12phr CB composites at different (b) frequencies, (c) crosslink-densities and (d) 3.5phr CNT composite at different temperatures.....	63
Figure 5.6: Evolution of the second peak with time for 12 phr CB sample.	65
Figure 5.7: Second peaks summarized after 1 hour for (a) different CB content, (b) 12 phr CB at different temperatures, (c) 3.5 phr CNT sample at different frequencies and (d) 3.5 phr CNT sample with different crosslink densities.....	66
Figure 5.8: Change in (a) relative resistance and (b) dynamic resistance amplitude against temperature for different CB content. Change in relative resistance for 12phr CB sample (c) with different crosslink densities, (d) at different dynamic strains. (e) CNT samples with different filler levels and (f) 12CB sample tested with less force. [<i>For all the cases, the temperature sweeps are performed from high (60°C) to low temperatures</i>]	68
Figure 5.9: Dependence of the second peak on temperature for samples (a) with different concentrations of carbon black, (b) 12CB with different crosslink densities and (c) with different concentrations of CNT	70
Figure 5.10: Dependence of elastic modulus (E') and mean conductance over dynamic strain for (a) different CB content and (b) 12 CB sample at 50 °C. Dependence of loss modulus (E'') and mean conductance over dynamic strain for (c) 13 CB sample at 35 °C and (d) 12 CB sample at 50 °C.	72
Figure 5.11: (a) Stress hysteresis profiles (b) Resistance hysteresis profiles of 12phr carbon black sample at different temperatures plotted from dynamic temperature sweep experiments.	73
Figure 6.1: Relaxation profiles for samples with various carbon black loading (a) relative resistance and (b) relative mean stress. [Symbols represent the experimental data and dotted lines represent the fitted curves]	77
Figure 6.2: Relative resistance plots with fitting for 12CB samples tested at different (a) temperatures, (b) frequency and (c) crosslink density. Relative mean stress plots of the same samples at different (d) temperatures, (e) frequency and (f) crosslink density. [Symbols represent the experimental data and dotted lines represent the fit]	79
Figure 6.3: Summary of relaxation parameters of various carbon black and carbon nanotubes samples. (a) Coefficients of relative stress versus coefficients of relative resistance (b) residual values of relative stress versus residual values of relative resistance.....	80
Figure 6.4: Phase shifts between strain, stress, and resistance	81
Figure 6.5: An example (a) resistance signal, (b) its Fourier transformed data and (c) the sine function fitting for a 12phr CB sample (Open circles: experimental data & solid line: Multi-sine fit).	82
Figure 6.6: $\tan \delta$ plots from a time sweep experiment performed for samples containing different CB loading [Filled symbols and solid line: $\tan \delta_{\sigma-\varepsilon}$ and open crossed symbols and dash line: $\tan \delta_{R-\varepsilon}$]	84
Figure 6.7: $\tan \delta$ values summarized after 1 hour from time sweep experiments for (a) 12 CB samples at different temperatures, (b) 12 CB	

samples with different crosslink density, (c) 3.5 CNT sample at different dynamic strain and (d) 3.5 CNT sample at different frequencies	85
Figure 6.8: $\tan \delta$ plots for temperature sweep experiments performed for (a) samples with different CB content, (b) 12 phr CB samples at different dynamic strain and (c) 3.5 phr CNT sample with different crosslink density	87
Figure 6.9: $\tan \delta$ plots for temperature sweep experiments performed for (a) samples with different carbon black concentrations (b) 12 phr CB samples at different loading conditions	88
Figure 6.10: Peak amplitudes (A_1 and A_2) summarized for (a) samples with different filler content and 12 phr CB sample at different (b) loads, (c) temperature and (d) crosslink density.	90
Figure 6.11: Peak amplitudes (A_1 and A_2) summarized for (a) samples with different filler content and (b) 12 phr CB sample at different loads. Amplitude ratios A_2 / A_1 summarized for (c) samples with different filler content and (d) 12 phr CB sample at different loads	92
Figure 7.1: (a) relative resistance and (b) relative mean stress plots with fitting for SSBR samples with different types of CCB.(c) relative resistance and (d) relative mean stress plots with fitting for SSBR samples with N330 CCB at different temperature.(e) relative resistance and (f) relative mean stress plots with fitting for SSBR samples with N330 CCB at different frequency. [Symbols represent the experimental data and dotted lines represent the fit]	94
Figure 7.2: $\tan \delta$ values summarized after 1 hour from time sweep experiments for (a) SSBR with different CCB and SSBR/N330 samples at different (b) temperatures and (c) frequencies	96
Figure 7.3: (a) $\tan \delta$ and (b) resistance amplitude ratios (A_2/A_1) for SSBR with different types of carbon blacks.	97
Figure 7.4: Dependence of mean conductance and elastic modulus (E') on the dynamic strain for different carbon blacks	98
Figure 7.5: (a) relative resistance and (b) relative mean stress plots with fitting for different rubbers. [<i>Symbols represent the experimental data and dotted lines represent the fit</i>]	99
Figure 7.6: $\tan \delta$ values summarized after 1 hour from time sweep experiments for different rubbers.....	101
Figure 7.7: Mean resistance values for 12CB sample tested in compression mode.....	102
Figure 7.8: (a) Changes in resistance of a rubber sample during the dynamic experiment and (b) corresponding changes in interparticle distance for the sample calculated using tunneling theory	103
Figure 8.1: Sensor embedded in tire-tread to detect tire pressure and sense road conditions [181]. Reproduced from Continental Tires – Press release August 12, 2017.....	108

List of tables

Table 2.1: Few initial works on the development of conductive rubber	9
Table 3.1 Basic properties of the utilized SSBR.....	25
Table 3.2 Basic properties of the utilized NR.....	26
Table 3.3 Basic properties of the utilized BR.....	26
Table 3.4 Basic properties of the utilized Printex XE-2B grade.....	27
Table 3.5: Basic properties of the utilized Nanocyl NC7000 grade	28
Table 3.6: Basic rubber compounding formulation (ingredients) with CNT.....	31
Table 3.7: Basic rubber compounding formulation (ingredients) with conductive carbon black (CB)	31
Table 3.8: Compound formulations of conductive carbon black and carbon nanotube with SSBR and aromatic process oil	32
Table 3.9: Compound formulations of conductive carbon black with different rubbers.....	32
Table 3.10 : Compound formulations of conventional carbon blacks with SSBR.....	32
Table 3.11: Various tests conditions utilized for the dynamic piezoresistivity study under strain-driven mode	37
Table 3.12: Various tests conditions utilized for the dynamic piezoresistivity study under force driven mode	38
Table 4.1: Fitting parameters for different samples with 2 phr of sulfur.....	48
Table 4.2: Fitting parameters for 12 phr carbon black and 4 phr CNT samples with a different sulfur content.....	50
Table 4.3: Fitting parameters for 3.5 phr CNT and 10.5 phr carbon black samples with different process oil content.....	52
Table 4.4: Sensitivity rating for various elastomeric composites Low strain (L): 10-50% strain; Medium strain (M): 50-100% strain: High strain (H): > 100% strain.	53
Table 6.1: Relative resistance and relative mean stress fit data for samples with different carbon black loading	77
Table 6.2: Relative resistance and relative mean stress fit data at various test conditions.....	78
Table 7.1: Relative resistance and relative mean stress fit data for SSBR filled with 60 phr of different CCB & SSBR filled with 60phr N330 at different conditions	95
Table 7.2: Relative resistance and relative mean stress fit data for different rubbers.....	100

Eidesstattliche Erklärung

Ich versichere, dass

(a) ich die vorliegende Arbeit mit dem Titel “Exploring the piezoresistive characteristics of solution styrene butadiene rubber composites under static and dynamic conditions - A novel route to visualize filler network behavior in rubbers” ohne unzulässige Hilfe Dritter und ohne Benutzung anderer als der angegebenen Hilfsmittel angefertigt habe. Die aus fremden Quellen direkt oder indirekt übernommenen Gedanken sind als solche kenntlich gemacht.

(b) ich die vorliegende Arbeit bisher weder im Inland noch im Ausland in gleicher oder ähnlicher Form einer anderen Prüfungsbehörde zum Zwecke einer Promotion oder eines anderen Prüfungsverfahrens vorgelegt habe und diese auch zu keinem Zeitpunkt veröffentlicht worden ist.

(c) ich bei der Auswahl und Auswertung des Materials sowie bei der Herstellung des Manuskripts die Unterstützungsleistungen der im Antrag genannten Betreuer/innen in Anspruch genommen habe.

(d) keine weiteren Personen bei der geistigen Herstellung der vorliegenden Arbeit beteiligt waren.

(e) ich keine Hilfe eines/r Promotionsberaters/in in Anspruch genommen habe.

(f) keine, weder unmittelbar noch mittelbar, geldwerten Leistungen im Zusammenhang mit dem Inhalt der vorliegenden Dissertation an Dritte erfolgt sind.

Dresden, den

List of publications

Peer-reviewed journals

1. Eshwaran Subramani Bhagavatheswaran, Klaus Werner Stöckelhuber, Sankar Raman Vaikuntam, Sven Wießner, Petra Pötschke, Gert Heinrich, Amit Das, “Time and Temperature Dependent Piezoresistive Behavior of Conductive Elastomeric Composites”. *Rubber Chemistry and Technology*, **91**, 651-667, **2018**.
2. Aladdin Sallat, Amit Das, Jana Schaber, Ulrich Scheler, Eshwaran Subramani Bhagavatheswaran, Klaus W. Stöckelhuber, Gert Heinrich, Brigitte Voit, Frank Böhme, “Viscoelastic and self-healing behavior of silica filled ionically modified poly(isobutylene-co-isoprene) rubber”. *RSC Advances*, **8**, 26798, **2018**.
3. Sankar Raman Vaikuntam, Eshwaran Subramani Bhagavatheswaran, Klaus Werner Stöckelhuber, Sven Wießner, Gert Heinrich, Amit Das, “Entwicklung von Hochleistungs-Elastomercomposites aus S-SBR und aus via Alkoxidroute hergestelltem Silica”. *Gummi Fasern Kunststoffe – Teil 2*, **4**, 170-177, **2018**
4. Eshwaran Subramani Bhagavatheswaran, Sankar Raman Vaikuntam, Klaus Werner Stöckelhuber, Sven Wießner, Gert Heinrich, Amit Das, “High-performance elastomeric strain sensors based on nanostructured carbon fillers for potential tire applications”. *Materials Today Communications*, **14**, 240–248, **2018**.
5. Sankar Raman Vaikuntam, Klaus Werner Stöckelhuber, Eshwaran Subramani Bhagavatheswaran, Sven Wiessner, Ulrich Scheler, Kay Saalwaechter, Petr Formanek, Gert Heinrich, Amit Das, “Entrapped Styrene Butadiene Polymer Chains by Sol-Gel Derived Silica Nanoparticles with Hierarchical Raspberry Structures”. *J. Phys. Chem. B*, **122**, 2010–2022, **2018**
6. Sankar Raman Vaikuntam, Eshwaran Subramani Bhagavatheswaran, Klaus Werner Stöckelhuber, Sven Wießner, Gert Heinrich, Amit Das, “Entwicklung von Hochleistungs-Elastomercomposites aus S-SBR und aus via Alkoxidroute hergestelltem Silica”. *Gummi Fasern Kunststoffe*, **3**, 106-112, **2018**
7. Tamil Selvan Natarajan, Eshwaran Subramani Bhagavatheswaran, Klaus Werner Stöckelhuber, Sven Wiessner, Petra Pötschke, Gert Heinrich, Amit Das, “Strong strain sensing performance of natural rubber nanocomposites. *ACS Applied Materials and Interfaces*, **9**, 4860–4872, **2017**

8. Sankar Raman Vaikuntam, Eshwaran Subramani Bhagavatheswaran, Klaus Werner Stöckelhuber, Sven Wießner, Gert Heinrich, Amit Das, “Development of high performance rubber composites from alkoxide-based silica and solution styrene–butadiene rubber”. *Rubber Chemistry and Technology*, **3**, 467–486, **2016**
9. Tamil Selvan Natarajan, Subramani Bhagavatheswaran Eshwaran, Amit Das, Klaus Werner Stöckelhuber, Sven Wießner, Petra Pötschke, Golok B. Nando, Alexander I. Chervanyov, Gert Heinrich, “Piezoresistive natural rubber-multiwall carbon nanotube nanocomposite for sensor applications”. *Sensors and Actuators A: Physical*, **239**, 102–113, **2016**
10. Vaikuntam Sankar Raman, Amit Das, Klaus Werner Stöckelhuber, Subramani Bhagavatheswaran Eshwaran, Jagannath Chanda, Mikhail Malanin, Uta Reuter, Andreas Leuteritz, Regine Boldt, Sven Wiessner, Gert Heinrich, “Improvement of mechanical performance of solution styrene butadiene rubber by controlling the concentration and the size of in-situ derived sol-gel silica particles”. *RSC Advances*, **6**, 33643–33655, **2016**
11. Eshwaran Subramani Bhagavatheswaran, Meenali Parsekar, Amit Das, Hai Hong Le, Sven Wiessner, Klaus Werner Stöckelhuber, Gerd Schmaucks, Gert Heinrich, “Construction of an Interconnected Nanostructured Carbon Black Network: Development of Highly Stretchable and Robust Elastomeric Conductors”. *The Journal of Physical Chemistry C*, **119**, 21723–21731, **2015**
12. Subramani Bhagavatheswaran Eshwaran, Debdipta Basu, Sankar Raman Vaikuntam, Burak Kutlu, Sven Wiessner, Amit Das, Kinsuk Naskar, Gert Heinrich, “Exploring the role of stearic acid in modified zinc aluminum layered double hydroxides and their acrylonitrile butadiene rubber nanocomposites”. *Journal of Applied Polymer Science*, **132**, 41539, **2015**
13. Subramani Bhagavatheswaran Eshwaran, Debdipta Basu, Burak Kutlu, Andreas Leuteritz, Udo Wagenknecht, Klaus Werner Stöckelhuber, Kinsuk Naskar, Amit Das, Gert Heinrich, “Stearate Modified Zinc-Aluminum Layered Double Hydroxides and Acrylonitrile Butadiene Rubber Nanocomposites”. *Polymer-Plastics Technology and Engineering*, **53**, 65–73, **2014**

Oral presentations

1. DKT 2018 in Nürnberg, Germany.
2. Technomer 2017 in Chemnitz, Germany.
3. PPS Europe Africa 2017 in Dresden, Germany.
4. 2017 Northern European Rubber Seminar in Dresden, Germany.
5. Frontiers of Rubber Science and Technology in Dresden, Germany.
6. 190th ACS Technical meeting in Pittsburgh, U.S.A.
7. Nanotech 2016 in Tokyo, Japan.
8. 188th ACS Technical meeting in Cleveland, U.S.A.
9. International Rubber Conference 2015 in Nuremberg, Germany.
10. 15th European Polymer Federation in Dresden, Germany.
11. 2015 Northern European Rubber Seminar in Cologne, Germany.
12. 2014 Northern European Rubber Seminar in Tampere, Finland.

Poster presentations

1. International Rubber Conference 2015 in Nuremberg, Germany.
2. Rubber fall Colloquium 2014 in Hannover, Germany